

Response to Major Revision Comment by Topical Editor

The length of the text is way too much, and it was quite painful to read throughout the document. This problem became much worse after the revision, although previous reviewer pointed out this issue. Of cause, authors have reason to add new texts for addressing reviewer's comments as authors mentioned it in their reply letter. But, still, due to the absence of readability, it is indeed very painful to read through the document. Actually, both previous referees refused to review the revised manuscript, and this is the first case in my long experience as an editor.

I agree that authors addressed all issues raised by previous referees. It's OK. But, the manuscript should be re-organized to reduce the amount of main text substantially (like, less than half). I believe that majority of the text in the section 4 and some figures can be moved to the supplemental information.

Thank you for taking the time to go through this iteration of this manuscript. We understand the issues that you and the referees have raised, and have accordingly reduced the main text body from 21 to 11 pages, and its total length (including Figures, etc) from 45 to 27 pages. These reductions have entailed a mix of deletion and the movement of large sections of the text and Figures into the Supplement, focusing largely on Section 4, as you have helpfully pointed out. On the other hand we were somewhat perplexed by the reported refusal to referee the previous version of the manuscript. All prior specific and general comments by referees were responded to, and indeed we had substantially reduced and restructured the text as per a non-specific suggestion to do so, while as a native English speaker the first author finds the charge of 'unreadability' rather puzzling. Since this manuscript has been in review for over seven months, we were surprised to learn that we should cut the text body by a factor of two or more at this late stage, given that this was never specifically raised in such a context previously. Again, we understand and agree that the length of the document posed problems of overburden for the reader in general and the referees specifically, however we felt this necessarily reflected the very broad content of such a study, given that it appeals to both the modelling and field work communities, and would need to satisfy their rigor and interest across a large number of domains (primary production, hydrology, data, soil science and thermodynamics, and the rather more niche specificities of the inland water continuum -DOC discharge, concentration, evasion, etc.) within the context of the model's structure and function, or lack thereof. We look forward to moving on to the next iteration of this manuscript's evolution, and thank you for your patience with and participation in that process.

1 **Title :**
2 **ORCHIDEE MICT-LEAK (r5459), a global model for the production, transport and**
3 **transformation of dissolved organic carbon from Arctic permafrost regions, Part**
4 **2: Model evaluation over the Lena River basin.**

5
6 **Authors:**
7 **S.P.K. Bowring¹, R. Lauerwald², B. Guenet¹, D. Zhu¹, M. Guimbertea^{1,3}, P. Regnier²,**
8 **A. Tootchi³, A. Ducharme³, P. Ciais¹**

9
10 **Affiliations:**
11 [1] Laboratoire des Sciences du Climat et de l'Environnement, LSCE, CEA, CNRS, UVSQ,
12 91191 Gif Sur Yvette, France
13 [2] Department of Geoscience, Environment & Society, Université Libre de Bruxelles,
14 Bruxelles, Belgium
15 [3] Sorbonne Université, CNRS, EPHE, Milieux environnementaux, transferts et
16 interaction dans les hydro-systèmes et les sols, Metis, 75005 Paris, France
17

18 **Abstract**
19 In this second part of a two-part study, we perform a simulation of the carbon and water
20 budget of the Lena catchment with the land surface model ORCHIDEE MICT-LEAK,
21 enabled to simulate dissolved organic carbon (DOC) production in soils and its transport
22 and fate in high latitudes inland waters. The model results are evaluated in their ability
23 to reproduce the fluxes of DOC and carbon dioxide (CO₂) along the soil-inland water
24 continuum, and the exchange of CO₂ with the atmosphere, including the evasion
25 outgassing of CO₂ from inland waters. We present simulation results over years 1901-
26 2007, and show that the model is able to broadly reproduce observed state variables
27 and their emergent properties across a range of interacting physical and biogeochemical
28 processes, including: 1) Net primary production (NPP), respiration and riverine
29 hydrologic amplitude, seasonality and inter-annual variation; 2) DOC concentrations,
30 bulk annual flow and their volumetric attribution at the sub-catchment level; 3) High
31 headwater versus downstream CO₂ evasion, an emergent phenomenon consistent with
32 observations over a spectrum of high latitude observational studies. (4) These quantities
33 obey emergent relationships with environmental variables like air temperature and
34 topographic slope that have been described in the literature. This gives us confidence in
35 reporting the following additional findings: Of the ~34TgC yr⁻¹ left over as input to soil
36 matter after NPP is diminished by heterotrophic respiration, 7 TgC yr⁻¹ is leached and
37 transported into the aquatic system. Of this, over half (3.6 TgC yr⁻¹) is evaded from the
38 inland water surface back into the atmosphere and the remainder (3.4 TgC yr⁻¹) flushed
39 out into the Arctic Ocean, mirroring empirically derived studies. These riverine DOC
40 exports represent ~1.5% of NPP. DOC exported from the floodplains is dominantly
41 sourced from recent, more 'labile' terrestrial production, in contrast to DOC leached
42 from the rest of the watershed with runoff and drainage, which is mostly sourced from
43 recalcitrant soil and litter. All else equal, both historical climate change (a
44 spring/summer warming of 1.8°C over the catchment) and rising atmospheric CO₂
45 (+85.6ppm) are diagnosed from factorial simulations to contribute similar, significant
46 increases in DOC transport via primary production, although this similarity may not
47 hold in the future.
48

49 1 Introduction

50
51 A new branch of the high latitude-specific land surface component of the IPSL Earth
52 System model, ORCHIDEE MICT-LEAK (r5459), was enabled to simulate new model
53 processes of soil dissolved organic carbon (DOC) and CO₂ production, and their
54 advective/diffusive vertical transport within a discretized soil column as well as their
55 transport and transformation within the inland water network, in addition to improved
56 representation of hydrological and carbon processes in floodplains. These additions,
57 processes first coded in the model ORCHILEAK (Lauerwald et al., 2017) and
58 implemented within the high latitude base model ORCHIDEE-MICT v8.4.1 (Guimbarteau
59 et al., 2018), were described in detail in Part 1 of this study, depicted graphically, in
60 Figure S1a,b. This second part of our study deals with the validation and application of
61 our model. We validate simulation outputs against observation for present-day and run
62 transient simulations over the historical period (1901-2007) using the Lena River basin
63 as test case. The simulation setup and rationale for choice of simulation basin are
64 outlined below.

65 2 Simulation Rationale

66 The Lena river basin, which is bounded by the region 52-72°N; 102-142°E, was chosen
67 as the basin for model evaluation because it is the largest DOC discharge contribution
68 amongst the Arctic rivers, according to some estimates (Raymond et al., 2007; Holmes et
69 al., 2012), with its 2.5 million km² area (befitting our coarse-grid resolution) discharging
70 almost 20% of the summed discharge of the largest six Arctic rivers, its large areal
71 coverage by Podzols (DeLuca and Boisvenue, 2012), and the dominance of DOC versus
72 particulate organic carbon (POC) with 3-6Tg DOC-C yr⁻¹ vs. 0.03-0.04 Tg POC-C yr⁻¹
73 (Semiletov et al., 2011) in the total OC discharge load –factors all broadly representative
74 of the Eurasian Arctic rivers. Climatological input to the model is from the Global Soil
75 Wetness Project Phase 3 (GSWP3) v.0 data, based on 20th Century reanalysis using the
76 NCEP land-atmosphere model and down-scaled to a 0.5°, 3-hourly resolution covering
77 the period 1901 to 2007 (Supplement, Table S1). This is then up-scaled to 1° resolution
78 and interpolated to a 30 minute timestep to comply with the timestep of ORCHIDEE's
79 surface water and energy balance calculation period. Precipitation was partitioned into
80 rainfall and snowfall, and a correction for wind-induced undercatch was also applied.
81 These are described in greater detail in Guimbarteau et al. (2018). Over the simulation
82 period under this dataset, the Lena basin experiences a mean thaw period warming of
83 1.8°C, while atmospheric CO₂ concentrations increase by 85.6ppm. The GSWP3 dataset
84 was chosen due to its relative performance in simulating the inter-annual variability and
85 seasonality of Pan-Arctic riverine discharge in ORCHIDEE-MICT (Guimbarteau et al.,
86 2018), as compared to another data-driven climate forcing product, CRUNCEP v7
87 (Kalnay et al., 1996; New et al., 1999). Indeed, under CRUNCEP v7, ORCHIDEE-MICT
88 was shown to underestimate river discharge by as much as 83% over the Yukon basin.
89 An improved floodplains area input file for the Lena basin (Tootchi et al., 2019) was
90 used to drive the simulation of floodplain dynamics (Supplement, Table S1).

91 3 Simulation Setup

92 As detailed in Part 1 (Section 3.1), the soil carbon stock used by our model was
93 reconstituted from a 20,000 year soil carbon spinup of an ORCHIDEE-MICT run from

Simon Bowring 8/10/y 14:40

Supprimé: .

Simon Bowring 8/10/y 14:40

Supprimé: In essence, plant litter and soil carbon are transformed by microbial degradation to DOC and CO₂; the DOC is itself either respired to CO₂ or adsorbed, or transformed to particulate soil carbon. DOC can then be transferred by precipitation-dependent water flow laterally across the terrestrial landmass, in surface or subsurface flows to streams and rivers, whereupon it may either be respired within the water column or exported to the marine realm. A flow diagram depicting these flows and the residence times of the respective carbon pools, reproduced from Part 1 of this study, is given

Simon Bowring 8/10/y 14:41

Supprimé: Compared to other Eurasian rivers, the Lena is relatively well studied, which provides data across the range of soil, hydrologic, geochemical and ecological domains over space and time, that enable us to perform adequate model evaluation.

Simon Bowring 8/10/y 14:41

Supprimé: .

... [1]

Simon Bowring 8/10/y 14:41

Supprimé: forcing is

Simon Bowring 8/10/y 14:42

Supprimé: climatological forcing

Simon Bowring 8/10/y 14:42

Supprimé: for its prior suitability as input

Simon Bowring 8/10/y 14:43

Supprimé: .

Simon Bowring 8/10/y 14:43

Supprimé: The model structure is described in Part 1 of this study, however we describe how the fluxes are generated with respect to the results obtained by this study in some detail in the initial description of the results, below (Section 4.1).

Simon Bowring 8/10/y 14:43

Supprimé: of this study

134 Guimberteau et al. (2018) and run to quasi-steady state equilibrium for the Active and
135 Slow carbon pools (Supplement, Fig. S1b) under the new soil carbon scheme used in the
136 model configuration of the present study (Fig. 1). After some adjustment runs to account
137 for model read/write norms, the model was then run in transient mode under historical
138 climate, land cover and atmospheric CO₂ concentrations (Fig. 1). Simulations were run
139 over the Lena river basin (Fig. 3a) for the climate, CO₂ and vegetation input forcing data
140 (Supplement, Table S1) over 1901-2007 at a 1 degree resolution (Fig. 1), to evaluate the
141 simulated output of relevant carbon fluxes and hydrologic variables against their
142 observed values, as well as those of emergent phenomena arising from their interplay
143 (Fig. 1). We evaluate at the basin scale because the isolation of a single geographic unit
144 allows for a more refined analysis of simulated variables than doing the same over the
145 global Pan-Arctic, much of which remains poorly accounted for in empirical databases
146 and literature. The literature studies used in this evaluation are summarised in Table
147 S2. In order to derive an understanding of the environmental drivers of carbon cycling in
148 the Lena watershed and analyse the model sensitivity to the corresponding forcing data,
149 alternative simulations were run with constant climate and CO₂ conditions (Table 1, and
150 Supplement Table S1). Thus a factorial simulation was devised, consisting of 2 factors
151 and 3 simulations whose inputs were otherwise identical but for the investigated factor
152 (Table 1).

Simon Bowring 8/10/y 14:43
Supprimé: different data
Simon Bowring 8/10/y 14:44
Supprimé: between ORCHIDEE-MICT and this model version
Simon Bowring 8/10/y 14:44
Supprimé: . A summary of the step-wise procedure for simulation setup described above is detailed graphically in

Simon Bowring 8/10/y 14:43
Supprimé: ... [2]

155 4 Results and Interpretation

156 We refer to different simulations performed in this study according to the sensitivity
157 factors to which they are subjected. The transient, historical climate and atmospheric
158 CO₂ -forced simulations are hereafter referred to as the "Control" (CTRL) scenario, for
159 ease of interpretation . The "CLIM" and "CO₂" scenarios are those simulations for which
160 climate variability and atmospheric CO₂ were held constant at their pre-industrial levels,
161 respectively (Table 1). The following evaluation sections compare observations solely
162 against the CTRL. The subsequent section will evaluate this comparison against the
163 factorial simulations described above. The overall carbon budgets and their fluxes as
164 generated by each of the simulations are shown in Figs. 2 and 11 and discussed in detail
165 at the end of the evaluation. In the following we report first the broad results of model
166 simulations with respect to the carbon cycle, and follow with an evaluation of river
167 water and DOC discharge, DOC concentration and seasonality and river surface CO₂
168 outgassing, against available empirical data. Evaluation of NPP and Soil Respiration,
169 which are not considered primary to this study, is covered in Supplementary Text S1.

Simon Bowring 8/10/y 14:45
Supprimé: .
Simon Bowring 8/10/y 14:45
Supprimé: .
Simon Bowring 9/10/y 10:51
Mis en forme: Indice
Simon Bowring 8/10/y 14:45
Supprimé: Below, we examine that budget's component parts, in the following sequential order: In section 4.1 we briefly look through the overall carbon budget of the entire basin, discussing component fluxes of the budget, their values and what they mean. Section 4.2 evaluates DOC discharge, followed by DOC concentrations in export (4.3), dissolved CO₂ transport in rivers and its evasion from the river surface (4.4), emergent phenomena with respect to CO₂ evasion compared to river size (4.5.1) and DOC concentrations and slope (4.5.2), followed by DOC reactivity pools (4.6). NPP and soil respiration rates, evaluated at the Pan-Arctic scale for ORCHIDEE-MICT in Guimberteau et al. (2018), are evaluated for the Lena basin in the Supplement (Text S2). Wherever possible, model output are compared with available in situ observations, while emergent relationships between fluxes or concentrations and environmental controls found in observations are also drawn from the model output, to provide a 'process oriented' evaluation of the model. In Section 4.7 we discuss the overall drivers of the fluxes simulated by our model with respect to the two CLIM and CO₂ factorial simulations and the implications of these for the future.

Simon Bowring 9/10/y 10:53
Supprimé: .

171 4.1 Model Output: Carbon Budget

172 Fig. 2 summarises the simulated components of the carbon (C) cycle across the Lena
173 basin, averaged over the decade 1998-2007. C inputs to terrestrial ecosystems are
174 dominated by photosynthetic input (GPP). GPP assimilates (875 TgC yr⁻¹) are either
175 used as metabolic substrate by plants and lost as CO₂ by plant respiration processes
176 (376 TgC yr⁻¹) or soil respiration processes (465 TgC yr⁻¹), leaving behind annual growth
177 in terrestrial C storage (net biome productivity (NBP)), an atmospheric CO₂ sink of 34
178 TgC yr⁻¹. Further C inputs are delivered to the terrestrial surface via a combination of
179 atmospheric deposition, rainwater dissolved C, and the leaching of canopy C
180 compounds. These sum to a flux transported to the soil surface (4.6 TgC yr⁻¹) by
181 throughfall (see Part 1, Section 2.5).

224
225 Simon Bowring 8/10/y 14:45
226

227 | DOC in the soil solution as well as a fraction of dissolved CO₂ produced in the root zone
228 | from root and microbial respiration is exported to rivers along the model's two
229 | hydrological export vectors, surface runoff and deep drainage (Part 1, Section 2.6). For
230 | the Lena basin simulations, these fluxes of C exported from soils amount to 5.1 and 0.2
231 | TgC yr⁻¹, for DOC and CO₂ respectively. Three water pools, representing streams, rivers
232 | and groundwater and each containing dissolved CO₂ and well as DOC of different
233 | reactivity, are routed through the landscape and between grid cells following the river
234 | network in the catchment (Part 1, Section 2.7). In addition, seasonally flooded soils
235 | located in low, flat grid cells next to the river network (see Part 1, Section 2.8) export
236 | DOC (0.57 TgC yr⁻¹) and CO₂ (1.54 TgC yr⁻¹) to the river network when their inundation
237 | occurs. Part of this leached inundated material is re-infiltrated back into the soil from
238 | the water column during floodplain recession ('Return' flux, 0.45 TgC yr⁻¹). During its
239 | transport through inland waters, DOC can be decomposed into CO₂ (2.1 TgC yr⁻¹) and a
240 | fraction of river CO₂ produced from DOC and transferred from soil escapes to the
241 | atmosphere (3.6 TgC yr⁻¹) through gas exchange kinetics (Part 1, Section 2.10). This flux
242 | is termed 'CO₂ evasion' in Fig. 2 of this study. Carbon that survives the inland water
243 | reactor is exported to the coastal ocean in the form of DOC (3.16 TgC yr⁻¹) and CO₂ (0.26
244 | TgC yr⁻¹).
245

246 | **Supprimé:** In the soil, DOC is produced by
247 | the decomposition of litter and soil organic
248 | carbon (SOC) pools (see Part 1, Section 2.4
249 | and Fig. 2) and can be ad- or de- sorbed to
250 | solid particles (see Part 1 of this study,
251 | Section 2.11), while there is a continuous
252 | exchange of DOC with (solid) soil organic
253 | carbon. The interplay between
254 | decomposition and sorption leads to DOC
255 | concentration changes in the soil solution.
256

257 Simon Bowring 8/10/y 14:49

258 | **Supprimé:** These fluxes and their
259 | interpretation within the context of the
260 | Land-Ocean-Aquatic Continuum (LOAC) are
261 | returned to in Section 4.8 of this study.
262

263 Simon Bowring 8/10/y 14:49

264 | **Supprimé:** , otherwise known as ice-out or
265 | spring freshet
266

267 Simon Bowring 8/10/y 14:50

268 | **Supprimé:** Given that DOC fluxes are
269 | almost directly proportional to river
270 | discharge in the Lena basin (Fig. 3), this
271 | sub-optimal performance with regard to
272 | hydrology during August to October
273 | seeming to be the main cause of a
274 | substantial underestimation in simulated
275 | bulk DOC outflow. Another cause may
276 | simply be the lack of peat representation in
277 | the model, for which DOC flux
278 | concentrations in outflowing fluvial water
279 | can be very high (e.g. Frey et al., 2005;
280 | 2009: see Section 4.5.1).
281 | Deficiencies in modelled hydrology
282 | hydrology correspond to those found in Fig.
283 | 12 of Guimbertea et al. (2018), indicating
284 | that the modifications made in this model
285 | version, which focus on the DOC cycle, have
286 | not further degraded the hydrological
287 | performance of the model, the causes of
288 | which are described below. Low simulated
289 | discharge for the Lena basin, particularly
290 | during the late summer and autumn, is
291 | consistent with prior, Pan-Arctic
292 | simulations conducted by Guimbertea et
293 | al. (2018), who ran ORCHIDEE-MICT using
294 | both the GSWP3 and CRU-NCEP v7 datasets
295 | and evaluated them over the period 1981-
296 | 2007. Despite the substantially better
297 | hydrological performance of ORCHIDEE
298 | under GSWP3 climate, they described a
299 | near-systematic underestimation of ... [3]

300 Simon Bowring 8/10/y 15:05

301 | **Supprimé:** it seems that
302

303 Simon Bowring 8/10/y 14:53

304 | **Supprimé:** Deficiencies in modelled
305 | hydrology correspond to those found in Fig.
306 | 12 of Guimbertea et al. (2018), indicating
307 | that the modifications made in this model
308 | version, which focus on the DOC cycle, have
309 | not further degraded the hydrological
310 | performance of the model, the causes of
311 | which are described below. Low simulated
312 | discharge for the Lena basin, particul ... [4]

244 4.2.1 Model Evaluation: River Discharge

245 | Simulated river water discharge captures the key feature of Arctic river discharge – that
246 | of a massive increase in flow to ~80,000 m³s⁻¹ in April-June caused by melting snow and
247 | ice, but underestimates observed river discharge in late summer by around 70% (Figs.
248 | 3c, 4b). In addition, the mean spring (June) discharge peak flows are slightly
249 | underestimated or out of phase in simulations (Figs. 3c, 4b) compared to observations
250 | (Ye et al., 2009): this is caused by a large amount of water throughput being simulated in
251 | May (~10,000 m³ s⁻¹) in excess of observed rates. Finally, during the winter low-flow
252 | period, the model consistently under-estimates water flow-through volumes reaching
253 | the river main stem (see Fig. 3c, winter months). Although this underestimate is not
254 | severe relative to annual bulk flows, the divergence is large as a percentage of
255 | observations (see right-hand axis, Fig. 3c), and may point to an issue in how ice is
256 | represented in the model, such as the fact that solid ice inclusions in the soil column are
257 | not represented, or the possibility that much slower groundwater dynamics than those
258 | represented in the model are feeding discharge. In addition to this, the presence of a
259 | dam on the Vilui tributary of the Lena has been shown to reduce main stem winter low-
260 | flow rates by up to 90% (Ye et al., 2003), similar to the discrepancy of our low-flow
261 | rates: given that our model only simulates 'natural' hydrological flows and thus does not
262 | include dams, we expect that this effect is also at play. Causal factors for the apparently
263 | poor performance of the hydrological module range from poor model representations
264 | (or lack thereof), climatological dataset choices and deficiencies in evaluation datasets
265 | themselves, and are covered in detail in the Supplement (Text S2).
266

267 4.2.2 Model Evaluation: DOC Annual Discharge

268 | Our CTRL simulation shows that the yearly sum of DOC output to the Arctic Ocean has
269 | increased steadily over course of the 20th Century, from ~1.4Tg DOC-C yr⁻¹ in 1901 to
270 | ~4Tg DOC-C yr⁻¹ in 2007 (Fig. 4a). Smoothing the DOC discharge over a 30-year
271 |

430 running mean shows that the increasing trend (Fig. 4a) over this averaging scale is
431 almost linear, at ~ 0.11 TgC per decade, or a net increase of 40% using this averaging
432 scale. Empirically based estimates of total contemporary DOC entering the Laptev Sea
433 from Lena river discharge vary around $\sim 2.5\text{--}5.8$ TgC-DOC (Cauwet and Sidorov, 1996;
434 Dolman et al., 2012; Holmes et al., 2012; Lara et al., 1998; Raymond et al., 2007;
435 Semiletov et al., 2011).

436 Note however that modelled aggregate DOC discharge is strongly affected by the
437 underestimation of river water discharge. Fig. 4a shows the average simulated DOC
438 discharge (red bar) of the last decade (1998–2007) of 3.2 TgC yr^{-1} , to be compared with
439 estimates of 3.6 TgC yr^{-1} (black bar) from Lara et al. (1998) and 5.8 TgC yr^{-1} (orange bar)
440 from Raymond et al. (2007) and 5.7 TgC yr^{-1} from Holmes et al. (2012). The most recent
441 and elaborate of those estimates is that of Holmes et al. (2012) who used a rating curve
442 approach based on 17 samples collected from 2003 to 2006 and covering the full
443 seasonal cycle, which was then applied to 10 years of daily discharge data (1999–2008)
444 for extrapolation. Given that their estimate is also based on Arctic-GRO-1/PARTNERS
445 data (<https://www.arcticgreatrivers.org/data>), which stands as the highest temporal
446 resolution dataset to date, their estimate is likely the most accurate of the DOC discharge
447 estimates. Compared to their average annual estimate of 5.7 TgC yr^{-1} , our simulated
448 DOC export is low by around 43%, [due largely to the poor performance of the hydrology
449 module, The DOC discharge underestimate is discussed in depth in Supplement \(Text
450 S2\).](#)

451 4.3 Model Evaluation: DOC Concentrations in lateral transport

452 While total DOC discharge captures the integral of biogeochemical processes leading the
453 fluvial outflow, simulations of this are highly sensitive to the performance of modelled
454 hydrology and climatological input data. A more precise measure for the performance
455 of the newly-introduced DOC production and transport module, which is less sensitive
456 to reproduction of river water discharge, is DOC concentration. This is because while
457 the total amount of DOC entering river water depends on the amount of water available
458 as a vehicle for this flux (hydrology), the concentration of DOC depends on the rate of
459 soil carbon leaching, itself depending largely on the interaction of soil biogeochemistry
460 with primary production and climatic factors. This we evaluate in Figure 5a, This shows
461 that for the majority of the thaw period or growing season (April–September), which
462 corresponds to the period during which over 90% of DOC production and transport
463 occurs, the model largely tracks the observed seasonality of DOC concentrations in
464 Arctic-GRO data averaged over 1999–2007. There is a large overestimate of the DOC
465 concentration in May owing to inaccuracies in simulating the onset of the thaw period,
466 while the months June–September underestimate concentrations by an average of 18%.
467 On the other hand, frozen period (November–April) DOC concentrations are
468 underestimated by between $\sim 30\text{--}50\%$. This is due to deficiencies in representing
469 wintertime soil hydrological water flow in the model, which impedes water flow when
470 the soil is frozen, as discussed in Section [S2](#). Because of this deficiency, slow-moving
471 groundwater flows that contain large amounts of DOC leachate are under-represented.
472 This interpretation is supported by the fact that in both observations and simulations, at
473 low discharge rates (corresponding to wintertime), DOC concentrations exhibit a strong
474 positive correlation with river discharge, while this relationship becomes insignificant at
475

Simon Bowring 8/10/y 15:01

Supprimé: whose causes are discussed
below

Simon Bowring 8/10/y 15:00

Supprimé: [... \[5\]](#)

Simon Bowring 8/10/y 15:11

Mis en forme: Ne pas ajuster l'espace
entre le texte latin et asiatique, Ne pas
ajuster l'espace entre le texte et les
nombres asiatiques

Simon Bowring 8/10/y 15:18

Supprimé: 4.2.1

484 higher levels of river discharge (Fig. 5b). Thus wintertime DOC concentrations suffer
485 from the same deficiencies in model representation as those for water discharge. In
486 other words, the standalone representation of DOC leaching is satisfactory, while when
487 it is sensitive to river discharge, it suffers from the same shortfalls identified in Sections
488 [S2](#) and [S3](#), [Modelled DOC concentrations in stream, river and ground water are](#)
489 [evaluated against data and discussed in the Supplement \(Text S5\)](#).
490

491 **4.4 In-Stream CO₂ Production, Transport, Evasion**

492

493 In our model, the fate of DOC once it enters the fluvial system is either to remain as DOC
494 and be exported to the ocean, or to be degraded to dissolved CO₂ (CO_{2(aq)}), which is
495 itself either also transported to the marine system or outgassed from the fluvial surface
496 to the atmosphere (see Part 1, Section 2.10 and [Text S6](#)). As noted in Part 1 of this study,
497 although the model as a whole conducts simulations at the 1 degree scale, the routing of
498 water and carbon, as well as the evasion of the latter, occurs at the sub-grid scale, such
499 that we are able to simulate spatially explicit rivers whose size approximates Strahler
500 order 4, and through the 'fast' water pool in the model are able to simulate streams of
501 Strahler order 1-3. The seasonality of riverine dissolved CO₂ concentrations (CO_{2(aq)},
502 mgC L⁻¹) is evaluated in [Fig. 4c](#) to compare CO_{2(aq)} concentrations with DOC bulk flows,
503 since CO_{2(aq)} concentrations follow an inverse seasonal pattern to those of DOC, being
504 highest during the winter baseflow period and lowest in summer due to dilution during
505 its high discharge phase (Semiletov et al., 2011). The simulated flow of CO_{2(aq)} at Kusur
506 ([Fig. 4c](#), dashed red) reproduces the seasonality of observations from Cauwet and
507 Sidorov (1996), who sampled the Lower Lena ([Fig. 3a](#)), but somewhat underestimates
508 concentrations. Also included in [Fig. 4c](#) is the basin average for all non-zero values,
509 whose shape also tracks that of observations. Thus the model represents on the one
510 hand increasing hydrological flow mobilising increasing quantities and concentrations
511 of DOC while on the other hand those same increasing hydrological flows increasing the
512 flux, but decreasing the concentration, of CO_{2(aq)} throughput.
513

514 [Evaluation of modelled CO₂ evasion is beset by problems, not least that no data on this](#)
515 [quantity have to our knowledge been recorded for the Lena \(see Text S6\)](#). [Figure 6](#)
516 summarises some of the results from the simulated water body CO₂ outgassing flux.
517 Year-on-year variation in basin-wide evasion from river, stream and floodplain sources
518 combined exhibits a marked increasing trend over the course of the 20th Century,
519 increasing from a minimum of ~1.6 TgCO₂-C yr⁻¹ in 1901 to a maximum of ~4.4 TgCO₂-C
520 yr⁻¹ in 2007 (+300%, [Fig. 7a](#)). Smoothing the data over a 30 year running average yields
521 a damped net increase in basin-wide evasion of ~30% ([Fig. 7a](#)). Thus yearly evasion
522 flux is some 105% of yearly DOC discharge to the coast from the Lena basin and 51% of
523 C exported from soils to headwaters as CO₂ or DOC. If we compare the mean yearly rate
524 of increase in absolute (TgC yr⁻¹) CO₂ evasion and DOC discharge based on linear
525 regression over the whole simulation period, it appears that the rate of increase of both
526 fluxes has been strikingly similar over the simulated 20th Century, with mean increases
527 of 11.1 GgC yr⁻¹ and 11.5 GgC yr⁻¹ per year for evasion and export, respectively. [A](#)
528 [summary and evaluation of the source and seasonal heterogeneity of evasion is](#)
529 [discussed in the Text S7](#).

530
531 As previously discussed, the proportion of total basin-wide CO₂ evasion attributable to
532

Simon Bowring 8/10/y 15:18
Supprimé:
Simon Bowring 8/10/y 15:18
Supprimé: 4.2.1 and 4.2.2
Simon Bowring 8/10/y 15:16
Supprimé: ... [6]
Simon Bowring 8/10/y 15:20
Supprimé: The latter two outcomes also apply to CO _{2(aq)} produced in the soil by organic matter degradation and subsequently transported by runoff and drainage flows to the water column. As shown in Fig. 2 , a large proportion of DOC (38%, 2.1 TgC yr ⁻¹) that enters the water column is degraded to CO _{2(aq)} during transport, which adds to the 1.65 TgC yr ⁻¹ of direct CO _{2(aq)} input from the terrestrial land surface. Of this bulk CO ₂ exported into and generated within the water column, 3.6 TgC yr ⁻¹ evades from the water surface to the atmosphere before reaching the river delta. In what follows, we evaluate first inputs of CO _{2(aq)} to the water column in terms of their seasonality, before evaluating CO ₂ evasion rates and the relation of this to smaller and larger water bodies (river versus stream).
Simon Bowring 8/10/y 15:22
Supprimé: ... [7]
Simon Bowring 9/10/y 08:58
Supprimé: d
Simon Bowring 9/10/y 08:58
Supprimé: d
Simon Bowring 9/10/y 08:58
Supprimé: d
Simon Bowring 9/10/y 08:58
Supprimé: d
Simon Bowring 10/10/y 11:06
Mis en forme: Indice
Simon Bowring 8/10/y 15:24
Supprimé: To our knowledge, no direct measurements for CO ₂ evasion from the surface of the Lena river are available in the literature. We refer to Denfeld et al. (2013) for evaluating our evasion flux results, since their basin of study, the Kolyma River, is the most geographically proximate existing dataset to the Lena, despite biogeographical differences between the two basins – namely that the Kolyma is almost entirely underlain by continuous permafrost. ... [8]
Simon Bowring 9/10/y 09:00
Supprimé: 7
Simon Bowring 10/10/y 11:08
Supprimé:) (
Simon Bowring 9/10/y 09:05
Supprimé:
Simon Bowring 10/10/y 11:08
Supprimé: .
Simon Bowring 8/10/y 15:27
Supprimé: The heterogeneity of CO ₂ evasion from different sources in the ... [9]

headwater streams and rivers is substantially greater than their proportion of total basin surface area. Figure 6b represents the mean monthly fractional contribution of each surface hydrological water pool to the total evasion flux (unitless) over the period 1998-2007. This shows that over the entirety of the thaw period, the stream water pool takes over from the river water pool as the dominant evasion source, particularly at the height of the freshet period, where its fractional contribution rises to >75%. The stream fraction of August outgassing is ~57% of the annual total, which is higher than the ~40% found for streams in Denfeld et al. (2013). However, the values between the two studies are not directly comparable, different basins notwithstanding, due to differences between how 'streams' are defined in the model and in the field (expanded on in Text S8). Also shown in Fig. 6b is the gradual onset of evasion from the floodplain reservoir in April, as the meltwater driven surge in river outflow leads to soil inundation and the gradual increase of proportional evasion from these flooded areas over the course of the summer, with peaks in June-August as water temperatures over these flooded areas likewise peak. We stress the importance of these simulation results as they concur with large numbers of observational studies (cited above) which show smaller headwater streams' disproportionately large contribution to total outgassing (Fig. 7c), this being due to their comparatively high outgassing rates (Fig. 7e). In addition, the contribution of floodplains to evasion, an otherwise rarely studied feature of high latitude biomes, is shown here to be significant. A Hovmöller plot (Fig. 7d) of the monthly longitude-averaged stream reservoir fraction of total evasion, allows us to infer that: (i) The dominance of stream evasion begins in the most southern upstream headwaters in the lower latitude thaw period (April-May), and trickles northward over the course of the next two months, following the riverflow. (ii) The intensity of this evasion is greatest in the lower latitude regions of the basin, which we speculate is the result of higher temperatures causing a greater proliferation of small thaw water-driven flows and evasion. (iii) Areas where the stream fraction is not dominant or only briefly dominant during the summer (58-60°N, 63-64°N, 70-71°N) are all areas where floodplain CO₂ evasion plays a prominent role at that latitudinal band.

We evaluate the approximate rate of modelled areal CO₂ efflux from the water surface against observations from Denfeld et al. (2013). (The 'approximate' caveat is treated in the Supplementary Text S9). The comparison of simulated results with those from Denfeld et al. (2013) are displayed in Fig. 6d, which shows boxplots for simulated CO₂ evasion from the stream water reservoir and river water reservoir averaged over 1998-2007. The empirical (Kolyma river) analogue of this data, from which this plot is inspired (Fig. 4d in Denfeld et al., 2013), is shown in inset. Median efflux was 1.1 (6) versus 0.4 (0.8) for stream and river, respectively, in simulations (observations). Like the observations, simulated stream efflux had a substantially greater interquartile range, mean (24.6) and standard deviation (73) than total river efflux (1.3 and 7.2, respectively).

4.5. Emergent Phenomena: DOC and topographic slope, MAAT

Subsurface water infiltration fluxes and transformations of dissolved matter represent an important, if poorly understood and observationally under-represented biogeochemical pathway of DOC export to river main stems, involving the complex interplay of slope, parent material, temperature, permafrost material age and soil physical-chemical processes, such as adsorption and priming. In the Lena basin, as in

Simon Bowring 9/10/y 09:00
Supprimé: 7
Simon Bowring 9/10/y 09:05
Supprimé: c
Simon Bowring 8/10/y 15:32
Supprimé: .
Simon Bowring 8/10/y 15:31
Supprimé: the
Simon Bowring 8/10/y 15:31
Supprimé: study
Simon Bowring 8/10/y 15:34
Supprimé: This is because in ORCHIDEE MICT-L, the 'stream' water reservoir is water routed to the river network for all hydrologic flows calculated to not cross a 0.5 degree grid cell boundary (the resolution of the routing module, explained in Part 1, Section 2.6), which may not be commensurate with long, <20m width streams in the real-world, that were used in the Denfeld et al. (2013) study. In addition, this 'stream' water reservoir in the model does not include any values for width or area in the model, so we cannot directly compare our stream reservoir to the <20m width criterion employed by Denfeld et al. (2013) in their definition of an observed stream. Thus our 'stream' water reservoir encompasses substantially greater s ... [10]
Simon Bowring 9/10/y 09:00
Supprimé: 7
Simon Bowring 9/10/y 09:02
Supprimé: c
Simon Bowring 8/10/y 15:46
Supprimé: [11]
Simon Bowring 8/10/y 15:45
Supprimé: .
Simon Bowring 8/10/y 15:45
Supprimé: .
Simon Bowring 8/10/y 15:45
Supprimé: .
Simon Bowring 8/10/y 15:43
Supprimé: T
Simon Bowring 8/10/y 15:42
Supprimé: refers to the fact that m ... [12]
Simon Bowring 9/10/y 09:00
Supprimé: 7
Simon Bowring 9/10/y 09:03
Supprimé: e
Simon Bowring 8/10/y 16:21
Supprimé: in the figure, with whis ... [13]
Simon Bowring 8/10/y 15:44
Supprimé: Note that from ~700 n ... [14]
Simon Bowring 8/10/y 16:16
Supprimé: [15]
Simon Bowring 8/10/y 15:55
Supprimé: 2

821 other permafrost catchments, topographic slope has been shown to be a powerful
822 predictor for water infiltration depth, and concentration and age of DOC (Jasechko et al.,
823 2016; Kutscher et al., 2017; McGuire et al., 2005), with deeper flow paths and older,
824 lower DOC-concentrated waters found as the topographic slope increases. This
825 relationship was shown in Fig. 4 of Kutscher et al. (2017) who surveyed DOC
826 concentrations across a broad range of slope angle values in the Lena basin and found a
827 distinct negative relationship between the two. Comparing the Kutscher et al. (2017)
828 values with our model output, by plotting stream and river DOC concentrations
829 averaged per gridpoint over 1998–2007 against the topographic map used in the routing
830 scheme (Fig. 8) we find a similar negative relationship between the two variables. The
831 causes of this relationship and a discussion of the model's ability to represent it are
832 discussed in Supplementary Text S10. A positive, non-linear relationship between DOC
833 and mean annual air temperature (MAAT), discussed in prior empirical studies, is also
834 reproduced by the model (Fig. 7) and discussed in the Supplement Text S11.

Simon Bowring 9/10/y 09:08

Supprimé: 10

4.6 DOC Reactivity Pools

336 Here we examine the reactivity of DOC leached from the soil and litter to different
337 hydrological export pools. Surface runoff DOC export is dominated by refractory carbon
338 (Fig. 9), with export rates largely following discharge rates as they drain the basin with
339 an increasing delay when latitude increases. As the thaw period gets underway (April),
340 the fraction of labile carbon in surface runoff DOC increases substantially from south to
341 north, reflecting the hydrologic uptake of the previous year's un-decomposed high-
342 reactivity organic matter.

Simon Bowring 8/10/y 15:57

Supprimé: ... [16]

343 Refractory C-dominated drainage DOC export (Fig. 9) is highest in June through
344 October, with refractory export rate intensities per latitudinal band during this period
345 consistent with the fraction of inundated area (Fig. S1b) over these bands during the
346 year. The high refractory proportion of drainage flow is expected, as drainage leaches
347 older, relict soil and litter matter. Because of its longer residence time within the soil
348 column, labile DOC carried downward via soil infiltration will tend to be metabolised in
349 situ before it can be exported to the hydrological network, further increasing the
350 proportion of refractory carbon. By contrast floodplain DOC export (Fig. 9) is composed
351 of more nuanced mix of both reactivity classes, reflecting its relatively greater
352 dependence on the current year's 'fresh' biomass as source material (62% labile DOC
353 versus 38% refractory DOC, year-averaged) for carbon leaching.

Simon Bowring 9/10/y 09:09

Supprimé: 11a

354 For both the river and stream pool, mean DOC concentrations are dominated by
355 refractory carbon sources. When averaged over the year, the dominance of the
356 refractory DOC carbon pool over its labile counterpart is also evident for all DOC inputs
357 to the hydrological routing except for floodplain inputs, as well as within the 'flowing'
358 stream and river pools themselves. This is shown in Table 2, where the year-averaged
359 percentage of each carbon component of the total input or reservoir is subdivided
360 between the 'North' and 'South' of the basin, these splits being arbitrarily imposed as the
361 latitudinal mid-point of the basin itself (63N). This reinforces the generalised finding
362 from our simulations that refractory carbon dominates runoff and drainage inflows to
363 rivers (89% refractory, on average), while floodplains export mostly labile DOC to the
364 basin (64%), these values being effectively independent of this latitudinal sub-division
365 (Table 2). Nonetheless, there is a small consistent difference between North and South

Simon Bowring 9/10/y 09:09

Supprimé: 11a

876 in stream and river water DOC makeup, in that the labile portion decreases between
877 North and South ; this may be an attenuated reflection of the portion of labile DOC that is
878 decomposed to CO_2 within the water column during its transport northward, affecting
879 the bulk average proportions contained within the water in each 'hemisphere'.
880

881 5 Discussion

882

883 5.1 Land-Ocean Aquatic Continuum (LOAC)

884 5.1.1 LOAC Fluxes

885

886 Overall, our simulation results show that dissolved carbon entering the Lena river
887 system is significantly transformed during its transport to the ocean. Taking the average
888 throughput of carbon into the system over the last ten years of our simulation, our
889 results show that whereas 7 TgC yr^{-1} (after reinfiltration following flooding of 0.45 TgC
890 yr^{-1} ; see Fig. 2 'Return' flux) of carbon enters the Lena from terrestrial sources as
891 dissolved carbon and CO_2 , only 3.4 TgC yr^{-1} is discharged into the Laptev Sea and beyond
892 from the river mouth. The remainder (3.6 TgC yr^{-1}) is metabolised in the water column
893 during transport and evaded to the atmosphere (bottom panel, Fig. 10). The terrestrial
894 DOC inflow estimate is comparable to that made by Kicklighter et al. (2013), who
895 estimated in a modelling study terrestrial dissolved carbon loading of the Lena is ~ 7.7
896 TgC yr^{-1} .
897

Simon Bowring 9/10/y 09:10

Supprimé: 2a

898 The relative quantities of carbon inflow, evasion and outflow in the river system that are
899 presented for the Lena in Fig. 10 can be compared to the same relative quantities –that
900 is, the ratios of evasion:in and out:in, where 'in' refers to dissolved terrestrial input, –
901 from the global study by Cole et al. (2007), who estimated these fluxes from empirical or
902 empirically-derived data at the global scale. This is shown in the top panel of Fig. 10,
903 where we simplify the Cole et al. (2007) data to exclude global groundwater CO_2 flux
904 from the coast to the ocean (because our basin mask has a single coastal pixel whereas
905 coastal groundwater seepage is distributed along the entire continental boundary) and
906 the POC fraction of in-river transport and sedimentation (since ORCHIDEE MICT lacks a
907 POC erosion/sedimentation module) from their budget.
908

Simon Bowring 9/10/y 09:10

Supprimé: 2a

Simon Bowring 9/10/y 09:10

Supprimé: 2a

909 This gives global terrestrial dissolved carbon input of 1.45 PgC yr^{-1} , 0.7 PgC of which is
910 discharged to the ocean, and the other 0.75 PgC evaded to the atmosphere. Taking the
911 previously mentioned [evasion:in] and [out:in] ratios as a percentage, the outflow and
912 evasion fluxes for the Lena versus the global aggregate are remarkably similar, at 48.6
913 vs. 48.3% and 51.4 vs 51.7%, for the two respective flows. Thus our results agree with
914 the proposition that the riverine portion of the 'land-ocean aquatic continuum' (Regnier
915 et al., 2013) or 'boundless carbon cycle' (Battin et al., 2009) is indeed a substantial
916 reactor for matter transported along it. The drivers of changes in CO_2 and DOC export
917 from the soil over the simulation period (temperature and precipitation versus CO_2),
918 which we extract from our constant climate and CO_2 factorial simulations discussed in
919 the Simulation Setup, are similar, if somewhat dominated by temperature (Text S12).
920

Simon Bowring 8/10/y 16:24

Mis en forme: Indice

Simon Bowring 8/10/y 16:24

Mis en forme: Indice

Simon Bowring 8/10/y 16:25

Mis en forme: Indice

Simon Bowring 8/10/y 16:22

Supprimé: ... [17]

Simon Bowring 8/10/y 16:22

Supprimé: 3

Simon Bowring 9/10/y 09:10

Supprimé: 2a

921 5.1.2 LOAC export flux considerations

922

923 Despite our simulations' agreement with observations regarding the proportional fate of
924 terrestrial DOC inputs as evasion and marine export (Fig. 10), our results suggest

932 substantial and meaningful differences in the magnitude of those fluxes relative to NPP
933 in the Lena, compared to those estimated by other studies in temperate or tropical
934 biomes. Our simulations' cumulative DOC and CO₂ export from the terrestrial realm into
935 inland waters is equivalent to ~1.5 % of NPP.

936
937 This is considerably lower than Cole et al. (2007) and Regnier et al. (2013) who find
938 lateral transfer to approximate ~5% (1.9PgC yr⁻¹) of NPP at the global scale, while
939 Lauerwald et al. (2017) found similar rates for the Amazon. The cause of this
940 discrepancy with our results is beyond the scope of this study to definitively address,
941 given the lack of tracers for carbon source and age in our model. Nonetheless, our
942 analysis leads us to hypothesise the following.
943

944 Temperature limitation of soil microbial respiration at the end of the growing season
945 (approaching zero by October, SI Fig. S4d) makes this flux negligible from November
946 through May (SI Fig. S4d). In late spring, mobilisation of organic carbon is performed by
947 both microbial respiration and leaching of DOC via runoff and drainage water fluxes.
948 However, because the latter are controlled by the initial spring meltwater flux period,
949 which occurs before the growing season has had time to produce litter or new soil
950 carbon (May-June, Fig. 4b), aggregate yearly DOC transport reactivity is characterised by
951 the available plant matter from the previous year, which is overwhelmingly derived
952 from recalcitrant soil matter (Fig. 9) and is itself less available for leaching based on soil
953 carbon residence times.
954

955 This causes relatively low leaching rates and riverine DOC concentrations (e.g. Fig. 7), as
956 compared to the case of leaching from the same year's biological production.
957 Highlighting this point is floodplain domination by labile carbon sourced from that
958 year's production with a mean DOC concentration of 12.4 mgC L⁻¹ (1998-2007 average),
959 with mean riverine DOC concentrations around half that value (6.9 mgC L⁻¹).
960 Nonetheless the May-June meltwater pulse period dominates aggregate DOC discharge.
961 As this pulse rapidly subsides by late July, so does the leaching and transport of organic
962 matter. Warmer temperatures come in conjunction with increased primary production
963 and the temperature driven soil heterotrophic degradation of contemporary and older
964 matter (via active layer deepening). These all indicate that transported dissolved matter
965 in rivers, at least at peak outflow, is dominated by sources originating in the previous
966 year's primary production, that was literally 'frozen out' of more complete
967 decomposition by soil heterotrophs.
968

969 Further, we infer from the fact that all of our simulation grid cells fall within areas of low
970 (<-2°C) MAAT, far below the threshold MAAT (>3°C) proposed by Laudon et al. (2012)
971 for soil respiration-dominated carbon cycling systems (Fig. 7), that the Lena is
972 hydrologically-limited with respect to DOC concentration and its lateral flux. Indeed, the
973 seasonal discharge trend of the Lena –massive snowmelt-driven hydrological and
974 absolute DOC flux, coupled with relatively low DOC concentrations at the river mouth
975 (Fig. 4b, simulation data of Fig. 7), are in line with the Laudon et al. (2012) typology.

976
977 We therefore suggest that relatively low lateral transport relative to primary production
978 rates (e.g. as a percentage of net primary production, (%NPP)) in our simulations
979 compared to the lateral transport : NPP percentages reported from the literature in
980 other biomes is driven by meltwater (vs. precipitation) dominated DOC mobilisation,

Simon Bowring 9/10/y 09:50

Supprimé: 5

Simon Bowring 9/10/y 09:50

Supprimé: 5

Simon Bowring 9/10/y 09:09

Supprimé: 11a

Simon Bowring 9/10/y 09:07

Supprimé: 9

Simon Bowring 9/10/y 09:07

Supprimé: 9

Simon Bowring 9/10/y 09:07

Supprimé: 9

987 which occurs during a largely pre-litter deposition period of the growing season. DOC is
988 then less readily mobilised by being sourced from recalcitrant matter, leading to low
989 leaching concentrations relative to those from labile material. As discharge rates
990 decline, the growing season reaches its peak, leaving carbon mobilisation of fresh
991 organic matter to be overwhelmingly driven by in situ heterotrophic respiration.
992

993 While we have shown that bulk DOC fluxes scale linearly to bulk discharge flows (Fig.
994 3d), DOC concentrations (mgC L^{-1}) hold a more complex and weaker positive
995 relationship with discharge rates, with correlation coefficients (R^2) of 0.05 and 0.25 for
996 river and stream DOC concentrations, respectively (Fig. 13). This implies that while
997 increasing discharge reflects increasing runoff and an increasing vector for DOC
998 leaching, particularly in smaller tributary streams, by the time this higher input of
999 carbon reaches the river main stem there is a confounding effect of dilution by increased
1000 water fluxes which reduces DOC concentrations, explaining the difference between
1001 stream and river discharge vs. DOC concentration regressions in the Figure. Thus, and
1002 as a broad generalisation, with increasing discharge rates we can also expect somewhat
1003 higher concentrations of terrestrial DOC input to streams and rivers. Over the
1004 floodplains, DOC concentrations hold no linear relationship with discharge rates
1005 ($R^2=0.003$, SI Fig. S11), largely reflecting the fact that DOC leaching is here limited by
1006 terrestrial primary production rates more than by hydrology. To the extent that
1007 floodplains fundamentally require flooding and hence do depend on floodwater inputs
1008 at a primary level, we hypothesise that DOC leaching rates are not limited by that water
1009 input, at least over the simulated Lena basin.
1010

1011 As discussed above simulated DOC and CO_2 export as a percentage of simulated NPP
1012 over the Lena basin was 1.5% over 1998-2007. However, this proportion appears to be
1013 highly dynamic at the decadal timescale. As shown in Fig. S12, all lateral flux
1014 components in our simulations increased their relative throughput at a rate double to
1015 triple that of NPP or respiration fluxes over the 20th century, also doing so at a rate
1016 substantially higher than the rate increase in discharge. In addition, differentials of
1017 these lateral flux rates with the rates of their drivers (discharge, primary production)
1018 have on average increased over the century (Fig. S12). This suggests that there are
1019 potential additive effects of the production and discharge drivers of lateral fluxes that
1020 could lead to non-linear responses to changes in these drivers as the Arctic environment
1021 transforms, as suggested by the Laudon et al. (2012) data plotted in Fig. 4. Acceleration
1022 of the hydrological cycle compounded by temperature and CO_2 -driven increases in
1023 primary production could therefore increase the amount of matter available for
1024 leaching, increase the carbon concentration of leachate, and increase the aggregate
1025 generation of runoff to be used as a DOC transport vector. Given that these causal
1026 dynamics apply generally to permafrost regions, both low lateral flux as %NPP and the
1027 hypothesised response of those fluxes to future warming may be a feature particular to
1028 most high latitude river basins.
1029

1030 6. Conclusion

1031 This study has shown that the new DOC-representing high latitude model version of
1032 ORCHIDEE, ORCHIDEE MICT-LEAK, is able to reproduce with reasonable accuracy
1033 modern concentrations, rates and absolute fluxes of carbon in dissolved form, as well as
1034 the relative seasonality of these quantities through the year. When combined with a
1035

Simon Bowring 9/10/y 10:44
Supprimé: 6

Simon Bowring 9/10/y 10:45
Supprimé: 7

Simon Bowring 9/10/y 10:45
Supprimé: 7

1039 reasonable reproduction of real-world stream, river and floodplain dynamics, we
1040 demonstrate that this model is a potentially powerful new tool for diagnosing and
1041 reproducing past, present and potentially future states of the Arctic carbon cycle. Our
1042 simulations show that of the 34 TgC yr⁻¹ remaining after GPP is resired autotrophically
1043 and heterotrophically in the Lena basin, over one-fifth of this captured carbon is
1044 removed into the aquatic system. Of this, over half is released to the atmosphere from
1045 the river surface during its period of transport to the ocean, in agreement with previous
1046 empirically-derived global-scale studies. Both this transport and its transformation are
1047 therefore non-trivial components of the carbon system at these latitudes that we have
1048 shown are sensitive to changes in temperature, precipitation and atmospheric CO₂
1049 concentration. Our results, in combination with empirical data, further suggest that
1050 changes to these drivers –in particular climate –may provoke non-linear responses in
1051 the transport and transformation of carbon across the terrestrial-aquatic system's
1052 interface as change progresses in an Arctic environment increasingly characterised by
1053 amplified warming.

1054

1055 **Code and data availability**

1056 The source code for ORCHIDEE MICT-LEAK revision 5459 is available via
1057 <http://forge.ipsl.jussieu.fr/orchidee/wiki/GroupActivities/CodeAvalaibilityPublication/>
1058 ORCHIDEE_gmd-2018-MICT-LEAK_r5459

1059
1060 Primary data and scripts used in the analysis and other supplementary information that
1061 may be useful in reproducing the author's work can be obtained by contacting the
1062 corresponding author.

1063
1064 This software is governed by the CeCILL license under French law and abiding by the
1065 rules of distribution of free software. You can use, modify and/or redistribute the
1066 software under the terms of the CeCILL license as circulated by CEA, CNRS and INRIA at
1067 the following URL: <http://www.cecill.info>.

1068
1069

1070 **Authors' contribution**

1071 SB coded this model version, conducted the simulations and wrote the main body of the
1072 paper. RL gave consistent input to the coding process and made numerous code
1073 improvements and bug fixes. BG advised on the inclusion of priming processes in the
1074 model and advised on the study design and model configuration; DZ gave input on the
1075 modelled soil carbon processes and model configuration. PR contributed to the
1076 interpretation of results and made substantial contributions to the manuscript text. MG,
1077 AT and AD contributed to improvements in hydrological representation and floodplain
1078 forcing data. PC oversaw all developments leading to the publication of this study. All
1079 authors contributed to suggestions regarding the final content of the study.

1080

1081 **Competing interests**

1082 The authors declare no competing financial interests.

1083

1084 **Acknowledgements**

1085 Simon Bowring acknowledges funding from the European Union's Horizon 2020
1086 research and innovation program under the Marie Skłodowska-Curie grant agreement
1087 No. 643052, 'C-CASCADES' program. Simon Bowring received a PhD grant. Matthieu

1088 Guimberteau acknowledges funding from the European Research Council Synergy grant
1089 ERC-2013-SyG-610028 IMBALANCE-P. RL acknowledges funding from the European
1090 Union's Horizon 2020 research and innovation program under grant agreement
1091 no.703813 for the Marie Skłodowska-Curie European Individual Fellowship "C-Leak".
1092
1093

1094 **References:**

1095
1096 Battin, T. J., Luyssaert, S., Kaplan, L. A., Aufdenkampe, A. K., Richter, A. and Tranvik, L. J.:
1097 The boundless carbon cycle, *Nat. Geosci.*, doi:10.1038/ngeo618, 2009.
1098 Cauwet, G. and Sidorov, I.: The biogeochemistry of Lena River: Organic carbon and
1099 nutrients distribution, in *Marine Chemistry*, pp. 211–227, 1996.
1100 Cole, J. J., Prairie, Y. T., Caraco, N. F., McDowell, W. H., Tranvik, L. J., Striegl, R. G., Duarte,
1101 C. M., Kortelainen, P., Downing, J. A., Middelburg, J. J. and Melack, J.: Plumbing the global
1102 carbon cycle: Integrating inland waters into the terrestrial carbon budget, *Ecosystems*,
1103 doi:10.1007/s10021-006-9013-8, 2007.
1104 DeLuca, T. H. and Boisvenue, C.: Boreal forest soil carbon: Distribution, function and
1105 modelling, *Forestry*, 161–184, doi:10.1093/forestry/cps003, 2012.
1106 Dolman, A. J., Shvidenko, A., Schepaschenko, D., Ciais, P., Tchekabakova, N., Chen, T., Van
1107 Der Molen, M. K., Belelli Marchesini, L., Maximov, T. C., Maksyutov, S. and Schulze, E. D.:
1108 An estimate of the terrestrial carbon budget of Russia using inventory-based, eddy
1109 covariance and inversion methods, *Biogeosciences*, doi:10.5194/bg-9-5323-2012, 2012.
1110 Guimberteau, M., Zhu, D., Maignan, F., Huang, Y., Yue, C., Dantec-N d lec, S., Ottl, C., Jornet-
1111 Puig, A., Bastos, A., Laurent, P., Goll, D., Bowring, S., Chang, J., Guenet, B., Tifafi, M., Peng,
1112 S., Krinner, G., Ducharme, A. s., Wang, F., Wang, T., Wang, X., Wang, Y., Yin, Z., Lauerwald,
1113 R., Joetzjer, E., Qiu, C., Kim, H. and Ciais, P.: ORCHIDEE-MICT (v8.4.1), a land surface
1114 model for the high latitudes: model description and validation, *Geosci. Model Dev.*,
1115 11(1), 121–163, doi:10.5194/gmd-11-121-2018, 2018.
1116 Holmes, R. M., McClelland, J. W., Peterson, B. J., Tank, S. E., Bulygina, E., Eglington, T. I.,
1117 Gordeev, V. V., Gurtovaya, T. Y., Raymond, P. A., Repeta, D. J., Staples, R., Striegl, R. G.,
1118 Zhulidov, A. V. and Zimov, S. A.: Seasonal and Annual Fluxes of Nutrients and Organic
1119 Matter from Large Rivers to the Arctic Ocean and Surrounding Seas, *Estuaries and*
1120 *Coasts*, 35(2), 369–382, doi:10.1007/s12237-011-9386-6, 2012.
1121 Jasechko, S., Kirchner, J. W., Welker, J. M. and McDonnell, J. J.: Substantial proportion of
1122 global streamflow less than three months old, *Nat. Geosci.*, 9(2), 126,
1123 doi:10.1038/ngeo2636, 2016.
1124 Kalnay, E., Kanamitsu, M., Kistler, R., Collins, W., Deaven, D., Gandin, L., Iredell, M., Saha,
1125 S., White, G., Woollen, J., Zhu, Y., Chelliah, M., Ebisuzaki, W., Higgins, W., Janowiak, J., Mo,
1126 K. C., Ropelewski, C., Wang, J., Leetmaa, A., Reynolds, R., Jenne, R. and Joseph, D.: The
1127 NCEP/NCAR 40-year reanalysis project, *Bull. Am. Meteorol. Soc.*, doi:10.1175/1520-
1128 0477(1996)077<0437:TNYRP>2.0.CO;2, 1996.
1129 Kicklighter, D. W., Hayes, D. J., McClelland, J. W., Peterson, B. J., McGuire, A. D. and Melillo,
1130 J. M.: Insights and issues with simulating terrestrial DOC loading of Arctic river
1131 networks, *Ecol. Appl.*, 23(8), 1817–1836, doi:10.1890/11-1050.1, 2013.
1132 Kutscher, L., Mörth, C. M., Porcelli, D., Hirst, C., Maximov, T. C., Petrov, R. E. and
1133 Andersson, P. S.: Spatial variation in concentration and sources of organic carbon in the
1134 Lena River, Siberia, *J. Geophys. Res. Biogeosciences*, 122(8), 1999–2016,
1135 doi:10.1002/2017JG003858, 2017.
1136 Lara, R. J., Rachold, V., Kattner, G., Hubberten, H. W., Guggenberger, G., Skoog, A. and

1137 Thomas, D. N.: Dissolved organic matter and nutrients in the Lena River, Siberian Arctic:
 1138 Characteristics and distribution, Mar. Chem., doi:10.1016/S0304-4203(97)00076-5,
 1139 1998.
 1140 Lauerwald, R., Regnier, P., Camino-Serrano, M., Guenet, B., Guimberteau, M., Ducharne,
 1141 A., Polcher, J. and Ciais, P.: ORCHILEAK (revision 3875): A new model branch to simulate
 1142 carbon transfers along the terrestrial-aquatic continuum of the Amazon basin, Geosci.
 1143 Model Dev., 10, 3821–3859, doi:10.5194/gmd-10-3821-2017, 2017.
 1144 McGuire, K. J., McDonnell, J. J., Weiler, M., Kendall, C., McGlynn, B. L., Welker, J. M. and
 1145 Seibert, J.: The role of topography on catchment-scale water residence time, Water
 1146 Resour. Res., doi:10.1029/2004WR003657, 2005.
 1147 New, M., Hulme, M. and Jones, P.: Representing twentieth-century space-time climate
 1148 variability. Part I: Development of a 1961–90 mean monthly terrestrial climatology, J.
 1149 Clim., 1999.
 1150 Raymond, P. A., McClelland, J. W., Holmes, R. M., Zhulidov, A. V., Mull, K., Peterson, B. J.,
 1151 Striegl, R. G., Aiken, G. R. and Gurtovaya, T. Y.: Flux and age of dissolved organic carbon
 1152 exported to the Arctic Ocean: A carbon isotopic study of the five largest arctic rivers,
 1153 Global Biogeochem. Cycles, 21(4), doi:10.1029/2007GB002934, 2007.
 1154 Regnier, P., Friedlingstein, P., Ciais, P., Mackenzie, F. T., Gruber, N., Janssens, I. A.,
 1155 Laruelle, G. G., Lauerwald, R., Luyssaert, S., Andersson, A. J., Arndt, S., Arnosti, C., Borges,
 1156 A. V., Dale, A. W., Gallego-Sala, A., Goddérus, Y., Goossens, N., Hartmann, J., Heinze, C.,
 1157 Ilyina, T., Joos, F., Larowe, D. E., Leifeld, J., Meysman, F. J. R., Munhoven, G., Raymond, P.
 1158 A., Spahni, R., Suntharalingam, P. and Thullner, M.: Anthropogenic perturbation of the
 1159 carbon fluxes from land to ocean, Nat. Geosci., doi:10.1038/ngeo1830, 2013.
 1160 Semiletov, I. P., Pipko, I. I., Shakhova, N. E., Dudarev, O. V., Pugach, S. P., Charkin, A. N.,
 1161 Mcroy, C. P., Kosmach, D. and Gustafsson, Ö.: Carbon transport by the Lena River from its
 1162 headwaters to the Arctic Ocean, with emphasis on fluvial input of terrestrial particulate
 1163 organic carbon vs. carbon transport by coastal erosion, Biogeosciences, doi:10.5194/bg-
 1164 8-2407-2011, 2011.
 1165 Tootchi, A., Jost, A. and Ducharne, A.: Multi-source global wetland maps combining
 1166 surface water imagery and groundwater constraints, Earth Syst. Sci. Data, 11, 189–220,
 1167 doi:10.5194/essd-11-189-2019, 2019.
 1168 Ye, B., Yang, D., Zhang, Z. and Kane, D. L.: Variation of hydrological regime with
 1169 permafrost coverage over Lena Basin in Siberia, J. Geophys. Res. Atmos., 114, D7,
 1170 doi:10.1029/2008JD010537, 2009.
 1171
 1172
 1173
 1174
 1175

Tables and Figures:

Table 1: Summary describing of the factorial simulations undertaken to examine the relative drivers of lateral fluxes in our model.

Simulation Name	Abbreviation	Historical Input Data	Input* Held Constant
Control	CTRL	Climate, CO ₂ , Vegetation	None
Constant Climate	CLIM	CO ₂ , Vegetation	Climate
Constant CO ₂	CO ₂	Climate, Vegetation	CO ₂ (Pre-industrial)

*Historically-variable input

1181
1183
1184
1185
1186
1187

Table 2: Summary of the average carbon reactivity types comprising the hydrological inputs to rivers and streams (runoff, drainage and floodplain inputs), and within the rivers and streams themselves, subdivided between the 'North' and 'South' of the Lena basin (greater or less than 63N, respectively).

Simon Bowring 8/10/y 16:52

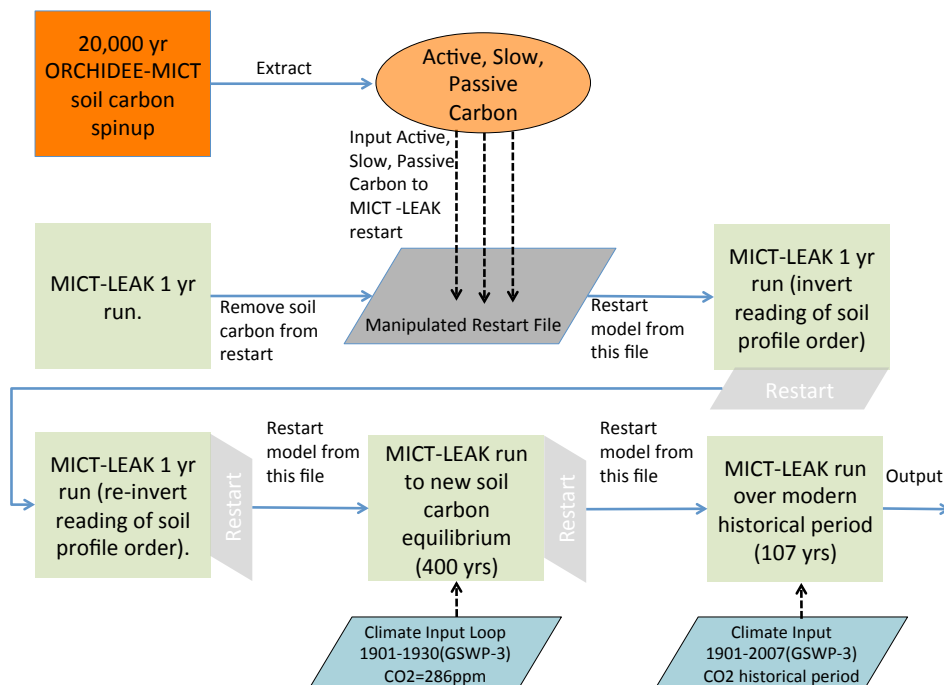
Supprimé: Permafrost Groundwater Provinces ... [18]

Simon Bowring 8/10/y 16:52

Supprimé: 3

Hydrological Source	Model Carbon Reactivity Pool	North	South
Runoff Input	Refractory	81%	83%
	Labile	19%	17%
Drainage Input	Refractory	96%	94%
	Labile	4%	6%
Flood Input	Refractory	36%	37%
	Labile	64%	63%
Streams	Refractory	91%	89%
	Labile	9%	11%
Rivers	Refractory	92%	90%
	Labile	8%	10%

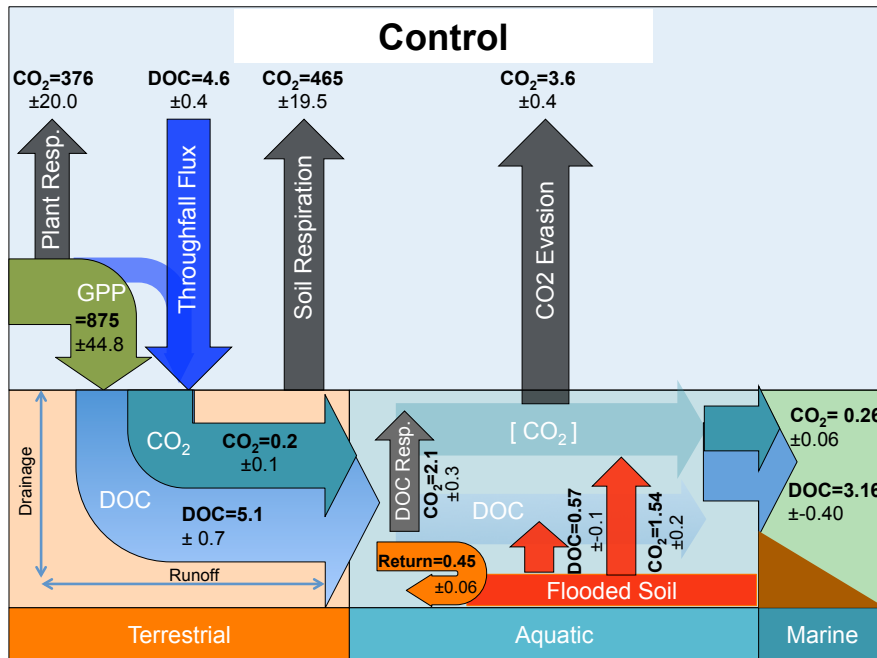
1188
1189



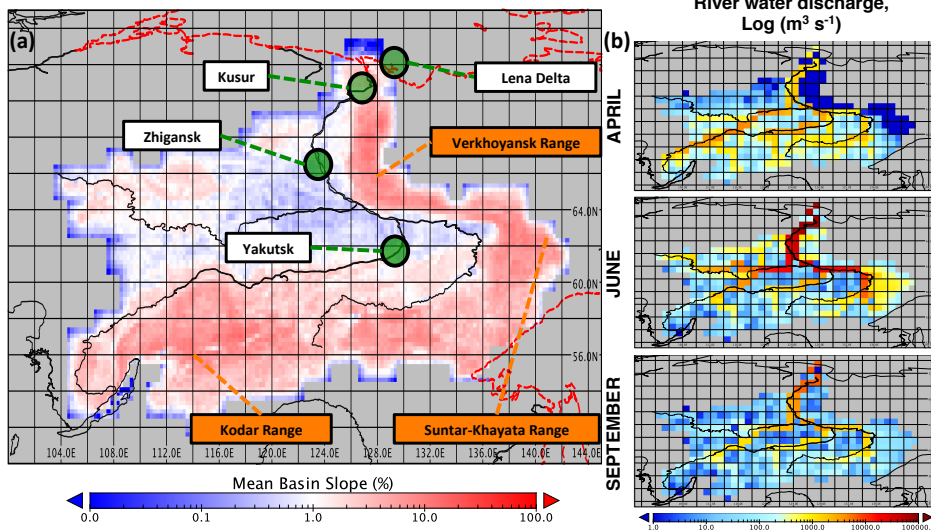
1190
1191
1192
1193
1194

Figure 1: Flow diagram illustrating the step-wise stages required to set up the model, up to and including the historical period. The two stages that refer to the inverted reading of restart soil profile order point to the fact that the restart inputs from ORCHIDEE-MICT are read by our model in inverse order, so that one year must be run in

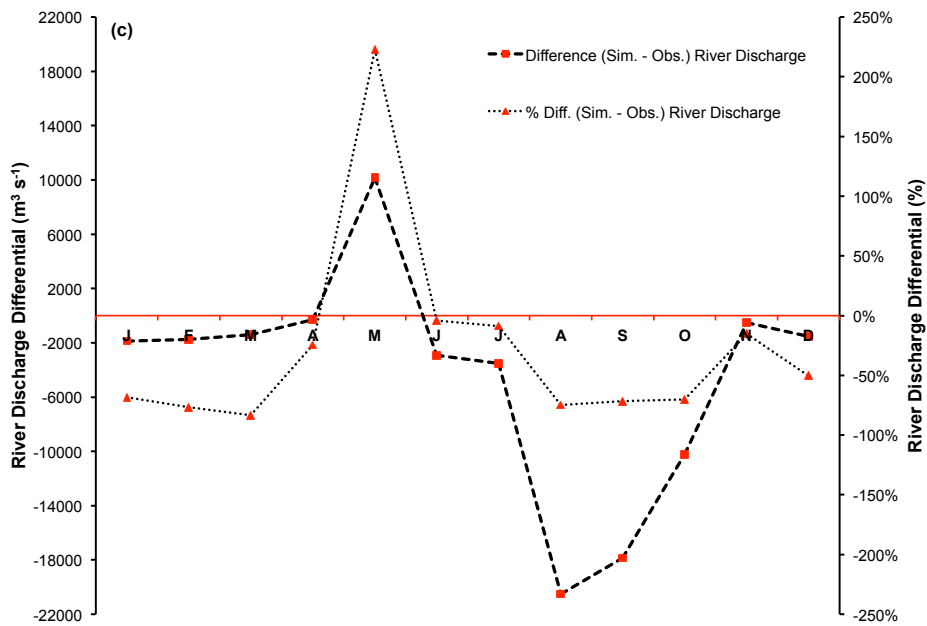
1198 which an activated flag reads it properly, before the reading of soil profile restarts is re-
 1199 inverted for all subsequent years.
 1200



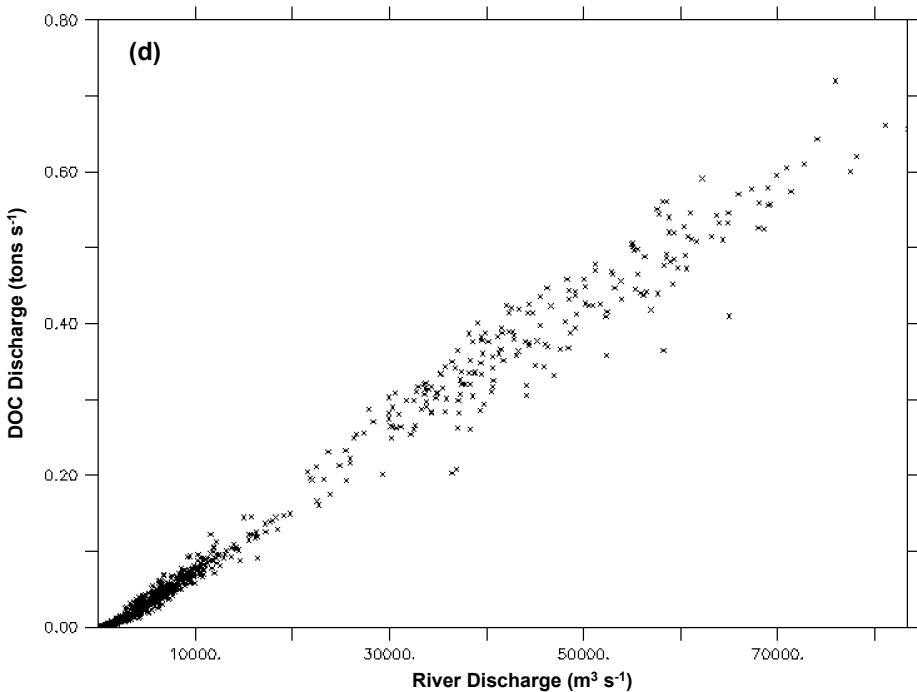
1201
 1202 **Figure 2:** Schematic diagrams detailing the major yearly carbon flux outputs (TgC yr^{-1})
 1203 from the Control simulation averaged over the period 1998-2007 as they are
 1204 transported across the land-aquatic continuum.
 1205



1206
1207
1208

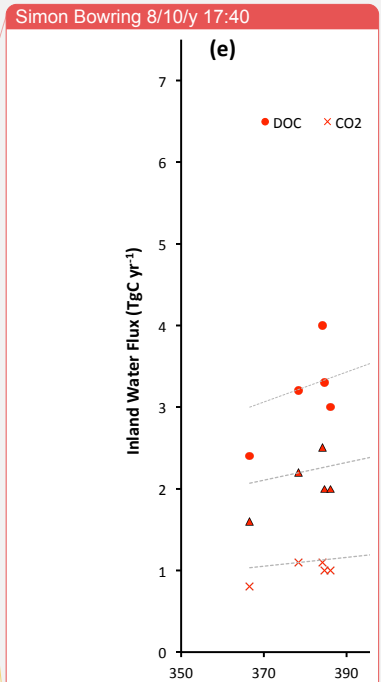


1209
1210



1211
1212 **Figure 3:** Map of the Lena (a) with the scale bar showing the mean grid cell topographic
1213 slope from the simulation, and the black line the satellite-derived overlay of the river
1214 main stem and sub-basins. Mountain ranges of the Lena basin are shown in orange.
1215 Green circles denote the outflow gridcell (Kusur) from which our simulation outflow
1216 data are derived, as well as the Zhigansk site, from which out evaluation against data
1217 from Raymond et al. (2007) are assessed. The regional capital (Yakutsk) is also included
1218 for geographic reference. Coastal outline and inland water bodies are shown as dashed
1219 red and solid black lines, respectively. (b) Maps of river water discharge ($\log(m^3 s^{-1})$) in
1220 April, June and September, averaged over 1998-2007. (c) The mean monthly river
1221 discharge differential between observed discharge for the Lena (Ye et al., 2009) and
1222 simulated discharge averaged over 1998-2007, in absolute ($m^3 s^{-1}$) and percentage
1223 terms. (d) Regression of simulated monthly DOC discharge versus simulated river
1224 discharge at the river mouth (Kusur) over the entire simulation period (1901-2007).
1225
1226 (a)

Unknown
Mis en forme: Police :Gras

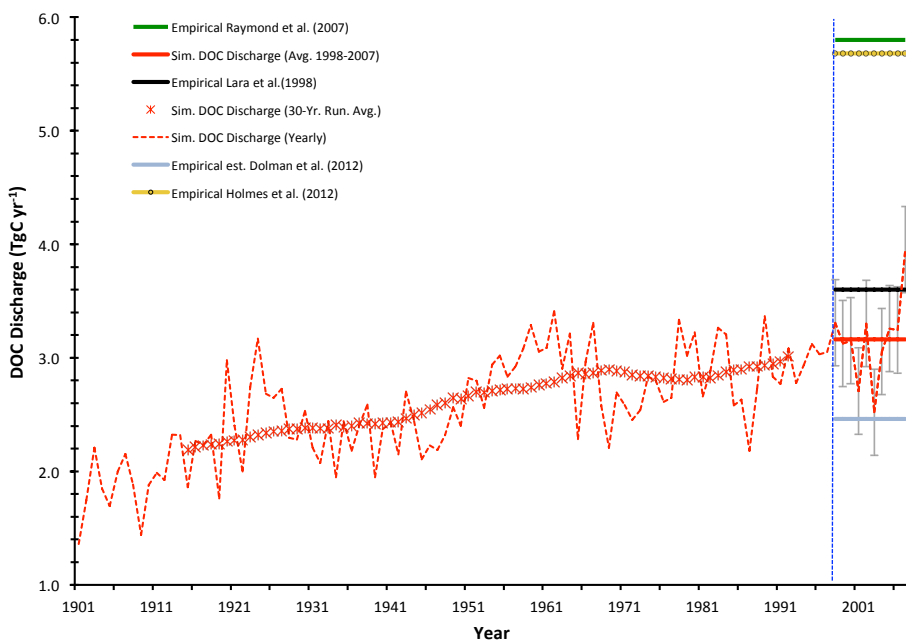


Supprimé:

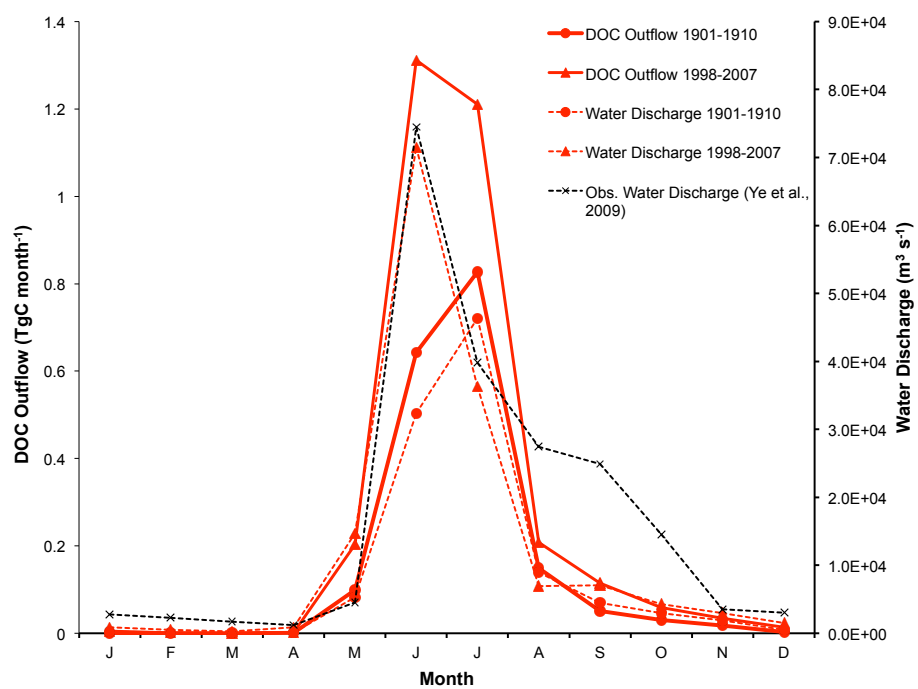
Unknown
Mis en forme: Police :Gras

Simon Bowring 8/10/y 17:40

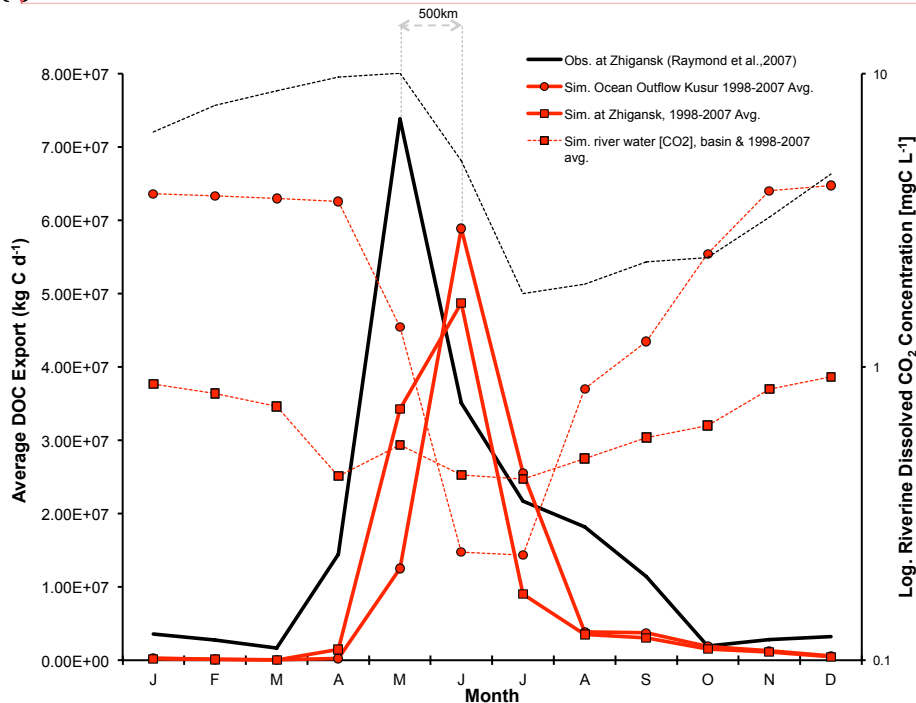
Supprimé: (e) Summed yearly lateral flux versus NPP values for DOC discharge, CO₂ discharge and CO₂ evasion (FCO₂) over the entire simulation period, with linear regression lines shown.



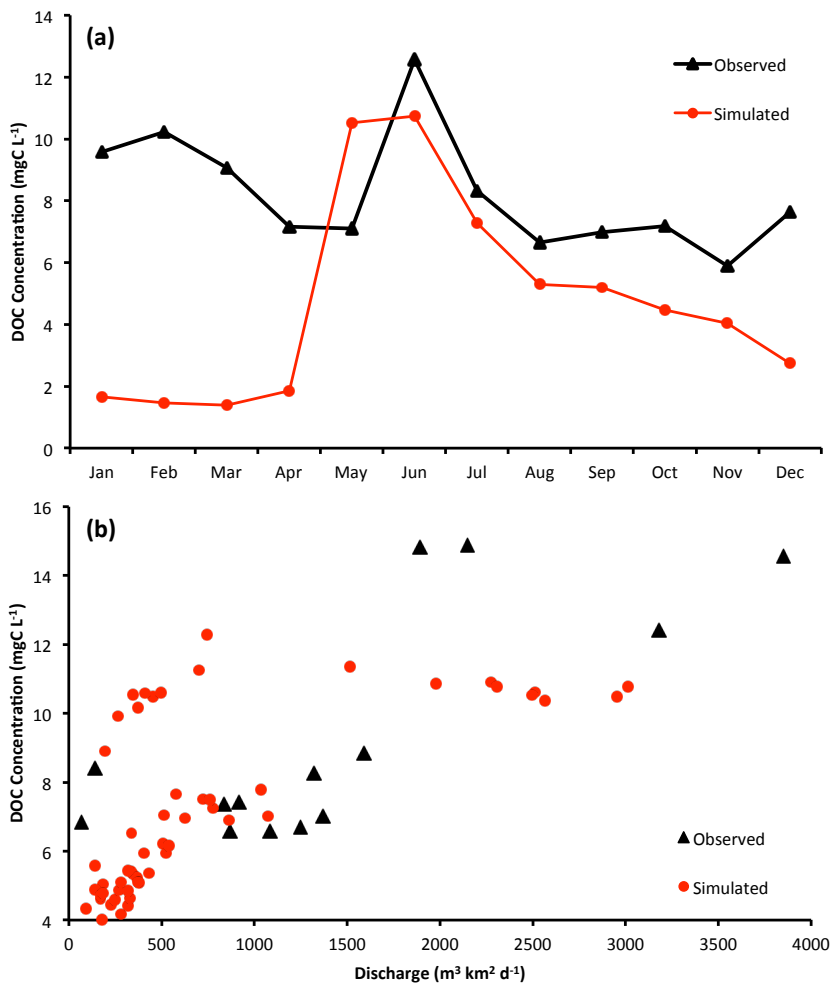
(b)



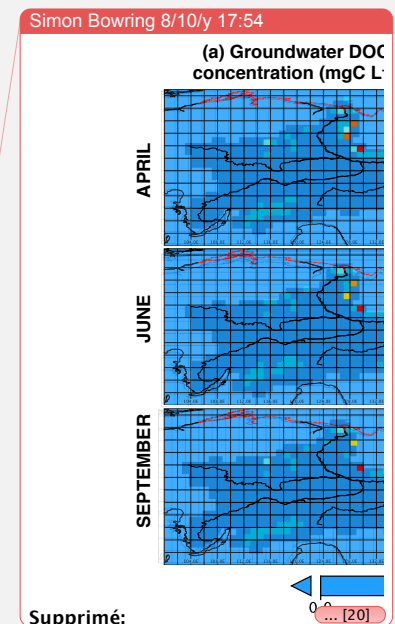
Simon Bowring 8/10/y 17:42
Supprimé: ...
Simon Bowring 8/10/y 17:42
Supprimé: ... [19]
Unknown
Mis en forme: Police :Gras

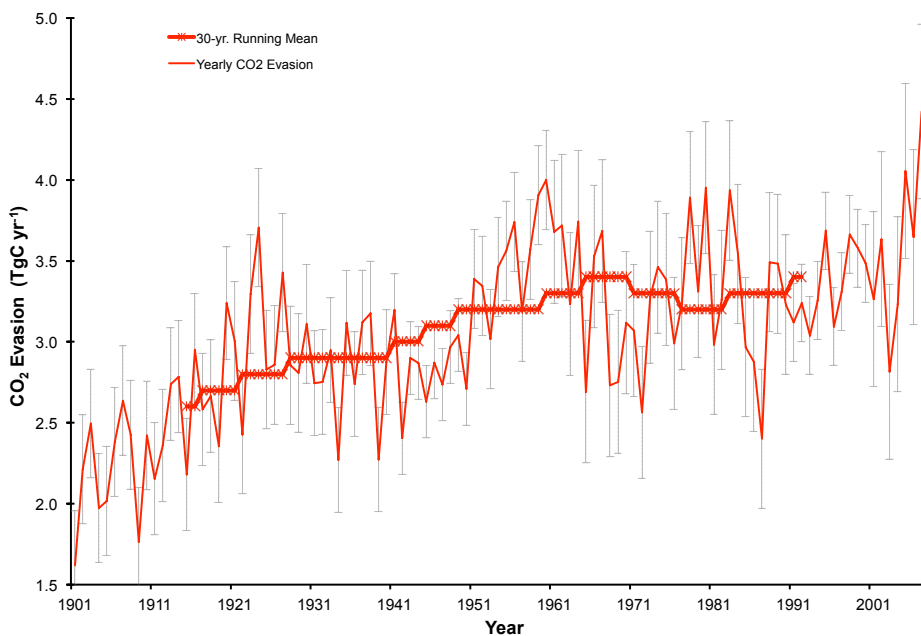
1241
1242

1243 **Figure 4: (a)** Yearly DOC discharged from the Lena river into the Laptev sea is shown
 1244 here in tC yr^{-1} , over the entire simulation period (dashed red line), with the smoothed,
 1245 30-year running mean shown in asterisk. Observation based estimates for DOC
 1246 discharge from Lara et al. (1998), Raymond et al. (2007), Dolman et al. (2012) and
 1247 Holmes et al. (2012) are shown by the horizontal black, green triangle, blue diamond
 1248 and yellow circle line colours and symbols, respectively, and are to be compared against
 1249 the simulated mean over the last decade of simulation (1998-2007, horizontal red line),
 1250 with error bars added in grey displaying the standard deviation of simulated values over
 1251 that period. **(b)** Average monthly DOC discharge (solid red, tC month^{-1}) and water
 1252 discharge (dashed red, $\text{m}^3 \text{s}^{-1}$) to the Laptev Sea over the period averaged for 1901-1910
 1253 (circles) and 1997-2007 (squares) are compared, with modern maxima closely tracking
 1254 observed values. Observed water discharge over 1936-2000 from R-ArcticNet v.4
 1255 (Lammers et al., 2001) and published in Ye et al. (2009) are shown by the dashed black
 1256 line. **(c)** Observed (black) and simulated (red) seasonal DOC fluxes (solid lines) and CO_2
 1257 discharge concentrations (dashed lines). Observed DOC discharge as published in
 1258 Raymond et al. (2007) from 2004-2005 observations at Zhigansk, a site $\sim 500\text{km}$
 1259 upstream of the Lena delta. This is plotted against simulated discharge for: (i) the Lena
 1260 delta at Kusur (red circles) and (ii) the approximate grid pixel corresponding to the
 1261 Zhigansk site (red squares) averaged over 1998-2008. Observed CO_2 discharge from a
 1262 downstream site (Cauwet & Sidorov, 1996; dashed black), and simulated from the
 1263 outflow site (dashed circle) and the basin average (dashed square) are shown on the
 1264 log-scale right-hand axis for 1998-2008.



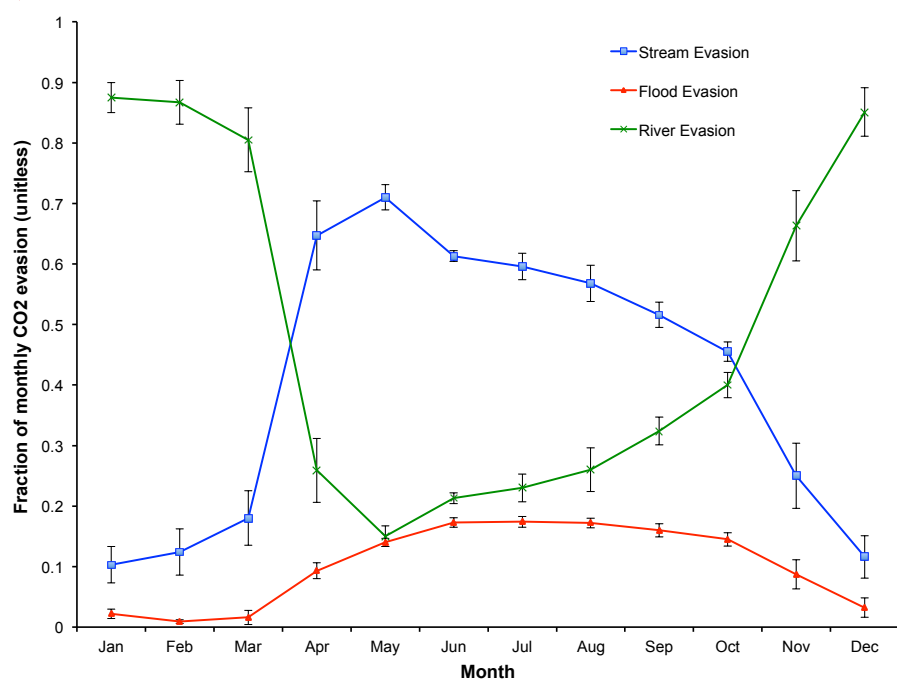
1270
1271 **Figure 5:** (a) Simulated and observed (Arctic-GRO/Holmes et al., 2012) DOC
1272 concentration seasonality for the Lena basin over the period 1999-2007. (b) Plots of
1273 DOC concentration versus river discharge as in observations (Raymond et al., 2007) and
1274 simulations, where simulations data points are monthly averages taken over the period
1275 1999-2007





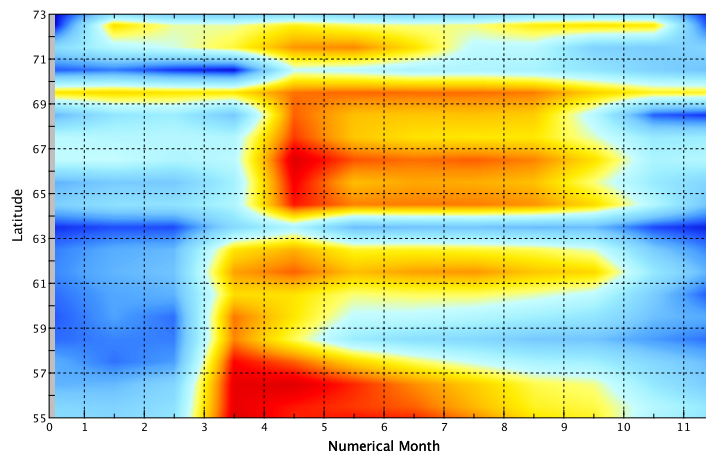
1281 | (b)

Simon Bowring 8/10/y 17:55
Supprimé: (b) ... [21]
 Simon Bowring 8/10/y 17:57
Supprimé: c



1283 | (c)

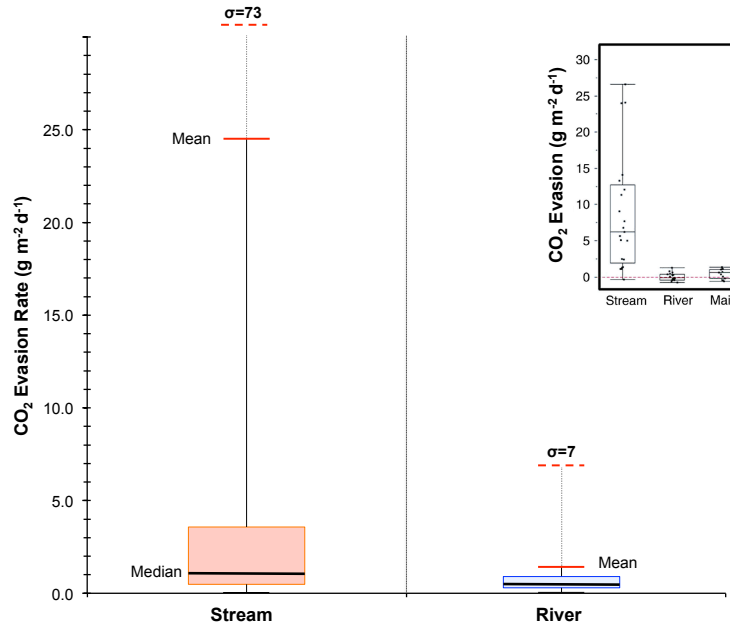
Simon Bowring 8/10/y 17:57
Supprimé: d



Fast Fraction of Total CO₂ Evasion (unitless)

1289
1290
1291
1292
1293 | (d)
1294

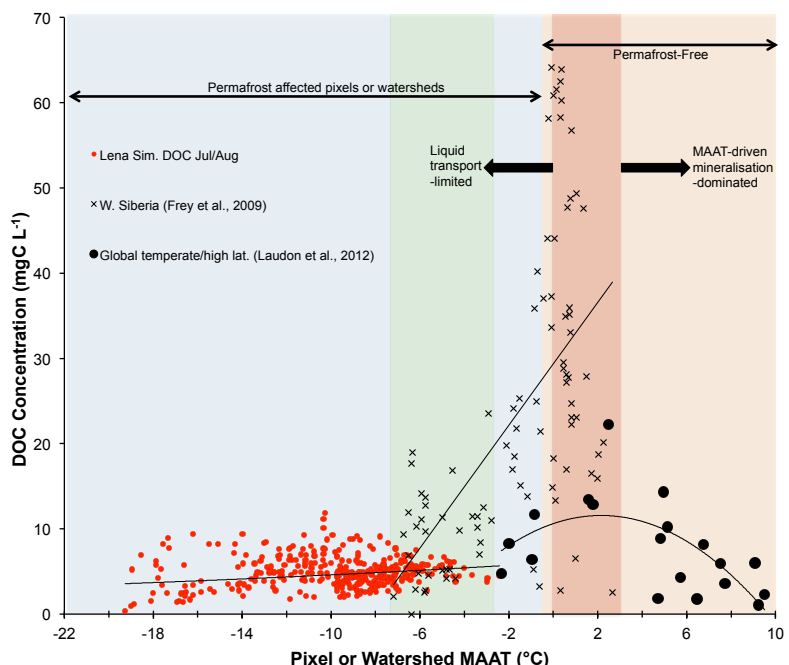
Simon Bowring 9/10/y 10:09
Supprimé: e



1295
1296 | **Figure 6:** CO₂ evasion from stream, river, flood reservoirs. (a) Timeseries of total
1297 yearly CO₂ evasion (tC yr⁻¹) summed over the three hydrological pools (red line) with

Simon Bowring 9/10/y 09:00
Supprimé: 7

1300 the 30-year running mean of the same variable overlain in thick red (asterisk). Error
 1301 bars give the standard deviation of each decade (e.g. 1901-1910) for each data point in
 1302 that decade. (b) The fraction of total CO_2 evasion emitted from each of the hydrological
 1303 pools for the average of each month over the period 1998-2007 is shown for river, flood
 1304 and stream pools (blue, green and red lines, respectively), with error bars depicting the
 1305 standard deviation of data values for each month displayed. (c) Hovmöller diagram
 1306 showing the monthly evolution of the stream pool fraction (range 0-1) per month and
 1307 per latitudinal band, averaged over the period 1998-2007. (d) Boxplot for approximate
 1308 (see text) simulated CO_2 evasion ($\text{gC m}^{-2} \text{ d}^{-1}$) from the streamwater reservoir and river
 1309 water reservoir averaged over 1998-2007. Coloured boxes denote the first and third
 1310 quartiles of the data range, internal black bars the median. Whiskers give the mean
 1311 (solid red bar) and standard deviation (dashed red bar) of the respective data.
 1312 Empirical data on these quantities using the same scale for rivers, streams and
 1313 mainstem of the Kolyma river from Denfeld et al., 2013 are shown inset.
 1314
 1315



1316
 1317 | **Figure 7:** Mean summertime DOC concentrations (mgC L^{-1}) plotted against mean annual
 1318 air temperature (MAAT, $^{\circ}\text{Celsius}$) for simulated pixels over the Lena river basin (red
 1319 circles), and observations for largely peat-influenced areas in western Siberia as
 1320 reported in Frey et al., 2009 (black crosses), and observations from a global non-peat
 1321 temperate and high latitude meta-analysis (black circles) reported in Laudon et al.
 1322 (2012). The blue region represents permafrost-affected areas, while the orange region
 1323 represents permafrost-free areas. The green region bounds the area of overlap in MAAT
 1324 between the observed and simulated datasets. The dark red shaded area corresponds to
 1325 the MAAT 'zone of optimality' for DOC production and transport proposed by Laudon et

Simon Bowring 8/10/y 17:56

Supprimé: (b) Log-scale Hovmöller diagram plotting the longitudinally-averaged difference (increase) in total CO_2 evaded from the Lena River basin between the average of the periods 1998-2007 and 1901-1910, over each monthly timestep, in (\log) $\text{gC m}^{-2} \text{ d}^{-1}$. Thus as the river drains northward the month-on-month difference in water-body CO_2 flux, between the beginning and end of the 20th Century is shown;

Simon Bowring 8/10/y 17:56

Supprimé: c

Simon Bowring 8/10/y 17:56

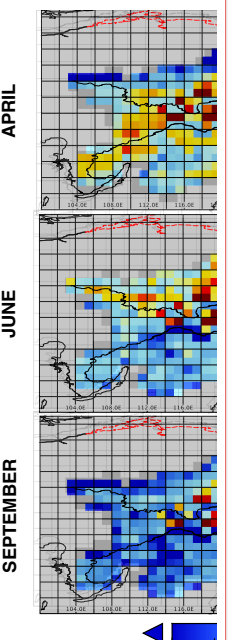
Supprimé: d

Simon Bowring 8/10/y 17:56

Supprimé: e

Simon Bowring 8/10/y 17:57

(a) 'Stream' CO_2

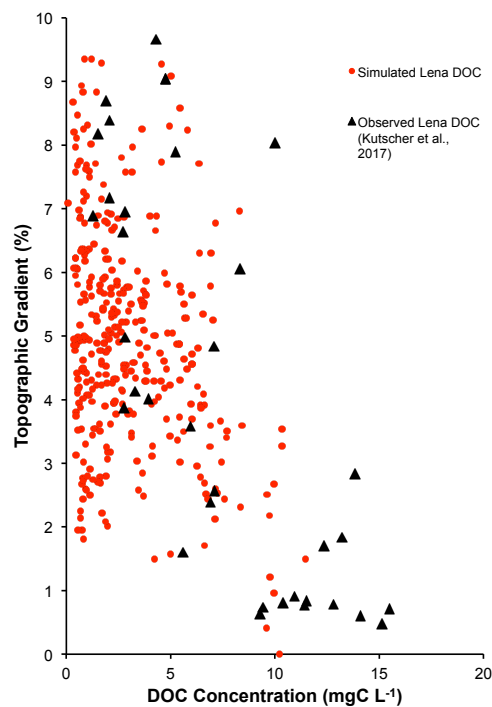


Supprimé:

Simon Bowring 9/10/y 09:07

Supprimé: 9

1343 al. (2012). Regression curves of DOC against MAAT for each of the separate datasets are
1344 shown for each individual dataset.
1345

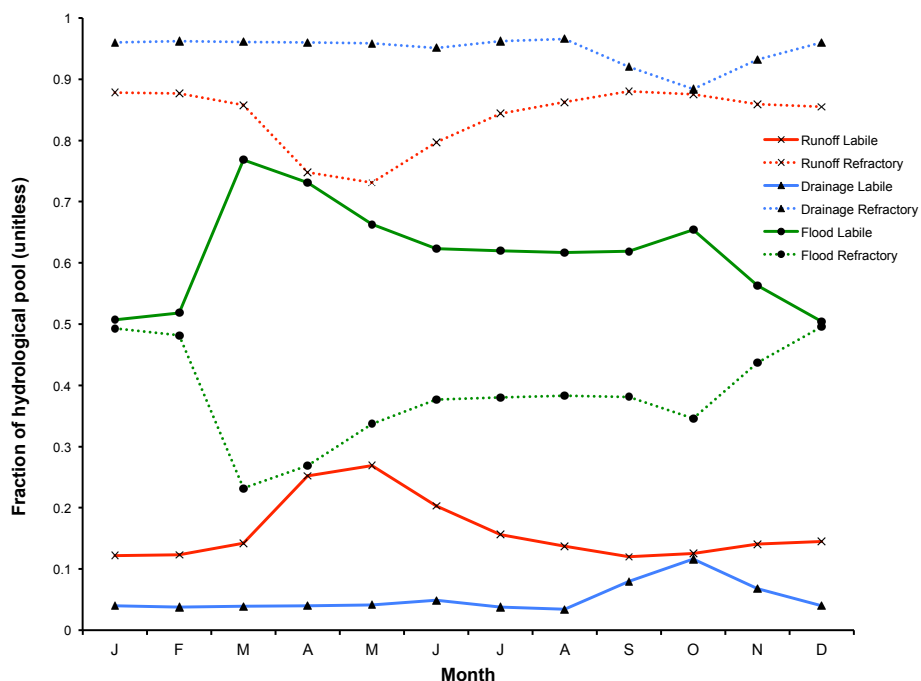


1346 | **Figure 8:** Variation of DOC concentrations versus topographic slope in Kutscher et al.,
1347 2017 (black triangles) and (red dots) as simulated and averaged for the summer months
1348 (JJA) over 1998-2007; observed values were measured during June and July 2012-2013.
1349
1350

1351 (a)
1352

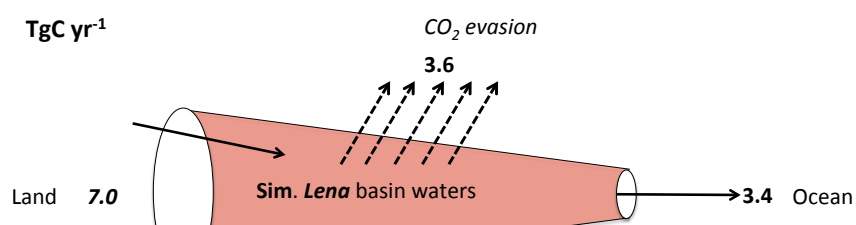
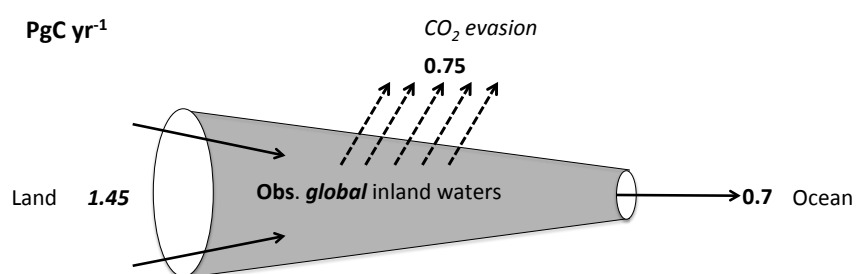
Simon Bowring 9/10/y 09:08

Supprimé: 10



1354
1355
1356 **Figure 9:** The mean monthly fraction of each hydrological pool's (runoff, drainage,
1357 floodplains) carbon reactivity constituents (labile and refractory) averaged across the
1358 simulation area over 1998-2008.
1359

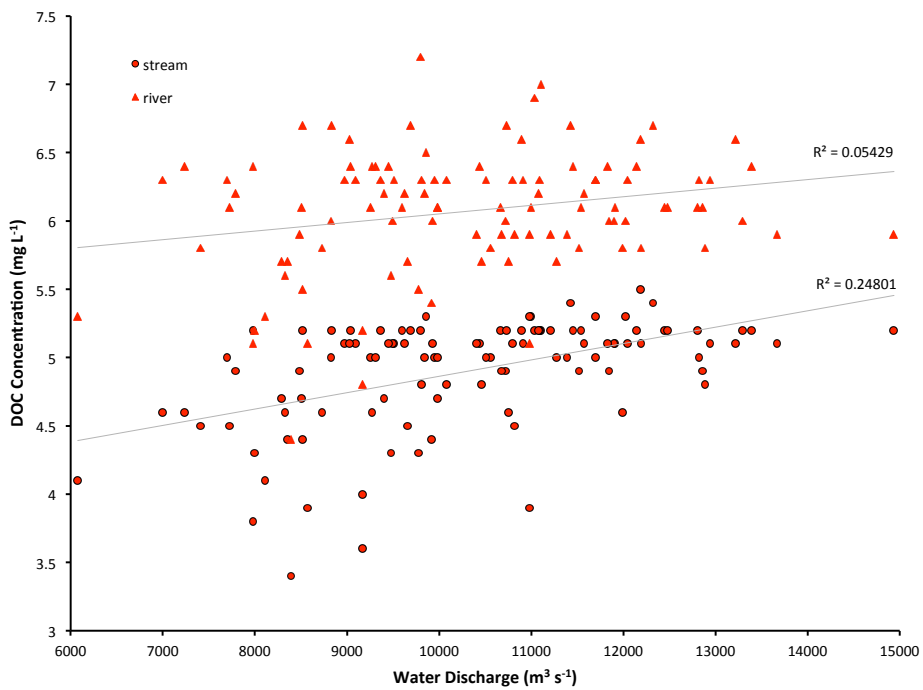
Simon Bowring 9/10/y 09:09
Supprimé: 11



Simon Bowring 9/10/y 09:11
Supprimé: (a)

1360

1363 | **Figure 10:** Simplified 'leaky pipe' diagram representing the transport and processing of
 1364 DOC within the land-ocean hydrologic continuum. The scheme template is taken from
 1365 Cole et al. (2007), where we reproduce their global estimate of DOC and non-
 1366 groundwater discharge portion of this flow in the top panel (PgC yr^{-1}), and the
 1367 equivalent flows from our Lena basin simulations in TgC yr^{-1} in the bottom panel. Thus
 1368 easy comparison would look at the relative fluxes within each system and compare them
 1369 to the other.
 1370
 1371



1372
 1373
 1374 **Figure 13:** Simulated basin-mean annual DOC concentrations (mg L^{-1}) for the stream
 1375 and river water pools regressed against mean annual simulated discharge rates ($\text{m}^3 \text{s}^{-1}$)
 1376 at Kusur over 1901-2007. Linear regression plots with corresponding R^2 values are
 1377 shown.
 1378
 1379
 1380

Simon Bowring 8/10/y 17:59
Supprimé: (b) ... [23]
 Simon Bowring 9/10/y 09:10
Supprimé: 2
 Simon Bowring 9/10/y 09:09
Supprimé: (a)
 Simon Bowring 9/10/y 09:41
Supprimé: (b-c): Schematic diagrams detailing the major yearly carbon flux outputs from simulations averaged over the period 1998-2007 as they are transformed and transported across the land-aquatic continuum. Figures (b) and (c) give the same fluxes as a percentage difference from the Control (CTRL-Simulation), for the constant climate and CO_2 simulations, respectively.

Given that DOC fluxes are almost directly proportional to river discharge in the Lena basin (Fig. 3d), this sub-optimal performance with regard to hydrology during August to October seeming to be the main cause of a substantial underestimation in simulated bulk DOC outflow. Another cause may simply be the lack of peat representation in the model, for which DOC flux concentrations in outflowing fluvial water can be very high (e.g. Frey et al., 2005; 2009: see Section 4.5.1).

Deficiencies in modelled hydrology correspond to those found in Fig. 12 of Guimberteau et al. (2018), indicating that the modifications made in this model version, which focus on the DOC cycle, have not further degraded the hydrological performance of the model, the causes of which are described below. Low simulated discharge for the Lena basin, particularly during the late summer and autumn, is consistent with prior, Pan-Arctic simulations conducted by Guimberteau et al. (2018), who ran ORCHIDEE-MICT using both the GSWP3 and CRU-NCEP v7 datasets and evaluated them over the period 1981-2007. Despite the substantially better hydrological performance of ORCHIDEE under GSWP3 climate, they described a near-systematic underestimation of summer/autumn discharge rates for both datasets over the Yukon, Mackenzie, Lena and Kolyma basins. Furthermore, the discrepancy of model output between climatological datasets was almost as large as the discrepancy between model output and observational data in that study, which analysed this in great depth, suggesting that the source of error is both a covariate of model process representation and parameterisation, as well as the climatological datasets themselves. Model hydrological representation and empirically derived climate input data are then subject to interaction with modelled soil (e.g. infiltration), vegetation (e.g. canopy interception) and thermodynamics (e.g. freezing and consequent partitioning of water transport) from which river discharge is computed, confounding full interpretation of sources of bias, briefly described below.

Model process deficiency in this regard was identified by Guimberteau et al. (2018) as residing in an overly restrictive representation of water impermeability through frozen topsoil, which decreases the residence time of running water by directing it to surface runoff rather than subsurface flow, and in the process increases the susceptibility of the total water volume to evapotranspiration from incoming shortwave radiation. This would bias both the timing (over-partitioning of water to high runoff periods) and volume of water (low bias) reaching the river stem and its eventual discharge into the ocean, respectively, as demonstrated by model output. Guimberteau et al. (2018) suggest that representation of sub-grid-scale infiltration mechanisms under frozen conditions, such as

soil freezing-drying that would enhance infiltration, be included in future, yet-to-be implemented iterations of ORCHIDEE. Furthermore, we suggest that the lack of representation of lakes in ORCHIDEE, which serve to increase the time lag between precipitation/melt and oceanic discharge, may likewise be a powerful source of bias in the timing of discharge fluxes represented by the model.

Unsurprisingly, simulated surface runoff has been shown to be strongly affected by differences in precipitation between datasets (Biancamaria et al., 2009; Fekete et al., 2004), while biases in these and evapotranspiration datasets that are used to both drive and evaluate the hydrological models, are a powerful source of water balance biases in high-latitude basins (Wang et al., 2015). Indeed, climatological dataset estimates for the spatial distribution of high latitude winter snowfall are generally problematic, owing to the low density of meteorological stations (Burke et al., 2013), wind-related issues with in-field collection and measurement that lead to systematic underestimates of snowfall rates (Yang et al., 2005), creating biases in the climatological datasets that only show up when the integrator of their model input -in this case river discharge -is modelled. In addition, the wintertime partitioning of precipitation between rain and snow, a function of 2m air temperatures in the forcing datasets, strongly affects the volume and timing of runoff (Guimberteau et al., 2018; Haddeland et al., 2011). Indeed, 69% of the spatial variance of the spring freshet has been attributed to snow water-equivalent bias during the pre-melt season (Rawlins et al., 2007). In addition, errors in forcing of soil evaporation due to inaccuracies in incoming shortwave radiation, as well as biases in the parameterisation of canopy interception -a function of simulated LAI -can lead to upward biases in evapotranspiration rates (Guimberteau et al., 2018).

Firstly, there is a quasi-linear positive relationship between DOC discharge and river discharge (Fig. 3d). This relation is common to Arctic rivers, as DOC loading experiences disproportionately large increases with increases in discharge (Fig. 4, Raymond et al., 2007), owing largely to the 'flushing' out of terrestrially fixed carbon from the previous year's production by the massive runoff generated by ice and snow melt during the spring thaw. Comparing simulated annual mean discharge rate ($\text{m}^3 \text{ s}^{-1}$) with long-term observations (Ye et al. 2003) over years 1940-2000 (Fig. 4c) shows that though absolute discharge rates are underestimated by simulations, their interannual variation reasonably tracks the direction and magnitude of observations. Linear regressions through each trend yield very similar yearly increases of 29 vs 38 $\text{m}^3 \text{ s}^{-1} \text{ yr}^{-1}$ for simulations and observations, respectively. The observed vs. simulated mean annual water discharge differential hovers at 36% (Figs. 3d, 4c), close to the 43% differential between observed and simulated DOC discharge, giving some indication that, given the linear relationship between water and DOC discharge, most of the DOC discrepancy can be explained by the performance of the hydrology and not the DOC module, the latter of which was the subject of developments added in ORCHIDEE M-L. Applying the regression slope of the relationship in Fig. 3d (9E-06 $\text{mgC per m}^3 \text{s}^{-1}$) to the mean river discharge discrepancy of 36%, we find that 84% of the

differential between observed and simulated discharge can be explained by the underperformance of the hydrology module.

Further sources of error are process exclusion and representation/forcing limitations. Indeed, separate test runs carried out using a different set of climatological input forcing show that changing from the GSWP3 input dataset to input from bias-corrected projections from the IPSL Earth System Model under the second Inter-Sectoral Impact Model Intercomparison Project (ISIMIP2b (Frieler et al., 2017; Lange, 2016, 2018)) protocol increases DOC discharge to the ocean to 4.14 TgC yr^{-1} (+37%), largely due to somewhat higher precipitation rates in that forcing dataset (see Table S3). Thus, the choice of input dataset itself introduces a significant degree of uncertainty to model output.

In addition, this model does not include explicit peatland formation and related dynamics, which is the subject of further model developments (Qiu et al., 2018) yet to be included in this iteration. With peatlands thought to cover ~17% of the Arctic land surface (Tarnocai et al., 2009), and with substantially higher leaching concentrations, this may be a significant omission from our model. The remaining biases likely arise from errors in the interaction of simulated NPP, respiration and DOC production and decomposition, which will impact on the net in and out -flow of dissolved carbon to the fluvial system. However, the DOC relationship with these variables is less clear-cut than with river discharge. Indeed, regressions (Fig. 3e) of annual DOC versus NPP (TgC yr^{-1}) show that DOC is highly sensitive to increases in NPP, but is less coupled to it (more scattered, $R^2=0.42$) than other simulated fluvial carbon variables shown, i.e. aquatic CO_2 evasion and soil CO_2 export to the river network. The differences in correlation and slope of the variables in Fig. 3e are expected: aquatic CO_2 evasion is least sensitive yet most tightly coupled to NPP ($R^2=0.52$), while CO_2 export to rivers is intermediate between the two ($R^2=0.43$). The greater correlation with NPP of DOC compared to evasion is understandable, given that DOC leaching is a covariate of both NPP and runoff, whereas evasion flux is largely dependent on organic inputs (production) and temperature (see Part 1).

4.2.3 Model Evaluation: DOC Discharge Seasonality

Figure 4b shows that the bulk of the DOC outflow occurs during the spring freshet or snow/ice-melting period of increased discharge, accounting for ~50-70% of the total Arctic outflow (Lammers et al., 2001; Ye et al., 2009), with peak water discharge rates in June of ~80,000 $\text{m}^3 \text{ s}^{-1}$. DOC concentrations increase, as meltwater flushes out DOC accumulated from the previous year's litter and SOC generation (Raymond et al., 2007; Kutscher et al., 2017). This is reproduced in our simulations, since DOC discharge peak occurs at the onset of the growing season, meaning it is generated from a temporally prior stock of organic carbon. Simulation of the hydrological dynamic is presented in maps of river discharge through the basin in Fig. 3b, which show low-flows in April with substantial hydrographic flow from upstream mountainous headwaters and Lake Baikal inflow in the south, peak flow in June dominated by headwaters, and little headwater input in September.

In Fig. 4b we observe the following: (i) DOC discharge fluxes closely track hydrological fluxes. (ii) The simulated modern river discharge peak approximates the historical

observed discharge peak, but slightly overestimates spring fluxes and substantially underestimates fluxes in the autumn, as explained above. (iii) The difference between the first and last decades of the simulation in Fig. 4b is mostly attributable to a large increase in the DOC flux mobilised by spring freshet waters. This suggests both greater peaks in simulated DOC flux and a shift to earlier peak timing, owing to an increase in river discharge, indicative of an earlier spring and a progressively warmer environment over the 20th Century. (iv) The maximum modelled modern monthly DOC flux rate of ~ 1.3 TgC month $^{-1}$ is comparable to the mean maximum DOC flux rate measured in a recent study (1.75 TgC month $^{-1}$, Kutscher et al., 2017, Fig. 2).

We compare the Raymond et al. (2007) modern DOC outflow (Fig. 4d, solid black line) from the Lena river at Zhigansk (Raymond et al., 2007) against simulated DOC outflow from both Zhigansk and Kusur (Fig. 4d). Simulated DOC flux is underestimated for both sites. Peakflow at Zhigansk seems to be attenuated over May and June in simulations, as opposed to May peakflow in observations. Peakflow at Kusur is definitively in June. This suggests that simulated outflow timing at Zhigansk may slightly delayed, causing a split in peak discharge when averaged in the model output. Thus the aggregation of model output to monthly averages from calculated daily and 30 minute timesteps can result in the artificial imposition of a normative temporal boundary (i.e. month) on a continuous series. This may cause the less distinctive 'sharp' peak seen in Fig. 4d, which is instead simulated at the downstream Kusur site, whose distance some 500km away from Zhigansk more clearly explains the delay difference in seasonality. We further evaluate our DOC discharge at the sub-basin scale, to test whether the fractional contribution of different DOC flows from each sub-basin correspond to those in their observed correlates from Kutscher et al., (2017). This comparison is depicted in Fig. S2, where the observed and simulated percentage DOC contributions of the Aldan, Vilui, and Upper and Lower Lena sub-basins to total flux rates are 19 (24%), 20(10%), 33 (38%) and 30 (28%) in simulations (observations) for the four sub-basins, respectively. While deviations between simulated and observed DOC fluxes can be expected, the nearly twofold value mismatch of the Vilui basin is due to its real-word damming, not represented here. On the other hand, we cannot explain the $\sim 5\%$ discrepancies in other sub-basin fluxes, particularly for the Aldan.

The spatial distribution of DOC concentrations are shown in maps of mean monthly DOC concentration for stream water, river water and groundwater (Fig. 6a,b,c, respectively) in April, June and September. For both the stream and river water reservoirs, DOC concentrations appear to have spatio-temporal gradients correlated with the flux of water over the basin during the thaw period, with high concentrations of $10\text{--}15$ mgC L $^{-1}$ driven by April meltwaters upstream of the basin, these high concentrations moving northward to the coldest downstream regions of the basin in June. Lower DOC concentrations of ~ 5 mgC L $^{-1}$ dominate the basin in September when the bulk of simulated lateral flux of DOC has dissipated into the Laptev Sea. In contrast, groundwater DOC concentrations are generally stable with time, although some pixels appear to experience some 'recharge' in their concentrations during the first two of the three displayed thaw months. Significantly, highest groundwater DOC concentrations of up to 20 mgC L $^{-1}$ are focussed on the highest

elevation areas of the Lena basin on its Eastern boundary, which are characterized by a dominance of Podzols (SI, Fig. 2b). This region, the Verkhoyansk range, is clearly visible as the high groundwater DOC concentration (2-20mgC L⁻¹) arc (in red) in Fig. 6a, as well as other high elevation areas in the south-western portion of the basin (Fig. 3a), while the low-lying central basin shows much smaller groundwater DOC concentrations (0-2mgC L⁻¹). The range of simulated groundwater DOC concentration comes close to those aggregated from the empirical literature by Shvartsev (2008), which finds from >9,000 observations that groundwater in permafrost regions exhibit a mean concentration of ~10 mgC L⁻¹ after peatlands and swamps (not simulated here) are removed (Table 2).

Page 6 : [7] Supprimé

Simon Bowring

08/10/19 15:22

Page 6 : [8] Supprimé

Simon Bowring

08/10/19 15:24

To our knowledge, no direct measurements for CO₂ evasion from the surface of the Lena river are available in the literature. We refer to Denfeld et al. (2013) for evaluating our evasion flux results, since their basin of study, the Kolyma River, is the most geographically proximate existing dataset to the Lena, despite biogeographical differences between the two basins –namely that the Kolyma is almost entirely underlain by continuous permafrost. The Kolyma River CO₂ evasion study measured evasion at 29 different sites along the river basin (~158-163°E; 68-69.5°N), with these sites distinguished from one another as 'main stem', 'inflowing river' or 'stream' on the basis of reach length. The study showed that during the summer low-flow period (August), areal river mainstem CO₂ evasion fluxes were ~0.35 gC m⁻² d⁻¹, whereas for streams of stream order 1-3 (widths 1-19m), evasion fluxes were up to ~7 gC m⁻² d⁻¹, and for non-mainstem rivers (widths 20-400m) mean net fluxes were roughly zero (Table 3 of Denfeld et al., 2013). Thus, while small streams have been observed to contribute to roughly 2% of the Kolyma basin surface area, their measured percentage contribution to total basin-wide CO₂ evasion ~40%, whereas for the main stem the surface area and evasion fractions were ~80% and 60%, respectively. Likewise, mean annual evasion rates of <0.8 up to around 7 gC m⁻² d⁻¹ have been found for the Ob and Pur rivers in Western Siberia (Serikova et al., 2018).

Results such as these, in addition to permafrost soil incubation experiments (e.g. Drake et al., 2015; Vonk et al., 2013, 2015b, 2015a) suggest that small streams, which represent the initial (headwater) drainage sites of these basins, rapidly process hydrologically leached carbon to the atmosphere, and that this high-reactivity carbon is a mix of recently thawed ancient permafrost material, as well as decomposing matter from the previous growth year. This is given as evidence that the total carbon processing of high-latitude rivers is significantly underestimated if only mainstem carbon concentrations are used in the accounting framework, since a large amount of carbon is metabolised to the atmosphere before reaching the site of measurement.

Page 6 : [9] Supprimé

Simon Bowring

08/10/19 15:27

The heterogeneity of CO₂ evasion from different sources in the model is most evident in

terms of their geographic distribution and relative intensity, as shown in the evasion flux rate maps over stream and river areas in April, June and September (Fig. 8a-b). Stream evasion (Fig.8a), tends to be broadly distributed over the whole basin, representing the fact that small streams and their evasion are the main hydrologic connectors outside of the main river and tributary grid cells, whereas river evasion (Fig. 8b) is clearly linked to the hydrographic representation of the Lena main stem itself, with higher total quantities in some individual grid cells than for the stream reservoir, yet distributed amongst a substantially smaller number of grid cells. Whereas the stream reservoir has greatest absolute evasion flux rates earlier in the year (April-May), maximum evasion rates occur later in the year and further downstream for the river reservoir, reflecting the fact that headwaters are first-order integrators of soil-water carbon connectivity, whereas the river mainstem and tributaries are of a secondary order.

The spatio-temporal pattern of increasing evasion over the simulation period is shown in Fig. 7b as a Hovmöller difference plot, between the last and first decade, of log-scale average monthly evasion rates per latitudinal band. This shows that the vast majority of outgassing increase occurs between March and June, corresponding to the progressive onset of the thaw period moving northwards over this timespan. Although relatively small, outgassing increases are apparent for most of the year, particularly at lower latitudes. This would suggest that the change is driven most acutely by relatively greater temperature increases at higher latitudes ('Arctic amplification' of climate warming, e.g. Bekryaev et al., 2010) while less acute but more temporally homogenous evasion is driven by seasonal warming at lower latitudes.

Page 7 : [10] Supprimé

Simon Bowring

08/10/19 15:34

This is because in ORCHIDEE MICT-L, the 'stream' water reservoir is water routed to the river network for all hydrologic flows calculated to not cross a 0.5 degree grid cell boundary (the resolution of the routing module, explained in Part 1, Section 2.6), which may not be commensurate with long, <20m width streams in the real-world, that were used in the Denfeld et al. (2013) study. In addition, this 'stream' water reservoir in the model does not include any values for width or area in the model, so we cannot directly compare our stream reservoir to the <20m width criterion employed by Denfeld et al. (2013) in their definition of an observed stream. Thus our 'stream' water reservoir encompasses substantially greater surface area and hydrologic throughput than that in the Denfeld et al. study.

Page 7 : [11] Supprimé

Simon Bowring

08/10/19 15:46

Page 7 : [12] Supprimé

Simon Bowring

08/10/19 15:42

refers to the fact that model output doesn't define a precise surface area for the stream water reservoir, which is instead bundled into a single value representing the riverine fraction of a grid cell's total surface area. To approximate the areal outgassing for the stream versus river water reservoirs, we weight the total non-floodplain inundated area of each grid cell by the relative total water mass of each of the two hydrological pools, then divide the total daily CO₂ flux simulated by the model by this value. The per-pool areal

estimate is an approximation since it assumes that rivers and streams have the same surface area: volume relationship. This is clearly not the case, since streams are generally shallow, tending to have greater surface area per increment increase in depth than rivers. Thus, our areal approximations are likely underestimated (overestimated) for streams (rivers), respectively.

Page 7 : [13] Supprimé

Simon Bowring

08/10/19 16:21

in the figure, with whiskers in their case denoting measured maxima and minima

Page 7 : [14] Supprimé

Simon Bowring

08/10/19 15:44

Note that from ~ 700 non-zero simulation datapoints, 7 were omitted as 'outliers' from the stream reservoir efflux statistics described below, because very low stream:river reservoir values skewed the estimation of total approximate stream surface area values very low, leading to extreme efflux rate values of $1\text{-}3000\text{gC m}^{-2} \text{d}^{-1}$ and are thus considered numerical artefacts of the areal approximation approach used here.

Page 7 : [15] Supprimé

Simon Bowring

08/10/19 16:16

4.5 Emergent Phenomena

4.5.1 DOC and mean annual air temperature

A key emergent property of DOC concentrations in soils and inland waters should be their positive partial determination by the temperature of the environment under which their rates of production occur, as has been shown in the literature on permafrost regions, most notably in Frey & Smith (2005) and Frey & McClelland (2009).

Increasing temperatures should lead to greater primary production, thaw, decomposition and microbial mobilisation rates, and hence DOC production rates, leading to (dilution effects notwithstanding) higher concentrations of DOC in thaw and so stream waters. Looking at this emergent property allows us to evaluate the soil-level production of both DOC and thaw water at the appropriate biogeographic and temporal scale in our model. This provides a further constraint on model effectiveness at simulating existing phenomena at greater process-resolution.

Figure 9 compares three datasets (simulated and two observational) of riverine DOC concentration (in mgC L^{-1}) plotted against mean annual air temperature (MAAT). The simulated grid-scale DOC versus MAAT averaged over July and August (for comparability of DOC with observational sampling period) of 1998-2007 is shown in red, and observed data compiled by Laudon et al. (2012) and Frey and Smith (2005) for sites in temperate/cold regions globally and peatland-dominated Western Siberia, respectively. The Laudon et al. (2012) data are taken from 49 observations including MAAT over the period 1997-2011 from catchments north of 43°N , and aggregated to 10 regional biogeographies, along with datapoints from their own sampling; those in the Frey and Smith study are from $55\text{-}68^\circ\text{N}$ and $\sim 65\text{-}85^\circ\text{E}$ (for site locations, see Laudon et al. (2012), Table 1 and 2; Frey and Smith (2005), Fig. 1).

Fig. 9 can be interpreted in a number of ways. First, this MAAT continuum spans the range of areas that are both highly and moderately permafrost affected and permafrost free (Fig. 9, blue and green versus orange shading, respectively), potentially allowing us a glimpse of the behaviour of DOC concentration as the environment transitions from the former to the latter. Simulated Lena DOC concentrations, all in pixels with $MAAT < -2^{\circ}C$ and hence all bearing continuous or discontinuous permafrost ('permafrost-affected' in the figure), only exhibit a weakly positive response to MAAT on the scale used ($y=6.05e^{0.03MAAT}$), although the consistent increase in DOC minima with MAAT is clearly visible. Second, the Laudon et al. (2012) data exhibit an increasing then decreasing trend over the range of MAAT (-2°C to 10°C) in their dataset, which they propose reflects an 'optimal' MAAT range (0-3°C) for the production and transport of DOC (Fig. 9, red shading). Below this optimum range, DOC concentrations may be limited by transport due to freezing, and above this, smaller soil carbon pools and temperature-driven decomposition would suppress the amount of DOC within rivers. Third, the lower end of the Laudon et al. (2012) MAAT values correspond to a DOC concentration in line with DOC concentrations simulated by our model. Fourth, DOC concentrations in the Frey and Smith (2005) data exhibit a broad scattering in permafrost-affected sites, with concentrations overlapping those of our simulations (Fig. 9, green shading), before rapidly increasing to very high concentrations relative to the Laudon et al. (2012) data, as sites transition to permafrost-free (red shading, $y=3.6^{MAAT}+29.4$).

Their data highlight the difference in DOC concentration regime between areas of high (Frey and Smith, 2005) and low (Laudon et al., 2012) peatland coverage and the different response of these to temperature changes. Fifth, because our simulation results largely correspond with the observed data where the MAAT ranges overlap (green shading), and because our model lacks peatland processes, we should expect our model to follow the polynomial regression plotted for the Laudon et al. (2012) data as temperature inputs to the model increase. Figure 9 implies that this increase should be on the order of a doubling of DOC concentration as a system evolves from a MAAT of -2°C to 2°C. With warming, we expect the response of DOC concentrations to reflect a mix of both observationally-derived curves, as a function of peatland coverage.

This relationship was found in temperate rivers by Lauerwald et al. (2012), and in a recent Pan-Arctic synthesis paper Connolly et al. (2018). The reasoning for the negative slope-DOC concentration relationship is that as elevation increases, temperature and primary production decreases. This leads to a thinner organic soil layer, meaning that mineral soil plays a stronger role in shallow hydrologic flowpaths, allowing for deeper infiltration and shorter residence time in a given soil layer. Further, steeper terrain leads to a lower soil water residence time and lower moisture than in flat areas. As a result, a given patch of soil matter will be exposed to leaching for less (residence) time, while the organic matter that is leached is thought to be adsorbed more readily to mineral soil particles, leading to either their re-stabilisation in the soil column or shallow retention and subsequent heterotrophic respiration in situ, cumulatively resulting in lower DOC concentrations in the hydrologic export (Kaiser and Kalbitz, 2012; Klaminder et al., 2011). This line of reasoning was

recently shown to apply also to deep organic permafrost soils (Zhang et al., 2017), although the degree to which this is the case in comparison to mineral soils is as yet unknown.

In addition, and as described in Part 1 (Section 2.5) of this study, MICT-L contains a provision for increased soil column infiltration and lower decomposition rates in areas underlain by Podzols and Arenosols. The map from the Harmonized World Soil Database (Nachtergaele, 2010), which is used as the input to this criterion, shows areas underlain by these soils in the Lena basin to also be co-incident with areas of high topographic slope (Fig. 3a, SI, Fig S3b). The 'Podzol effect' is to increase the rate of decomposition and infiltration of DOC, relative to all other soil types, thus also increasing the rate of DOC flux into groundwater (see Part 1 of this study, Section 2.5). Thus, our modelling framework explicitly resolves the processes involved in these documented dynamics –soil thermodynamics, solid vertical flow (turbation), infiltration as a function of soil textures and types, adsorption as a function of soil parameters (see Part 1 of this study, Section 2.11), DOC respiration as a function of soil temperature and hence depth (Part 1, Section 2.12), and lagging of DOC vertical flow behind hydrological drainage flow (summary Figure in Part 1, Fig. 1). We thus have some confidence in reporting that the simulated negative relationship of DOC concentration with topographic slope may indeed emerge from the model.

5.1.2 LOAC drivers

The constant climate (CLIM) and constant CO₂ (CO2) simulations described in Section 3 were undertaken to assess the extent –and the extent of the difference –to which these two factors are drivers of model processes and fluxes. These differences are summarised in Figs. 12(b-c), in which we show the same 1998-2007 –averaged yearly variable fluxes as in the CTRL simulation, expressed as percentages of the CTRL values given in Fig. 2. A number of conclusions can be drawn from these diagrams.

First, all fluxes are lower in the factorial simulations, which can be expected due to lower carbon input to vegetation from the atmosphere (constant CO₂) and colder temperatures (constant climate) inhibiting more vigorous growth and carbon cycling. Second, broadly speaking, both climate and CO₂ appear to have similar effects on all fluxes, at least within the range of climatic and CO₂ values to which they have subjected the model in these historical runs. With regard to lateral export fluxes in isolation, variable climate (temperature increase) is a more powerful driver than CO₂ increase (see below). Third, the greatest difference between the constant climate and CO₂ simulation carbon fluxes appear to be those associated with terrestrial inflow of dissolved matter to the aquatic network, these being more sensitive to climatic than CO₂ variability. This is evidenced by a 49% and 32% decline in CO₂ and DOC export, respectively, from the land to rivers in the constant climate simulation, versus a 27% and 23% decline in these same variables in the constant CO₂ simulation. Given that the decline in primary production and respiration in both factorial simulations was roughly the same, this difference in terrestrial dissolved input is

attributable to the effect of climate (increased temperatures) on the hydrological cycle, driving changes in lateral export fluxes.

This would imply that at these carbon dioxide and climatic ranges, the modelled DOC inputs are slightly more sensitive to changes in the climate rather than to changes in atmospheric carbon dioxide concentration and the first order biospheric response to this. However, while the model biospheric response to carbon dioxide concentration may be linear, thresholds in environmental variables such as MAAT may prove to be tipping points in the system's emergent response to change, as implied by Fig. 9, meaning that the Lena, as with the Arctic in general, may soon become much more temperature-dominated with regard to the drivers of its own change.

Page 15 : [18] Supprimé

Simon Bowring

08/10/19 16:52

Table 2: Mean observed groundwater CO₂ and DOC concentrations for global permafrost regions subdivided by biogeographic province and compiled by Shvartsev (2008) from over 9000 observations.

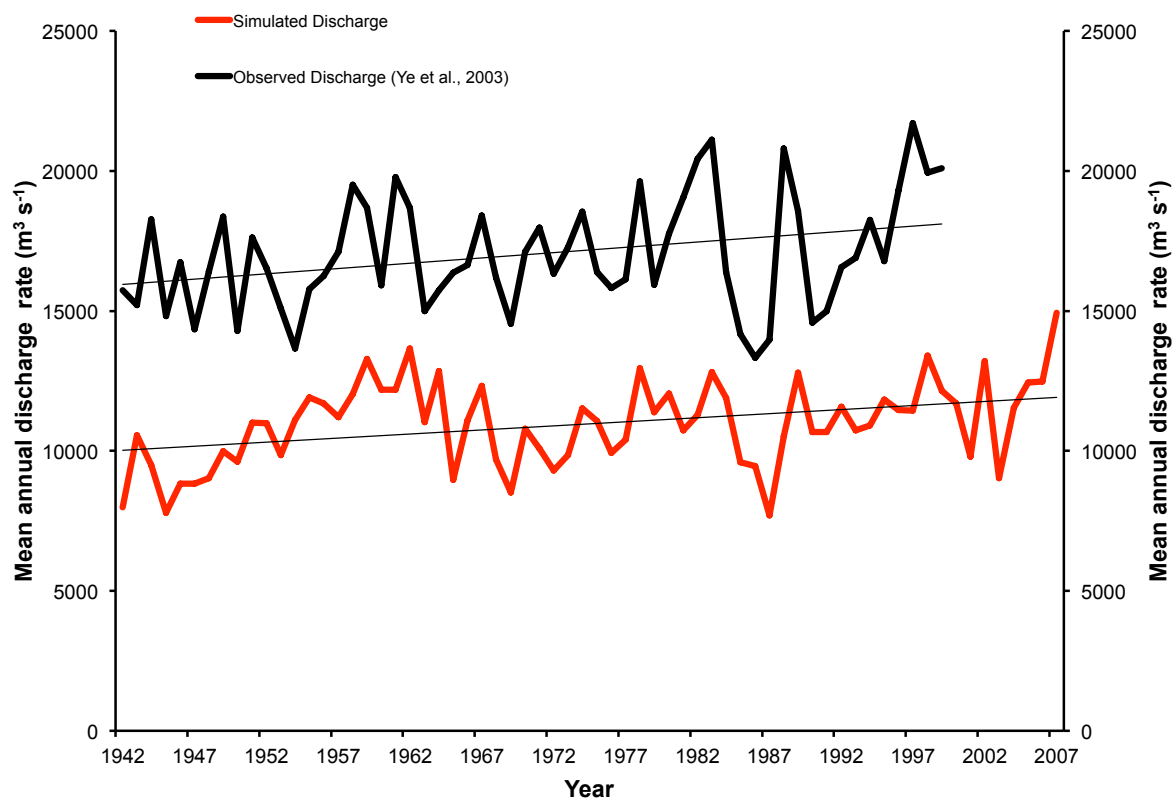
	Permafrost Groundwater Provinces				
	Swamp	Tundra	Taiga	Average	Average (-Swamp)
CO ₂ (mgC L ⁻¹)	12.3	14	10.8	12.4	12.4
DOC (mgC L ⁻¹)	17.6	10.1	9.3	12.3	9.7

Page 19 : [19] Supprimé

Simon Bowring

08/10/19 17:42

(c)



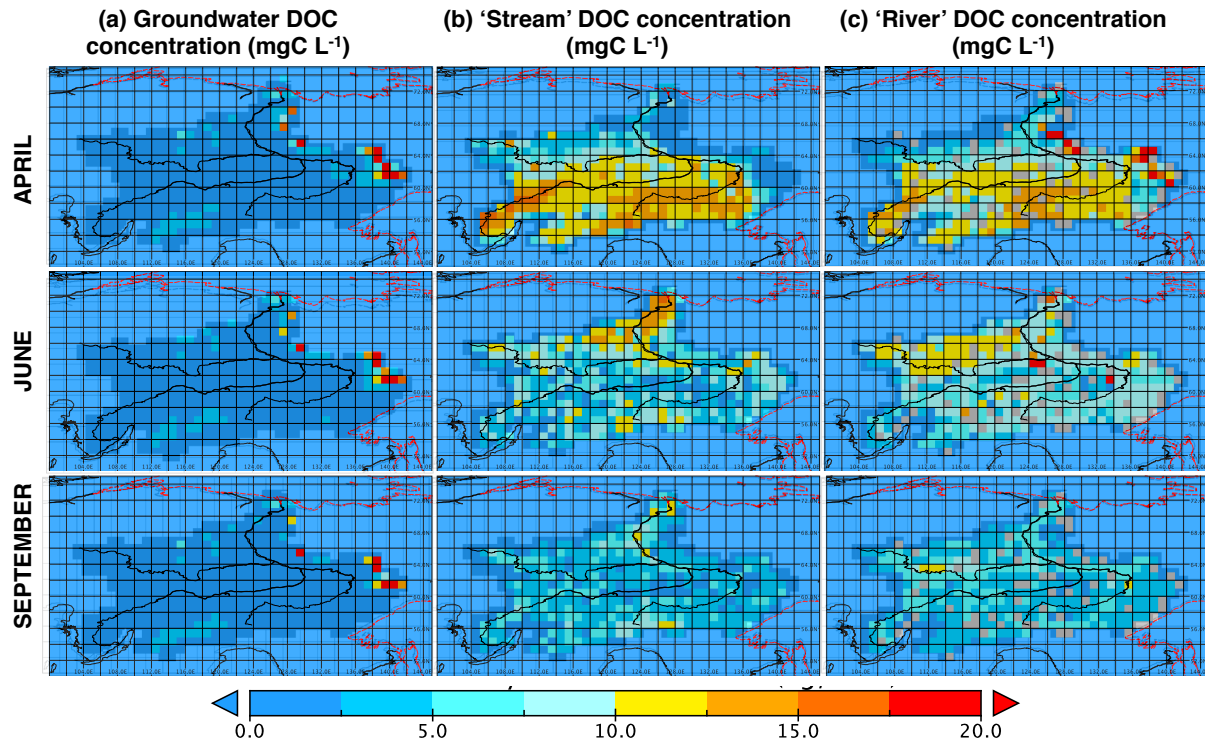


Figure 6: Maps of (a) DOC concentrations (mgC L^{-1}) in groundwater ('slow' water pool), (b) stream water pool, (c) river water pool in April, June and September (first to third rows, respectively), averaged over the period 1998-2007. The coastal boundary and a water body overlay have been applied to the graphic in red and black, respectively, and the same scale applies to all diagrams. All maps have the Lena basin area shaded in the background.

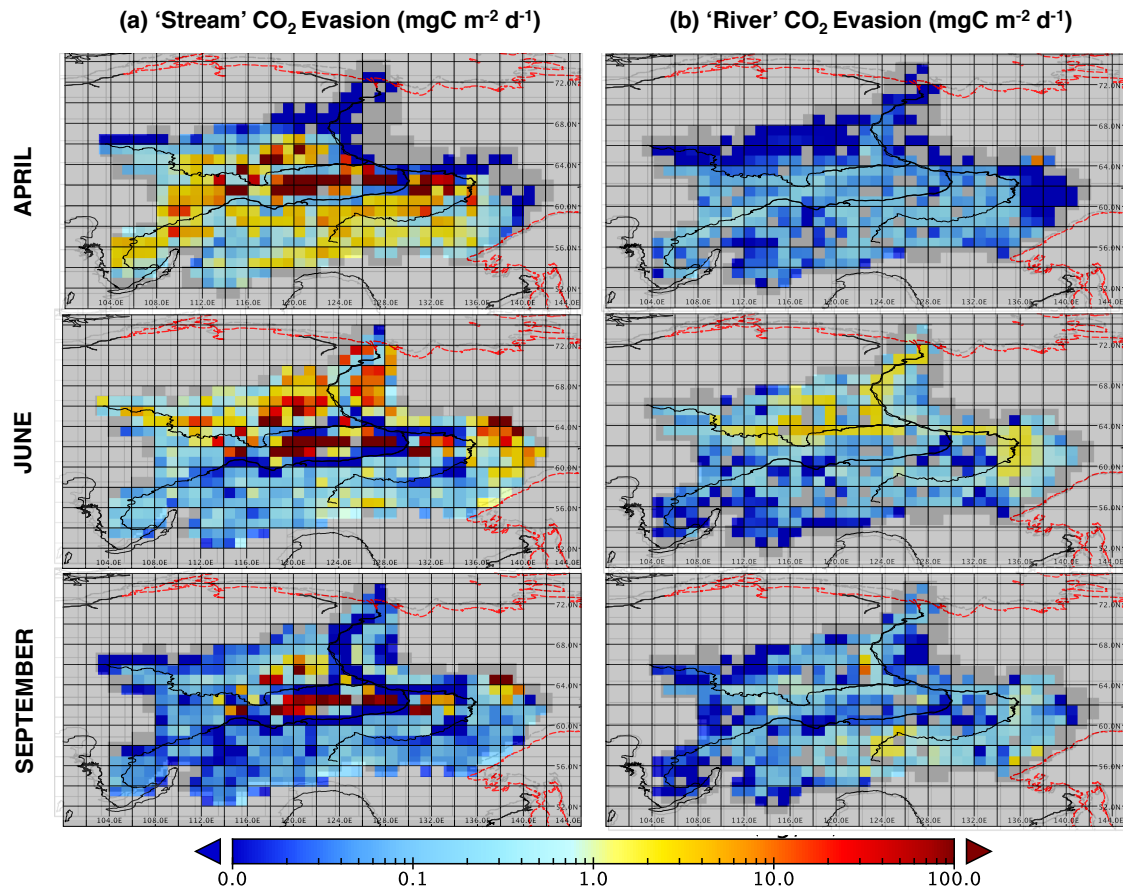
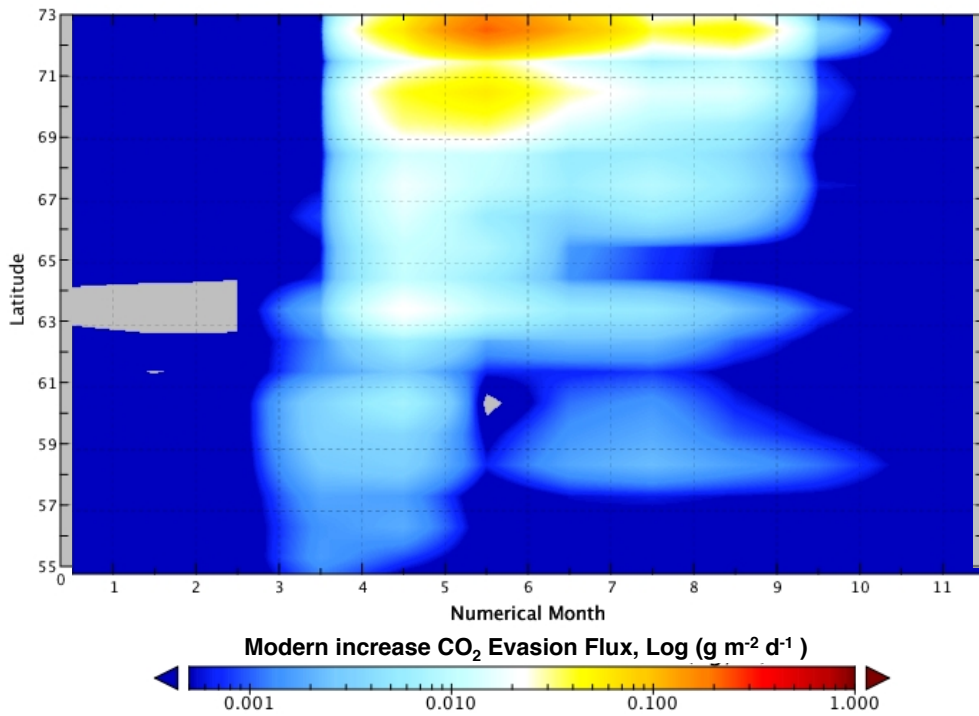
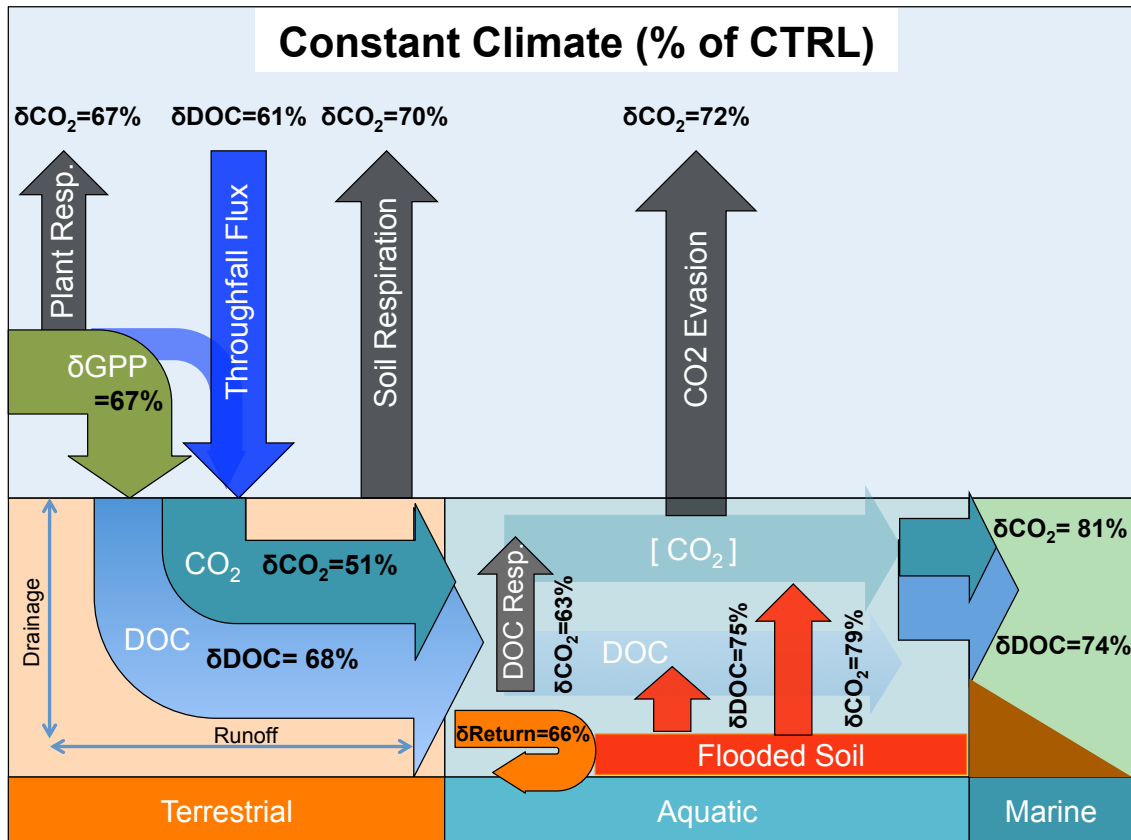


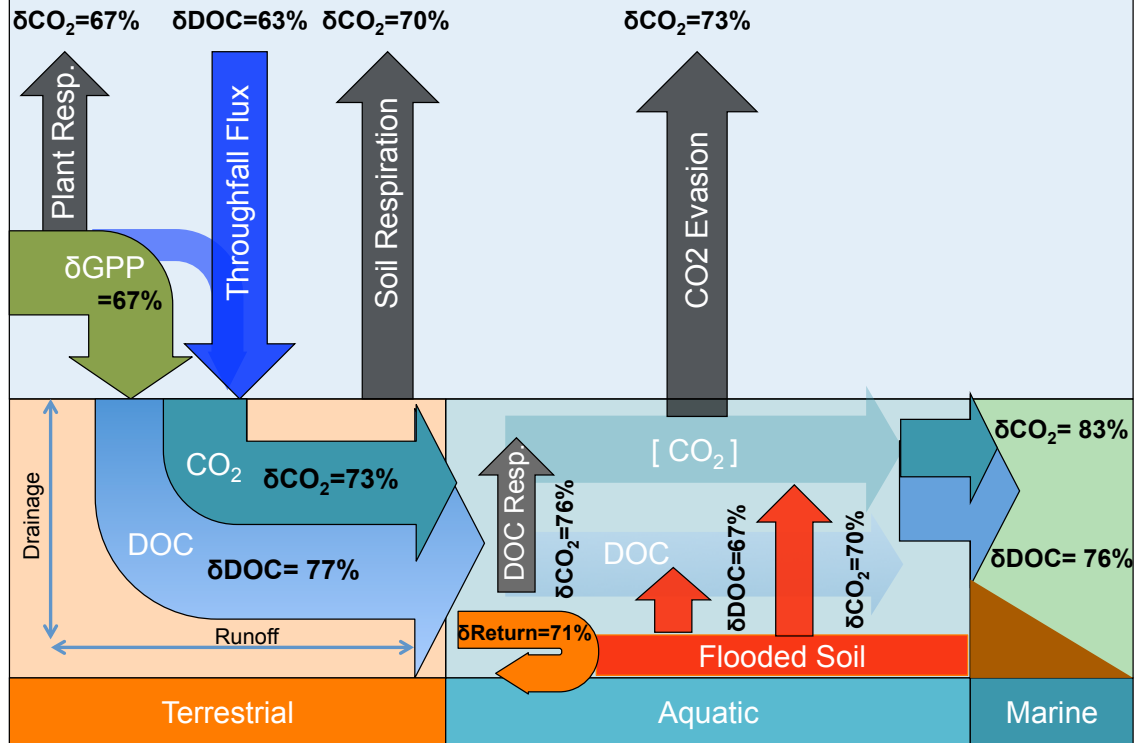
Figure 8: Maps of CO₂ evasion from the surface of the two fluvial hydrological pools in the model, (a) streams and (b) rivers in April, June and September. All maps use the same (log) scale in units of (mgC m⁻² d⁻¹).

(b)



(c)

Constant CO₂ (% of CTRL)



1 **Supplement of**

2
3 **ORCHIDEE MICT-LEAK (r5459), a global model for the production, transport and**
4 **transformation of dissolved organic carbon from Arctic permafrost regions, Part**
5 **2: Model evaluation over the Lena River basin.**

6 **Authors:**

7 S.P.K. Bowring¹, R. Lauerwald², B. Guenet¹, D. Zhu¹, M. Guimbertea^{1,3}, P. Regnier²,
8 A. Tootchi³, A. Ducharme³, P. Ciais¹

9 **Affiliations:**

10 [1] Laboratoire des Sciences du Climat et de l'Environnement, LSCE, CEA, CNRS, UVSQ,
11 91191 Gif Sur Yvette, France

12 [2] Department of Geoscience, Environment & Society, Université Libre de Bruxelles,
13 Bruxelles, Belgium

14 [3] Sorbonne Université, CNRS, EPHE, Milieux environnementaux, transferts et
15 interaction dans les hydrosystèmes et les sols, Metis, 75005 Paris, France

16 **Text S1: Evaluation of Simulated NPP and Soil Respiration**

17 Rates of yearly net primary production (NPP) for Russian and Siberian forests have been
18 inferred in situ from eddy flux and inventory techniques to range from 123-250 gC m⁻²
19 yr⁻¹ (Beer et al., 2006; Lloyd et al., 2002; Roser et al., 2002; Schulze et al., 1999;
20 Shvidenko and Nilsson, 2003). We likewise simulate a broad range of NPP carbon
21 uptake rates, of 61-469 gC m⁻² yr⁻¹ averaged per grid cell over the Lena basin, with a
22 mean value of 210 gC m⁻² yr⁻¹. NPP is heterogeneously distributed over space and
23 between PFTs (SI, Fig. S4c), with forests averaging 90 gC m⁻² yr⁻¹ and grasslands
24 averaging 104 gC m⁻² yr⁻¹ over the basin as a whole. Low values tended to originate in
25 basin grid cells with elevated topography or high mean slope, while the maximum value
26 was standalone, exceeding the next greatest by ~100 gC m⁻² yr⁻¹, and is most likely
27 caused by the edge effects of upscaling a coastal gridcell's small fraction of terrestrial
28 area where high productivity occurs in a small plot, to the grid cell as a whole. By
29 evaluating NPP we are also evaluating at a secondary level litter production, which is at
30 a third level a major component of DOC production.

31 Taken as a whole, gross primary production (GPP) was performed under simulations by
32 four PFT groups, with the largest basin-wide bulk contributions coming from boreal
33 needleleaf summer-green trees and C3 grasses (SI, Fig. S4a), the highest GPP uptake
34 rates (3 TgC pixel⁻¹ yr⁻¹) generated by boreal needleleaf evergreen trees, and the
35 remainder of GPP contributed by Boreal broad-leaved summer-green trees (SI, Fig. S4a).

36 Soil respiration rates, of combined soil heterotroph and plant root respiration in our
37 Control simulation, averaged 208 gC m⁻² yr⁻¹ (0.57 gC m⁻² d⁻¹) over the Lena basin over
38 the period 1990-2000, which is somewhat higher than those found by Elberling (2007)
39 in tundra soils over Svalbard, of 103-176 gC m⁻² yr⁻¹ (0.28-0.48 gC m⁻² d⁻¹). Sawamoto, et
40 al. (2000) measured in situ summertime soil respiration over the central Lena basin and
41 found rates of 1.6-34 gC m⁻² d⁻¹, while Sommerkorn (2008) observed rates of 0.1-3.9 gC
42 m⁻² d⁻¹ at higher latitudes, these appearing to vary with vegetation and fire history.

50 water table depth and temperature. Mean heterotrophic respiration rates of $1.6 \text{ gC m}^{-2} \text{ d}^{-1}$
51 are simulated here during July and August, in the range $0.05-2.2 \text{ gC m}^{-2} \text{ d}^{-1}$ for each of
52 the above PFT groups. The spatial distribution of, and difference in respiration rates
53 between PFT groups largely mirrors those for NPP (SI Fig. S4c), with maximum rates of
54 $1.4 \text{ gC m}^{-2} \text{ d}^{-1}$ over forested sites, versus a maximum of $2.2 \text{ gC m}^{-2} \text{ d}^{-1}$ over
55 grassland/tundra sites (SI, Fig. S4b).

56
57 Aggregated over the basin, results show that increases over the course of the 20th
58 Century were simulated for NPP, GPP, River Discharge, DOC, $\text{CO}_{2(\text{aq})}$, autotrophic and
59 heterotrophic respiration and CO_2 evasion, with percentage changes in the last versus
60 first decade of +25%, +27%, 38%, +73%, +60%, +30%, +33% and +63%, respectively.
61 (Fig. S12). It thus appears that rising temperatures and CO_2 concentrations
62 disproportionately favoured the metabolism of carbon within the soil and its
63 transport and mineralisation within the water column, fed by higher rates of primary
64 production and litter formation as well as an accelerated hydrological cycle.

67 Text S2: Deficiencies in Modelled Hydrology

68
69 Deficiencies in modelled hydrology correspond to those found in Fig. 12 of Guimbarteau
70 et al. (2018), indicating that the modifications made in this model version, which focus
71 on the DOC cycle, have not further degraded the hydrological performance of the model,
72 the causes of which are described below. Low simulated discharge for the Lena basin,
73 particularly during the late summer and autumn, is consistent with prior, Pan-Arctic
74 simulations conducted by Guimbarteau et al. (2018), who ran ORCHIDEE-MICT using
75 both the GSWP3 and CRU-NCEP v7 datasets and evaluated them over the period 1981-
76 2007. Despite the substantially better hydrological performance of ORCHIDEE under
77 GSWP3 climate, they described a near-systematic underestimation of summer/autumn
78 discharge rates for both datasets over the Yukon, Mackenzie, Lena and Kolyma basins.
79 Furthermore, the discrepancy of model output between climatological datasets was
80 almost as large as the discrepancy between model output and observational data in that
81 study, which analysed this in great depth, suggesting that the source of error is both a
82 covariate of model process representation and parameterisation, as well as the
83 climatological datasets themselves. Model hydrological representation and empirically
84 derived climate input data are then subject to interaction with modelled soil (e.g.
85 infiltration), vegetation (e.g. canopy interception) and thermodynamics (e.g. freezing
86 and consequent partitioning of water transport) from which river discharge is
87 computed, confounding full interpretation of sources of bias, briefly described below.

88
89 Model process deficiency in this regard was identified by Guimbarteau et al. (2018) as
90 residing in an overly restrictive representation of water impermeability through frozen
91 topsoil, which decreases the residence time of running water by directing it to surface
92 runoff rather than subsurface flow, and in the process increases the susceptibility of the
93 total water volume to evapotranspiration from incoming shortwave radiation. This
94 would bias both the timing (over-partitioning of water to high runoff periods) and
95 volume of water (low bias) reaching the river stem and its eventual discharge into the
96 ocean, respectively, as demonstrated by model output. Guimbarteau et al. (2018)
97 suggest that representation of sub-grid-scale infiltration mechanisms under frozen
98 conditions, such as soil freezing-drying that would enhance infiltration, be included in

99 future, yet-to-be implemented iterations of ORCHIDEE. Furthermore, we suggest that
100 the lack of representation of lakes in ORCHIDEE, which serve to increase the time lag
101 between precipitation/melt and oceanic discharge, may likewise be a powerful source of
102 bias in the timing of discharge fluxes represented by the model.

103
104 Unsurprisingly, simulated surface runoff has been shown to be strongly affected by
105 differences in precipitation between datasets (Biancamaria et al., 2009; Fekete et al.,
106 2004), while biases in these and evapotranspiration datasets that are used to both drive
107 and evaluate the hydrological models, are a powerful source of water balance biases in
108 high-latitude basins (Wang et al., 2015). Indeed, climatological dataset estimates for the
109 spatial distribution of high latitude winter snowfall are generally problematic, owing to
110 the low density of meteorological stations (Burke et al., 2013), wind-related issues with
111 in-field collection and measurement that lead to systematic underestimates of snowfall
112 rates (Yang et al., 2005), creating biases in the climatological datasets that only show up
113 when the integrator of their model input -in this case river discharge -is modelled. In
114 addition, the wintertime partitioning of precipitation between rain and snow, a function
115 of 2m air temperatures in the forcing datasets, strongly affects the volume and timing of
116 runoff (Guimberteau et al., 2018; Haddeland et al., 2011). Indeed, 69% of the spatial
117 variance of the spring freshet has been attributed to snow water-equivalent bias during
118 the pre-melt season (Rawlins et al., 2007). In addition, errors in forcing of soil
119 evaporation due to inaccuracies in incoming shortwave radiation, as well as biases in the
120 parameterisation of canopy interception -a function of simulated LAI -can lead to
121 upward biases in evapotranspiration rates (Guimberteau et al., 2018).

122 123 **Text S3: Deficiencies in Modelled DOC Discharge**

124
125 Firstly, there is a quasi-linear positive relationship between DOC discharge and river
126 discharge (Fig. 3d). This relation is common to Arctic rivers, as DOC loading experiences
127 disproportionately large increases with increases in discharge (Fig. 4, Raymond et al.,
128 2007), owing largely to the 'flushing' out of terrestrially fixed carbon from the previous
129 year's production by the massive runoff generated by ice and snow melt during the
130 spring thaw. Comparing simulated annual mean discharge rate ($m^3 s^{-1}$) with long-term
131 observations (Ye et al. 2003) over years 1940-2000 (Fig. S3) shows that though absolute
132 discharge rates are underestimated by simulations, their interannual variation
133 reasonably tracks the direction and magnitude of observations. Linear regressions
134 through each trend yield very similar yearly increases of 29 vs 38 $m^3 s^{-1} yr^{-1}$ for
135 simulations and observations, respectively. The observed vs. simulated mean annual
136 water discharge differential hovers at 36% (Figs. 3d, 4c), close to the 43% differential
137 between observed and simulated DOC discharge, giving some indication that, given the
138 linear relationship between water and DOC discharge, most of the DOC discrepancy can
139 be explained by the performance of the hydrology and not the DOC module, the latter of
140 which was the subject of developments added in ORCHIDEE M-L. Applying the
141 regression slope of the relationship in Fig. 3d (9E-06 mgC per $m^3 s^{-1}$) to the mean river
142 discharge discrepancy of 36%, we find that 84% of the differential between observed
143 and simulated discharge can be explained by the underperformance of the hydrology
144 module.

145
146 Further sources of error are process exclusion and representation/forcing limitations.
147 Indeed, separate test runs carried out using a different set of climatological input forcing

148 show that changing from the GSWP3 input dataset to input from bias-corrected
149 projections from the IPSL Earth System Model under the second Inter-Sectoral Impact
150 Model Intercomparison Project (ISIMIP2b (Frieler et al., 2017; Lange, 2016, 2018))
151 protocol increases DOC discharge to the ocean to 4.14 TgC yr⁻¹ (+37%), largely due to
152 somewhat higher precipitation rates in that forcing dataset (see Table S3). Thus, the
153 choice of input dataset itself introduces a significant degree of uncertainty to model
154 output.

155
156 In addition, this model does not include explicit peatland formation and related
157 dynamics, which is the subject of further model developments (Qiu et al., 2018) yet to
158 be included in this iteration. With peatlands thought to cover ~17% of the Arctic land
159 surface (Tarnocai et al., 2009), and with substantially higher leaching concentrations,
160 this may be a significant omission from our model. The remaining biases likely arise
161 from errors in the interaction of simulated NPP, respiration and DOC production and
162 decomposition, which will impact on the net in and out -flow of dissolved carbon to the
163 fluvial system. However, the DOC relationship with these variables is less clear-cut than
164 with river discharge. Indeed, regressions (Fig. S2) of annual DOC versus NPP (TgC yr⁻¹)
165 show that DOC is highly sensitive to increases in NPP, but is less coupled to it (more
166 scattered, $R^2=0.42$) than other simulated fluvial carbon variables shown, i.e. aquatic CO₂
167 evasion and soil CO₂ export to the river network. The differences in correlation and
168 slope of the variables in Fig. S2 are expected: aquatic CO₂ evasion is least sensitive yet
169 most tightly coupled to NPP ($R^2=0.52$), while CO₂ export to rivers is intermediate
170 between the two ($R^2=0.43$). The greater correlation with NPP of DOC compared to
171 evasion is understandable, given that DOC leaching is a covariate of both NPP and runoff,
172 whereas evasion flux is largely dependent on organic inputs (production) and
173 temperature (see Part 1).

174 175 **Text S4: Model Evaluation: DOC Discharge Seasonality**

176
177 Figure 4b shows that the bulk of the DOC outflow occurs during the spring freshet,
178 accounting for ~50-70% of the total Arctic outflow (Lammers et al., 2001; Ye et al.,
179 2009), in which DOC concentrations increase, as meltwater flushes out DOC
180 accumulated from the previous year's litter and SOC generation (Raymond et al., 2007;
181 Kutscher et al., 2017), reproduced in Fig. 4b. Simulation of the hydrological dynamic is
182 presented in maps of river discharge through the basin in Fig. 3b, which show low-flows
183 in April with substantial hydrographic flow from upstream mountainous headwaters
184 and Lake Baikal inflow in the south, peak flow in June dominated by headwaters, and
185 little headwater input in September.

186
187 In Fig. 4b we observe the following: (i) DOC discharge fluxes closely track hydrological
188 fluxes. (ii) The simulated modern river discharge peak approximates the historical
189 observed discharge peak, but slightly overestimates spring fluxes and substantially
190 underestimates fluxes in the autumn, as explained above. (iii) The difference between
191 the first and last decades of the simulation in Fig. 4b is mostly attributable to a large
192 increase in the DOC flux mobilised by spring freshet waters. This suggests both greater
193 peaks in simulated DOC flux and a shift to earlier peak timing, owing to an increase in
194 river discharge, indicative of an earlier spring and a progressively warmer environment
195 over the 20th Century. (iv) The maximum modelled modern monthly DOC flux rate of
196 ~1.3 TgC month⁻¹ is comparable to the mean maximum DOC flux rate measured in a

197 recent study (1.75 TgC month⁻¹, Kutscher et al., 2017, Fig. 2).
198

199 We compare the Raymond et al. (2007) modern DOC outflow (Fig. 4d, solid black line)
200 against simulated DOC outflow from both Zhigansk and Kusur (Fig. 4d). Simulated DOC
201 flux is underestimated for both sites. Peakflow at Zhigansk seems to be attenuated over
202 May and June in simulations, as opposed to May peakflow in observations. Peakflow at
203 Kusur is definitively in June. This suggests that simulated outflow timing at Zhigansk
204 may slightly delayed, causing a split in peak discharge when averaged in the model
205 output. Thus the aggregation of model output to monthly averages from calculated daily
206 and 30 minute timesteps can result in the artificial imposition of a normative temporal
207 boundary (i.e. month) on a continuous series. This may cause the less distinctive 'sharp'
208 peak seen in Fig. 4c, which is instead simulated at the downstream Kusur site, whose
209 distance some 500km away from Zhigansk more clearly explains the delay difference in
210 seasonality. We further evaluate our DOC discharge at the sub-basin scale, to test
211 whether the fractional contribution of different DOC flows from each sub-basin
212 correspond to those in their observed correlates from Kutscher et al., (2017). This
213 comparison is depicted in Fig. S5, where the observed and simulated percentage DOC
214 contributions of the Aldan, Vilui, and Upper and Lower Lena sub-basins to total flux
215 rates are 19 (24%), 20(10%), 33 (38%) and 30 (28)% in simulations (observations) for
216 the four sub-basins, respectively. While deviations between simulated and observed
217 DOC fluxes can be expected, the nearly twofold value mismatch of the Vilui basin is due
218 to its real-word damming, not represented here. On the other hand, we cannot explain
219 the ~5% discrepancies in other sub-basin fluxes, particularly for the Aldan.
220

221 **Text S5: Evaluation of Modelled DOC Concentrations in Stream, River, Ground
222 Water**

223 The spatial distribution of DOC concentrations are shown in maps of mean monthly DOC
224 concentration for stream water, river water and groundwater (Fig. S6a,b,c, respectively)
225 in April, June and September. For both the stream and river water reservoirs, DOC
226 concentrations appear to have spatio-temporal gradients correlated with the flux of
227 water over the basin during the thaw period, with high concentrations of 10-15 mgC L⁻¹
228 driven by April meltwaters upstream of the basin, these high concentrations moving
229 northward to the coldest downstream regions of the basin in June. Lower DOC
230 concentrations of ~5 mgC L⁻¹ dominate the basin in September when the bulk of
231 simulated lateral flux of DOC has dissipated into the Laptev Sea. In contrast,
232 groundwater DOC concentrations are generally stable with time, although some pixels
233 appear to experience some 'recharge' in their concentrations during the first two of the
234 three displayed thaw months. Significantly, highest groundwater DOC concentrations of
235 up to 20 mgC L⁻¹ are focussed on the highest elevation areas of the Lena basin on its
236 Eastern boundary, which are characterized by a dominance of Podzols (SI, Fig. S9b).
237 This region, the Verkhoyansk range, is clearly visible as the high groundwater DOC
238 concentration (2-20mgC L⁻¹) arc (in red) in Fig. S6a, as well as other high elevation areas
239 in the south-western portion of the basin (Fig. 3a), while the low-lying central basin
240 shows much smaller groundwater DOC concentrations (0-2mgC L⁻¹). The range of
241 simulated groundwater DOC concentration comes close to those aggregated from the
242 empirical literature by Shvartsev (2008), which finds from >9,000 observations that
243 groundwater in permafrost regions exhibit a mean concentration of ~10 mgC L⁻¹ after
244 peatlands and swamps (not simulated here) are removed (Table 2).
245

246
247
248
249
250
251
252
253
254

The high groundwater reservoir DOC concentrations simulated in high altitude regions by ORCHIDEE MICT-L is related to the fact that, in the model, DOC is rapidly produced and infiltrated deep into soil above the permafrost table, to the point that it reaches the simulated groundwater pool relatively quickly, allowing it to enter this reservoir before being metabolised through the soil column -hence allowing for the relatively high groundwater concentrations found in mountain areas. Because of the prevailing low temperatures, this DOC is not quickly decomposed by microbes and instead feed the groundwater DOC pool.

Simon Bowring 8/10/y 16:34
Mis en forme: Éviter veuves et orphelines

255
256

Text S6: Riverine CO₂ Evasion

257
258
259
260
261
262
263
264
265
266
267
268
269
270

In our model, the fate of DOC once it enters the fluvial system is either to remain as DOC and be exported to the ocean, or to be degraded to dissolved CO₂ (CO_{2(aq)}), which is itself either also transported to the marine system or outgassed from the fluvial surface to the atmosphere (see Part 1, Section 2.10). The latter two outcomes also apply to CO_{2(aq)} produced in the soil by organic matter degradation and subsequently transported by runoff and drainage flows to the water column. As shown in Fig. 2, a large proportion of DOC (38%, 2.1 TgC yr⁻¹) that enters the water column is degraded to CO_{2(aq)} during transport, which adds to the 1.65 TgC yr⁻¹ of direct CO_{2(aq)} input from the terrestrial land surface. Of this bulk CO₂ exported into and generated within the water column, 3.6 TgC yr⁻¹ evades from the water surface to the atmosphere before reaching the river delta. In what follows, we evaluate first inputs of CO_{2(aq)} to the water column in terms of their seasonality, before evaluating CO₂ evasion rates and the relation of this to smaller and larger water bodies (river versus stream).

Simon Bowring 8/10/y 15:20
Mis en forme: Police :Gras
Simon Bowring 8/10/y 15:20
Mis en forme: Police :Gras
Simon Bowring 8/10/y 18:13
Mis en forme: Police :Gras, Indice
Simon Bowring 8/10/y 15:20
Mis en forme: Police :Gras

271
272
273
274
275
276
277
278
279
280
281
282
283
284
285
286
287
288
289

To our knowledge, no direct measurements for CO₂ evasion from the surface of the Lena river are available in the literature. We refer to Denfeld et al. (2013) for evaluating our evasion flux results, since their basin of study, the Kolyma River, is the most geographically proximate existing dataset to the Lena, despite biogeographical differences between the two basins -namely that the Kolyma is almost entirely underlain by continuous permafrost. The Kolyma River CO₂ evasion study measured evasion at 29 different sites along the river basin (~158-163°E; 68-69.5°N), with these sites distinguished from one another as 'main stem', 'inflowing river' or 'stream' on the basis of reach length. The study showed that during the summer low-flow period (August), areal river mainstem CO₂ evasion fluxes were ~0.35 gC m⁻² d⁻¹, whereas for streams of stream order 1-3 (widths 1-19m), evasion fluxes were up to ~7 gC m⁻² d⁻¹, and for non-mainstem rivers (widths 20-400m) mean net fluxes were roughly zero (Table 3 of Denfeld et al., 2013). Thus, while small streams have been observed to contribute to roughly 2% of the Kolyma basin surface area, their measured percentage contribution to total basin-wide CO₂ evasion ~40%, whereas for the main stem the surface area and evasion fractions were ~80% and 60%, respectively. Likewise, mean annual evasion rates of <0.8 up to around 7 gC m⁻² d⁻¹ have been found for the Ob and Pur rivers in Western Siberia (Serikova et al., 2018).

Simon Bowring 8/10/y 15:15
Mis en forme: Police :Gras

290
291
292
293
294

Results such as these, in addition to permafrost soil incubation experiments (e.g. Drake et al., 2015; Vonk et al., 2013, 2015b, 2015a) suggest that small streams, which represent the initial (headwater) drainage sites of these basins, rapidly process hydrologically leached carbon to the atmosphere, and that this high-reactivity carbon is

295 a mix of recently thawed ancient permafrost material, as well as decomposing matter
296 from the previous growth year. This is given as evidence that the total carbon
297 processing of high-latitude rivers is significantly underestimated if only mainstem
298 carbon concentrations are used in the accounting framework, since a large amount of
299 carbon is metabolised to the atmosphere before reaching the site of measurement.
300

301 **Text S7: Spatio-Temporal Heterogeneity in CO₂ Evasion**

302
303 The heterogeneity of CO₂ evasion from different sources in the model is most evident in
304 terms of their geographic distribution and relative intensity, as shown in the evasion
305 flux rate maps over stream and river areas in April, June and September (Fig. S8a-b). Stream
306 evasion (Fig. S8a), tends to be broadly distributed over the whole basin,
307 representing the fact that small streams and their evasion are the main hydrologic
308 connectors outside of the main river and tributary grid cells, whereas river evasion (Fig.
309 S8b) is clearly linked to the hydrographic representation of the Lena main stem itself,
310 with higher total quantities in some individual grid cells than for the stream reservoir,
311 yet distributed amongst a substantially smaller number of grid cells. Whereas the
312 stream reservoir has greatest absolute evasion flux rates earlier in the year (April-May),
313 maximum evasion rates occur later in the year and further downstream for the river
314 reservoir, reflecting the fact that headwaters are first-order integrators of soil-water
315 carbon connectivity, whereas the river mainstem and tributaries are of a secondary
316 order.
317

Simon Bowring 8/10/y 15:28

Mis en forme: Police :Gras

Simon Bowring 8/10/y 15:28

Mis en forme: Police :Gras

318 The spatio-temporal pattern of increasing evasion over the simulation period is shown
319 in Fig. S7 as a Hovmöller difference plot, between the last and first decade, of log-scale
320 average monthly evasion rates per latitudinal band. This shows that the vast majority of
321 outgassing increase occurs between March and June, corresponding to the progressive
322 onset of the thaw period moving northwards over this timespan. Although relatively
323 small, outgassing increases are apparent for most of the year, particularly at lower
324 latitudes. This would suggest that the change is driven most acutely by relatively greater
325 temperature increases at higher latitudes ('Arctic amplification' of climate warming, e.g.
326 Bekryaev et al., 2010) while less acute but more temporally homogenous evasion is
327 driven by seasonal warming at lower latitudes.
328

329 **Text S8:**

330
331 This is because in ORCHIDEE MICT-L, the 'stream' water reservoir is water routed to the
332 river network for all hydrologic flows calculated to not cross a 0.5 degree grid cell
333 boundary (the resolution of the routing module, explained in Part 1, Section 2.6), which
334 may not be commensurate with long, <20m width streams in the real-world, that were
335 used in the Denfeld et al. (2013) study. In addition, this 'stream' water reservoir in the
336 model does not include any values for width or area in the model, so we cannot directly
337 compare our stream reservoir to the <20m width criterion employed by Denfeld et al.
338 (2013) in their definition of an observed stream. Thus our 'stream' water reservoir
339 encompasses substantially greater surface area and hydrologic throughput than that in
340 the Denfeld et al. study.
341

Simon Bowring 8/10/y 15:42

Mis en forme: Police :Gras

342 **Text S9:**

343

344 The 'approximate' caveat refers to the fact that model output doesn't define a precise
345 surface area for the stream water reservoir, which is instead bundled into a single value
346 representing the riverine fraction of a grid cell's total surface area. To approximate the
347 areal outgassing for the stream versus river water reservoirs, we weight the total non-
348 floodplain inundated area of each grid cell by the relative total water mass of each of the
349 two hydrological pools, then divide the total daily CO₂ flux simulated by the model by
350 this value. The per-pool areal estimate is an approximation since it assumes that rivers
351 and streams have the same surface area: volume relationship. This is clearly not the
352 case, since streams are generally shallow, tending to have greater surface area per
353 increment increase in depth than rivers. Thus, our areal approximations are likely
354 underestimated (overestimated) for streams (rivers), respectively. Note that from ~700
355 non-zero simulation datapoints used to generate Fig. 6d were omitted as 'outliers' from
356 the stream reservoir efflux statistics described below, because very low stream:river
357 reservoir values skewed the estimation of total approximate stream surface area values
358 very low, leading to extreme efflux rate values of 1-3000gC m⁻² d⁻¹ and are thus
359 considered numerical artefacts of the areal approximation approach used here.
360
361

362 Text S10: Emergent Phenomena: DOC and Topographic Slope

363
364 This relationship was found in temperate rivers by Lauerwald et al. (2012), and in a
365 recent Pan-Arctic synthesis paper Connolly et al. (2018). The reasoning for the negative
366 slope-DOC concentration relationship is that as elevation increases, temperature and
367 primary production decreases. This leads to a thinner organic soil layer, meaning that
368 mineral soil plays a stronger role in shallow hydrologic flowpaths, allowing for deeper
369 infiltration and shorter residence time in a given soil layer. Further, steeper terrain
370 leads to a lower soil water residence time and lower moisture than in flat areas. As a
371 result, a given patch of soil matter will be exposed to leaching for less (residence) time,
372 while the organic matter that is leached is thought to be adsorbed more readily to
373 mineral soil particles, leading to either their re-stabilisation in the soil column or
374 shallow retention and subsequent heterotrophic respiration in situ, cumulatively
375 resulting in lower DOC concentrations in the hydrologic export (Kaiser and Kalbitz,
376 2012; Klaminder et al., 2011). This line of reasoning was recently shown to apply also to
377 deep organic permafrost soils (Zhang et al., 2017), although the degree to which this is
378 the case in comparison to mineral soils is as yet unknown.
379

380 In addition, and as described in Part 1 (Section 2.5) of this study, MICT-L contains a
381 provision for increased soil column infiltration and lower decomposition rates in areas
382 underlain by Podzols and Arenosols. The map from the Harmonized World Soil Database
383 (Nachtergaele, Freddy, Harrij van Velthuizen, Luc Verelst, N. H. Batjes, Koos Dijkshoorn,
384 V. W. P. van Engelen, Guenther Fischer, Arwyn Jones, Luca Montanarella, Monica Petri,
385 Sylvia PrielerB, Xuezheng Shi, Edmar Teixera and David Wiberg, 2010), which is used as
386 the input to this criterion, shows areas underlain by these soils in the Lena basin to also
387 be co-incident with areas of high topographic slope (Fig. 3a, SI, Fig S9b). The 'Podzol
388 effect' is to increase the rate of decomposition and infiltration of DOC, relative to all
389 other soil types, thus also increasing the rate of DOC flux into groundwater (see Part 1 of
390 this study, Section 2.5). Thus, our modelling framework explicitly resolves the
391 processes involved in these documented dynamics –soil thermodynamics, solid vertical
392 flow (turbation), infiltration as a function of soil textures and types, adsorption as a

Simon Bowring 8/10/y 15:57
Mis en forme: Police :Gras

393 function of soil parameters (see Part 1 of this study, Section 2.11), DOC respiration as a
394 function of soil temperature and hence depth (Part 1, Section 2.12), and lagging of DOC
395 vertical flow behind hydrological drainage flow (summary Figure in Part 1, Fig. 1). We
396 thus have some confidence in reporting that the simulated negative relationship of DOC
397 concentration with topographic slope may indeed emerge from the model.
398

399 **Text S11: Emergent Phenomena: DOC and Mean Annual Air Temperature**

400
401 A key emergent property of DOC concentrations in soils and inland waters should be
402 their positive partial determination by the temperature of the environment under which
403 their rates of production occur, as has been shown in the literature on permafrost
404 regions, most notably in Frey & Smith (2005) and Frey & McClelland (2009). Increasing
405 temperatures should lead to greater primary production, thaw, decomposition and
406 microbial mobilisation rates, and hence DOC production rates, leading to (dilution
407 effects notwithstanding) higher concentrations of DOC in thaw and so stream waters.
408 Looking at this emergent property allows us to evaluate the soil-level production of both
409 DOC and thaw water at the appropriate biogeographic and temporal scale in our model.
410 This provides a further constraint on model effectiveness at simulating existing
411 phenomena at greater process-resolution.
412

413 Figure 7 compares three datasets (simulated and two observational) of riverine DOC
414 concentration (in mgC L^{-1}) plotted against mean annual air temperature (MAAT). The
415 simulated grid-scale DOC versus MAAT averaged over July and August (for
416 comparability of DOC with observational sampling period) of 1998-2007 is shown in
417 red, and observed data compiled by Laudon et al. (2012) and Frey and Smith (2005) for
418 sites in temperate/cold regions globally and peatland-dominated Western Siberia,
419 respectively. The Laudon et al. (2012) data are taken from 49 observations including
420 MAAT over the period 1997-2011 from catchments north of 43°N , and aggregated to 10
421 regional biogeographies, along with datapoints from their own sampling; those in the
422 Frey and Smith study are from $55\text{--}68^\circ\text{N}$ and $\sim 65\text{--}85^\circ\text{E}$ (for site locations, see Laudon et
423 al. (2012), Table 1 and 2; Frey and Smith (2005), Fig. 1).
424

425 Fig. 7 can be interpreted in a number of ways. First, this MAAT continuum spans the
426 range of areas that are both highly and moderately permafrost affected and permafrost
427 free (Fig. 7, blue and green versus orange shading, respectively), potentially allowing us
428 a glimpse of the behaviour of DOC concentration as the environment transitions from
429 the former to the latter. Simulated Lena DOC concentrations, all in pixels with $\text{MAAT} < -2^\circ\text{C}$
430 and hence all bearing continuous or discontinuous permafrost ('permafrost-
431 affected' in the figure), only exhibit a weakly positive response to MAAT on the scale
432 used ($y=6.05e^{0.03\text{MAAT}}$), although the consistent increase in DOC minima with MAAT is
433 clearly visible. Second, the Laudon et al. (2012) data exhibit an increasing then
434 decreasing trend over the range of MAAT (-2°C to 10°C) in their dataset, which they
435 propose reflects an 'optimal' MAAT range ($0\text{--}3^\circ\text{C}$) for the production and transport of
436 DOC (Fig. 7, red shading). Below this optimum range, DOC concentrations may be
437 limited by transport due to freezing, and above this, smaller soil carbon pools and
438 temperature-driven decomposition would suppress the amount of DOC within rivers.
439 Third, the lower end of the Laudon et al. (2012) MAAT values correspond to a DOC
440 concentration in line with DOC concentrations simulated by our model. Fourth, DOC
441 concentrations in the Frey and Smith (2005) data exhibit a broad scattering in

442 permafrost-affected sites, with concentrations overlapping those of our simulations (Fig.
443 7, green shading), before rapidly increasing to very high concentrations relative to the
444 Laudon et al. (2012) data, as sites transition to permafrost-free (red shading,
445 $y=3.6_{MAAT}+29.4$).
446

447 Their data highlight the difference in DOC concentration regime between areas of high
448 (Frey and Smith, 2005) and low (Laudon et al., 2012) peatland coverage and the
449 different response of these to temperature changes. Fifth, because our simulation
450 results largely correspond with the observed data where the MAAT ranges overlap
451 (green shading), and because our model lacks peatland processes, we should expect our
452 model to follow the polynomial regression plotted for the Laudon et al. (2012) data as
453 temperature inputs to the model increase. Figure 7 implies that this increase should be
454 on the order of a doubling of DOC concentration as a system evolves from a MAAT of -
455 2°C to 2°C. With warming, we expect the response of DOC concentrations to reflect a
456 mix of both observationally-derived curves, as a function of peatland coverage.
457

458 **Text S12: LOAC drivers**

459
460 The constant climate (CLIM) and constant CO₂ (CO2) simulations described in Section 3
461 were undertaken to assess the extent –and the extent of the difference –to which these
462 two factors are drivers of model processes and fluxes. These differences are
463 summarised in Figs. S10 (a-b), in which we show the same 1998-2007 –averaged yearly
464 variable fluxes as in the CTRL simulation, expressed as percentages of the CTRL values
465 given in Fig. 2. A number of conclusions can be drawn from these diagrams.
466

467 First, all fluxes are lower in the factorial simulations, which can be expected due to
468 lower carbon input to vegetation from the atmosphere (constant CO₂) and colder
469 temperatures (constant climate) inhibiting more vigorous growth and carbon cycling.
470 Second, broadly speaking, both climate and CO₂ appear to have similar effects on all
471 fluxes, at least within the range of climatic and CO₂ values to which they have subjected
472 the model in these historical runs. With regard to lateral export fluxes in isolation,
473 variable climate (temperature increase) is a more powerful driver than CO₂ increase
474 (see below). Third, the greatest difference between the constant climate and CO₂
475 simulation carbon fluxes appear to be those associated with terrestrial inflow of
476 dissolved matter to the aquatic network, these being more sensitive to climatic than CO₂
477 variability. This is evidenced by a 49% and 32% decline in CO₂ and DOC export,
478 respectively, from the land to rivers in the constant climate simulation, versus a 27%
479 and 23% decline in these same variables in the constant CO₂ simulation. Given that the
480 decline in primary production and respiration in both factorial simulations was roughly
481 the same, this difference in terrestrial dissolved input is attributable to the effect of
482 climate (increased temperatures) on the hydrological cycle, driving changes in lateral
483 export fluxes.
484

485 This would imply that at these carbon dioxide and climatic ranges, the modelled DOC
486 inputs are slightly more sensitive to changes in the climate rather than to changes in
487 atmospheric carbon dioxide concentration and the first order biospheric response to
488 this. However, while the model biospheric response to carbon dioxide concentration
489 may be linear, thresholds in environmental variables such as MAAT may prove to be
490 tipping points in the system's emergent response to change, as implied by Fig. 7.

491 | meaning that the Lena, as with the Arctic in general, may soon become much more
492 | temperature-dominated with regard to the drivers of its own change.
493 |
494 |
495 | **Supplementary Tables and Figures**
496 |
497 | **Table S1:** Data type, name and sources of data files used to drive the model in the study
498 | simulations.
499 |
500 |

Simon Bowring 8/10/y 16:34
Supprimé: Text S1: Groundwater DOC
Concentrations ... [1]
Simon Bowring 8/10/y 16:53
Mis en forme: Police :Gras

Data Type	Name	Source
Vegetation Map	ESA CCI Land Cover Map	(Bontemps et al., 2013)
Topographic Index	STN-30p	(Vorosmarty et al., 2000)
Stream flow direction	STN-30p	Vörösmarty et al., 2000
River surface area		(Lauerwald et al., 2015)
Soil texture class		(Reynolds et al., 1999)
Climatology	GSPW3 v0, 1 degree	http://hydro.iis.u-tokyo.ac.jp/GSPW3/
Potential floodplains	Multi-source global wetland maps	(Tootchi et al., 2019)
Poor soils	Harmonized World Soil Database map	(Nachtergaele, Freddy, Harrij van Velthuizen, Luc Verelst, N. H. Batjes, Koos Dijkshoorn, V. W. P. van Engelen, Guenther Fischer, Arwyn Jones, Luca Montanarella, Monica Petri, Sylvia PrielerB, Xuezheng Shi, Edmar Teixera and David Wiberg, 2010)
Spinup Soil Carbon Stock	20ky ORCHIDEE-MICT soil carbon spinup	(Guimberteau et al., 2018)

501 |
502 | **Table S2:** Literature sources for empirical evaluation of model output.
503 |

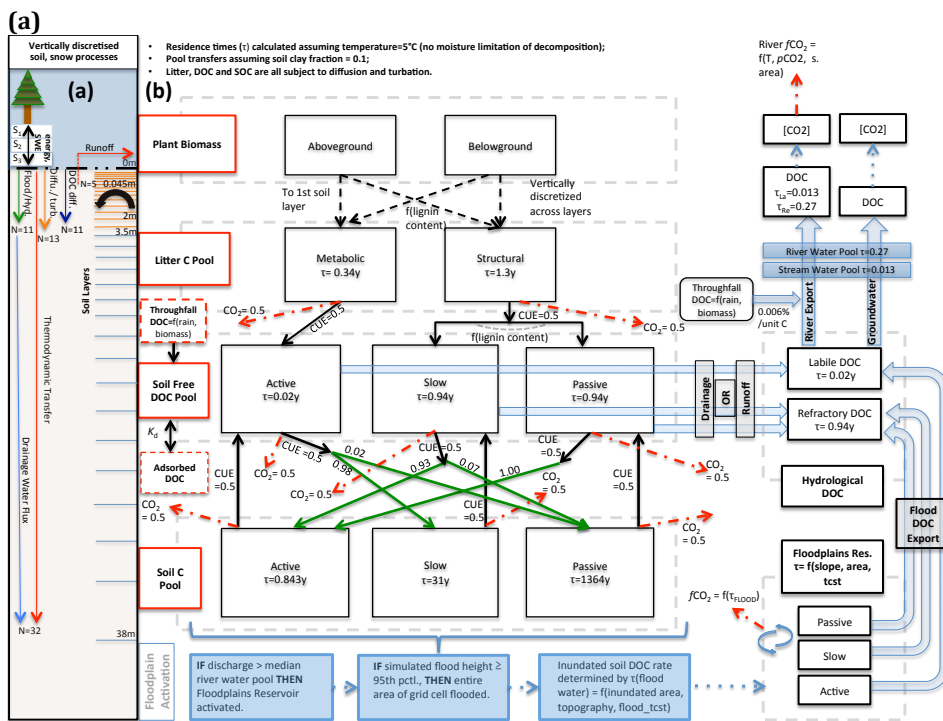
Empirical Evaluation Sources	
DOC Discharge	Cauwet and Sidorov (1996); Dolman et al. (2012); Holmes et al. (2012); Lara et al. (1998); Raymond et al. (2007); Semiletov et al. (2011); Kutscher et al. (2017).
Water Discharge	Ye et al. (2009); Lammers et al. (2001)
DOC concentration	Shvartsev (2008); Denfeld et al. (2013); Mann et al. (2015); Raymond et al. (2007); Semiletov et al. (2011); Arctic-GRO/PARTNERS (Holmes et al., 2012)
NPP	Beer et al. (2006); Lloyd et al. (2002); Roser et al. (2002); Schulze et al. (1999); Shvidenko and Nilsson, (2003)
Soil Respiration	Elberling (2007); Sawamoto et al. (2000); Sommerkorn (2008).
CO2 Evasion	Denfeld et al. (2013); Serikova et al. (2018).

504 |
505 | **Table S3:** Observed versus simulated DOC discharge (1998-2007), where we compare
506 | the output of two separate climatological datasets used as input to the model (GSPW3
507 | and ISIMIP 2b). Also shown are the simulated versus observed DOC discharge for the six
508 | largest Arctic rivers (the "Big Six") and for the Pan-Arctic as a whole.
509 |

	Simulated DOC to Ocean GSWP3	Simulated DOC to Ocean ISIMIP 2b	Observations (Holmes et al., 2012) PARTNERS/Arctic-GRO	
Lena	3.16	4.14	5.68	
Big 6		19.36	18.11	
Pan-Arctic		32.06	34.04	

513
514
515 **Table S4:** Mean observed groundwater CO_2 and DOC concentrations for global
516 permafrost regions subdivided by biogeographic province and compiled by Shvartsev
517 (2008) from over 9000 observations.
518

	Permafrost Groundwater Provinces			Average	Average (-Swamp)
	Swamp	Tundra	Taiga	Average	Average (-Swamp)
$\text{CO}_2 (\text{mgC L}^{-1})$	12.3	14	10.8	12.4	12.4
$\text{DOC} (\text{mgC L}^{-1})$	17.6	10.1	9.3	12.3	9.7



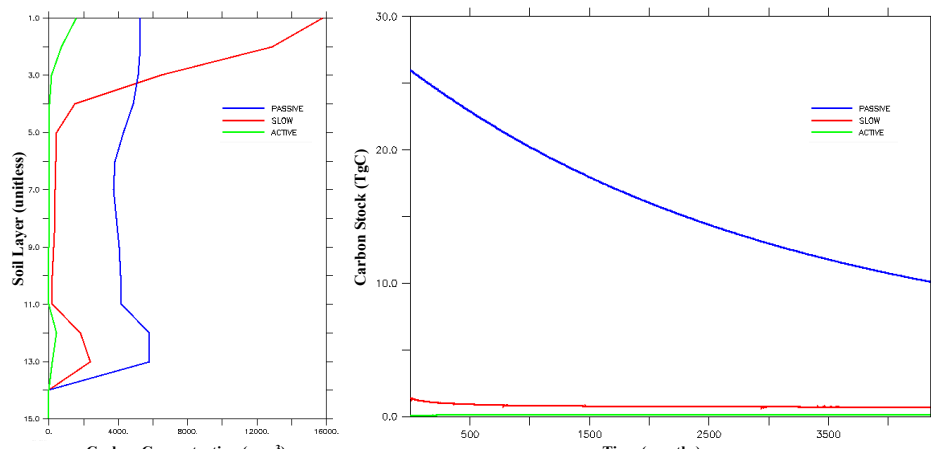
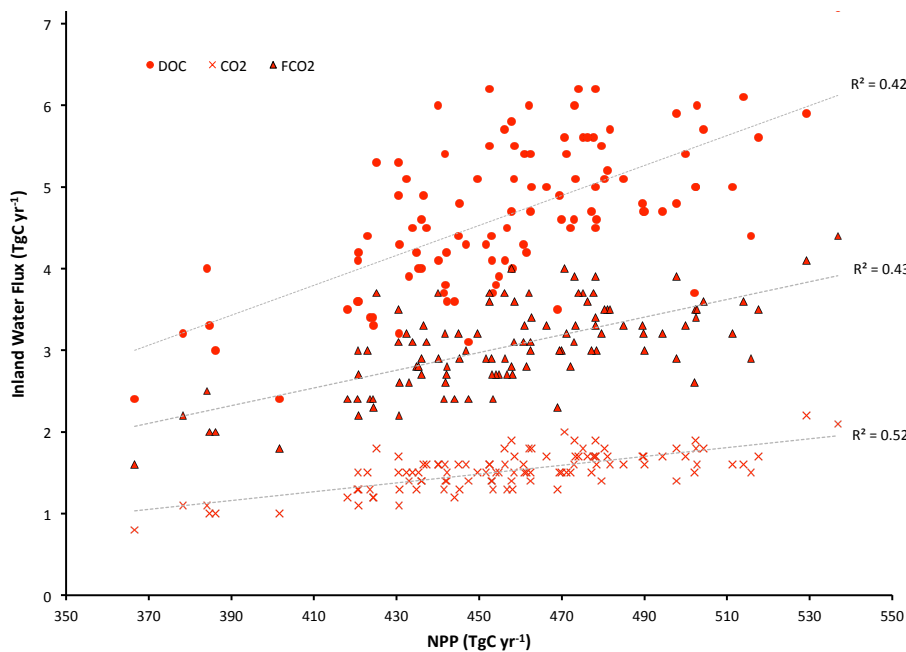
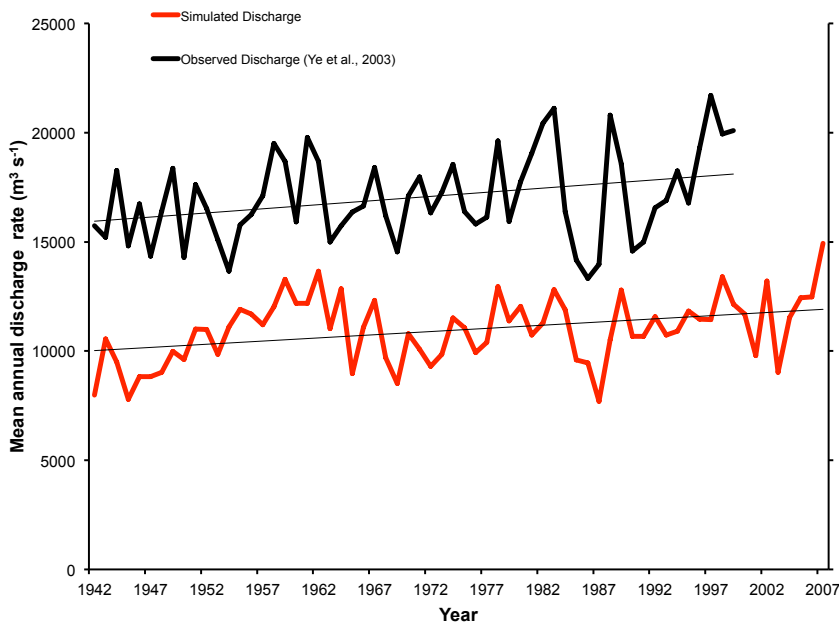


Figure S1: (a-b) Carbon and water flux map for core DOC elements in model structure relating to DOC transport and transformation, first published in Part 1 of this study. **(a)** Summary of the differing extent of vertical discretisation of soil and snow for different processes calculated in the model. Discretisation occurs along 32 layers whose thickness increases geometrically from 0-38m. N refers to the number of layers, SWE=snow water equivalent, S_n = Snow layer n. Orange layers indicate the depth to which diffusive carbon (turbation) fluxes occur. **(b)** Conceptual map of the production, transfer and transformation of carbon in its vertical and lateral (i.e., hydrological) flux as calculated in the model. Red boxes indicate meta-reservoirs of carbon, black boxes the actual pools as they exist in the model. Black arrows indicate carbon fluxes between pools, dashed red arrows give carbon loss as CO_2 , green arrows highlight the fractional distribution of DOC to SOC (no carbon loss incurred in this transfer), a feature of this model. For a given temperature ($5^{\circ}C$) and soil clay fraction, the fractional fluxes between pools are given for each flux, while residence times for each pool (τ) are in each box. The association of carbon dynamics with the hydrological module are shown by the blue arrows. Blue coloured boxes illustrate the statistical sequence which activates the boolean floodplains module. Note that for readability, the generation and lateral flux of dissolved CO_2 is omitted from this diagram, but is described at length in the Methods section. **(c)** (Left) Soil carbon concentrations per depth level for each soil carbon reactivity pool at the end of the spinup period. (Right) Evolution of each soil carbon pool over the course of the 400-year spinup quasi-equilibrium period.



548
549 **Figure S2:** Summed yearly lateral flux versus NPP values for DOC discharge, CO₂
550 discharge and CO₂ evasion (FCO₂) over the entire simulation period, with linear
551 regression lines shown.
552



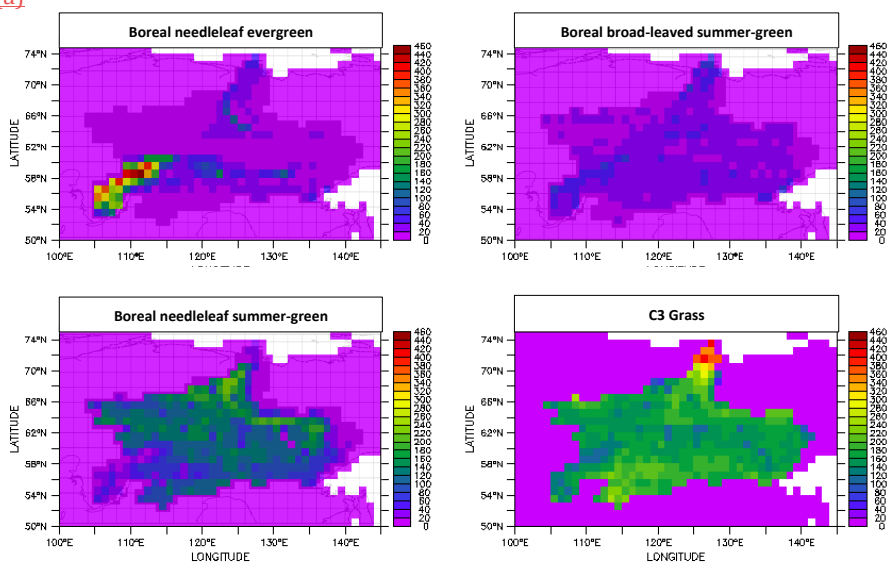
553

Unknown
Mis en forme: Police :Gras

554
555
556
557

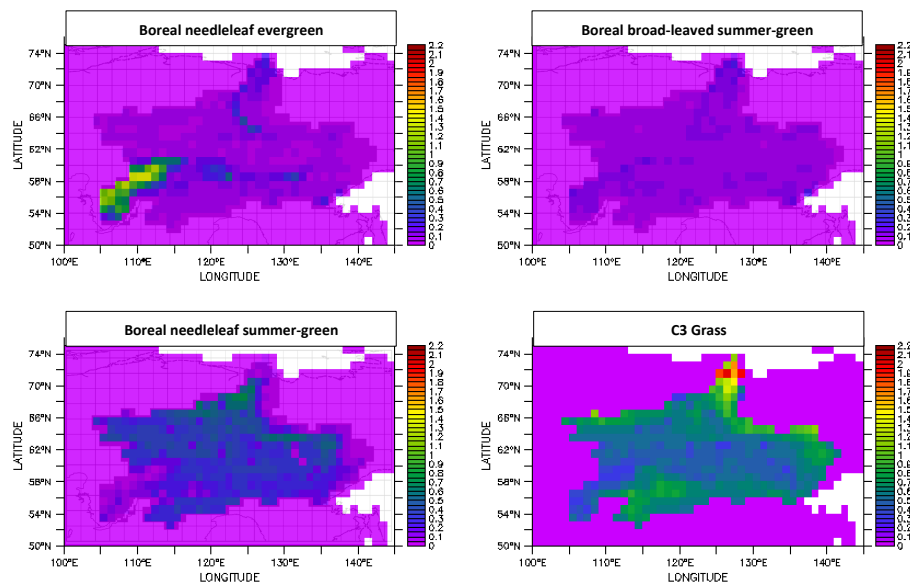
Figure S3: Observed versus simulated mean annual water discharge from the Lena river, where observations are taken from (Ye et al., 2003).

(a)



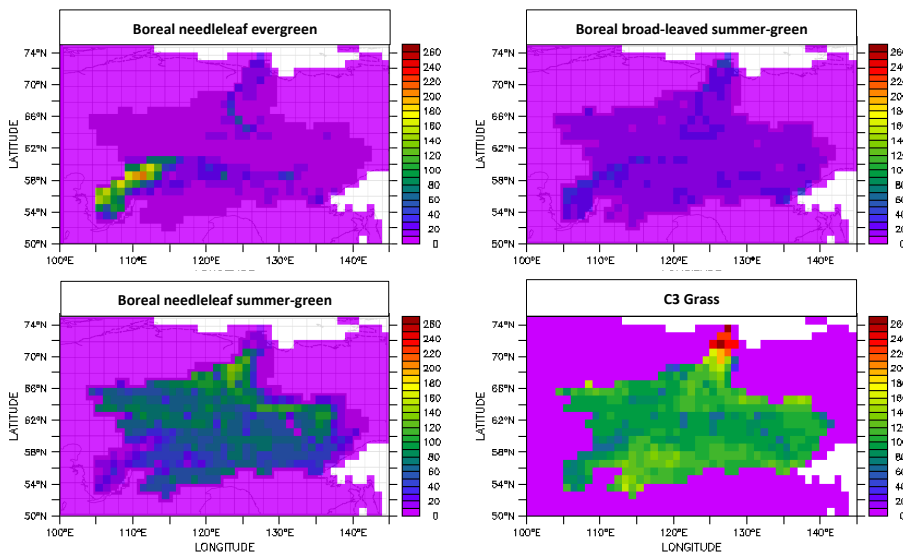
558
559

(b)



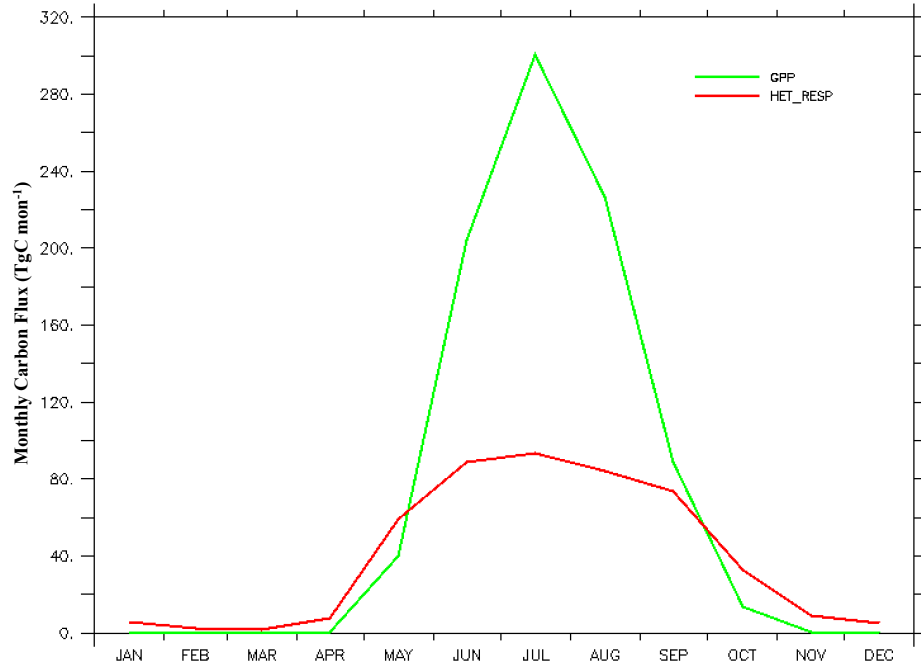
560
561

(c)



562
563

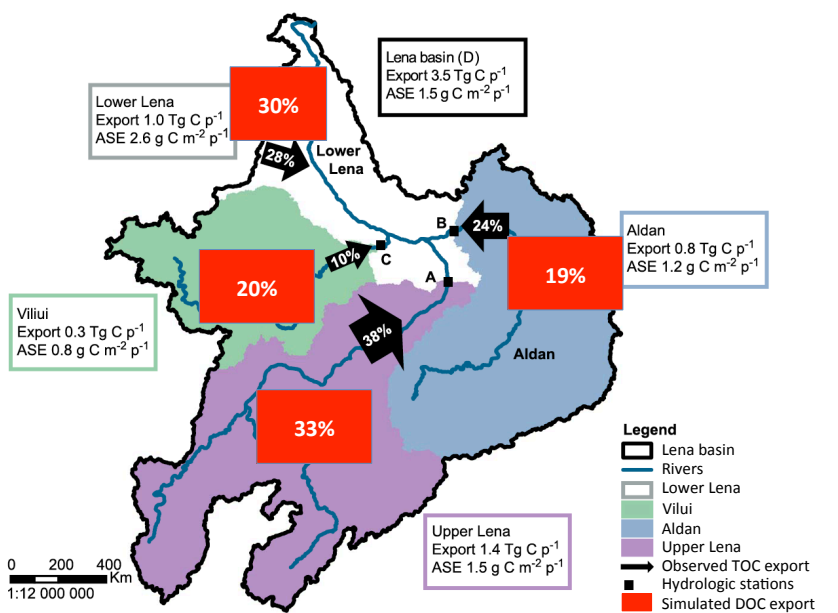
(d)



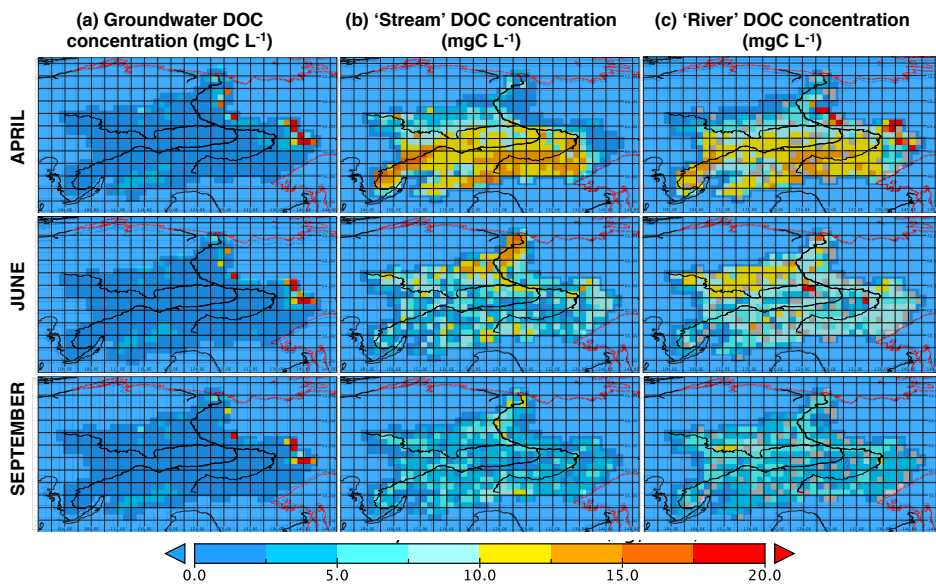
564
565
566
567
568
569

Figure S4: (a) Absolute yearly gross primary productivity (GPP, TgC yr^{-1}) for the four relevant PFT groups over the Lena basin, averaged over 1998-2007. (b) Mean July and August soil heterotrophic respiration rates ($\text{g m}^{-2} \text{ d}^{-1}$) for the same PFT groups as in (a), during the period 1998-2007. (c) Average yearly NPP ($\text{gC m}^{-2} \text{ yr}^{-1}$) averaged over the period 1998-2007. All maps have the Lena basin area shaded in the background. (d)

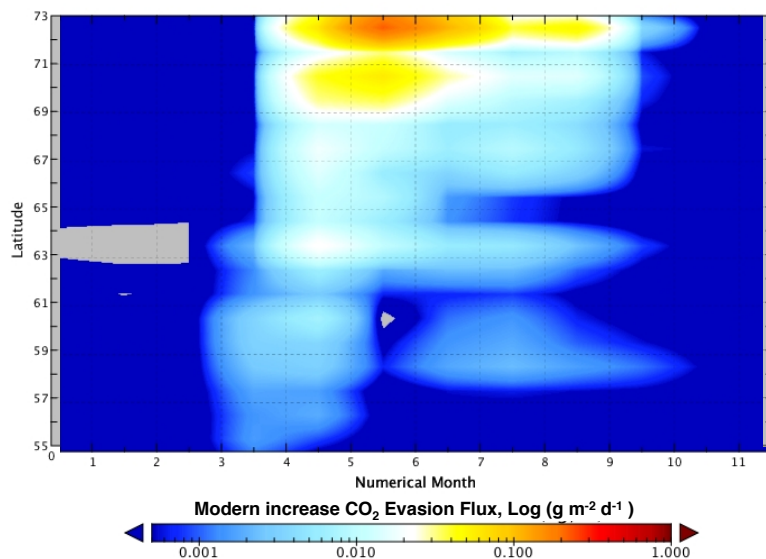
570 | Mean monthly carbon uptake (GPP) versus its heterotrophic respiration from the soil
571 | (Het Resp) in TgC per month, over the period 1998-2007.
572 |



573 |
574 |
575 | **Figure S5:** Map adapted from Fig. 2 in Kutscher et al. (2017) showing proportional sub-
576 | basin contributions of TOC outflow to total TOC discharge in June and July (designated
577 | as their sampling period 'p⁻¹' of 2012-2013, as observed in Kutscher et al., 2017 (black
578 | arrows), and DOC export contributions as simulated over the period 1998-2007 by
579 | ORCHIDEE MICT-L (red boxes). Simulation pixels used in the calculation are correlates
580 | of the real-world sampling locations unless the site coordinates deviated from a
581 | mainstem hydrographic flowpath pixel -in which case a nearest 'next-best' pixel was
582 | used. Here the percentages are out of the summed mean bulk DOC flow of each
583 | tributary, not the mean DOC discharge from the river mouth, because doing so would
584 | negate the in-stream loss of DOC via degradation to CO₂ while in-stream.
585 |
586 |



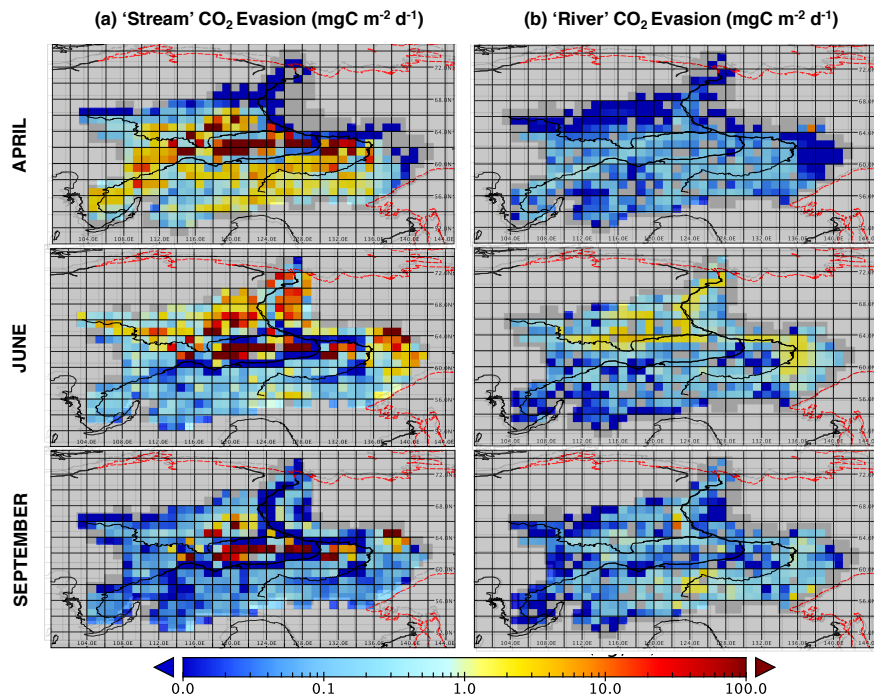
587
588 **Figure S6:** Maps of (a) DOC concentrations (mgC L⁻¹) in groundwater ('slow' water
589 pool), (b) stream water pool, (c) river water pool in April, June and September (first to
590 third rows, respectively), averaged over the period 1998-2007. The coastal boundary
591 and a water body overlay have been applied to the graphic in red and black,
592 respectively, and the same scale applies to all diagrams. All maps have the Lena basin
593 area shaded in the background.
594
595



596

597
598
599
600
601
602

Figure S7: Log-scale Hovmöller diagram plotting the longitudinally-averaged difference (increase) in total CO_2 evaded from the Lena River basin between the average of the periods 1998-2007 and 1901-1910, over each monthly timestep, in (log) $\text{gC m}^{-2} \text{d}^{-1}$. Thus as the river drains northward the month-on-month difference in water-body CO_2 flux, between the beginning and end of the 20th Century is shown.



603
604
605
606
607
608
609
610

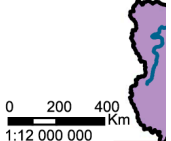
Figure S8: Maps of CO_2 evasion from the surface of the two fluvial hydrological pools in the model, (a) streams and (b) rivers in April, June and September. All maps use the same (log) scale in units of ($\text{mgC m}^{-2} \text{d}^{-1}$).

Simon Bowring 9/10/y 09:34

Lower Len:
Export 1.0
ASE 2.6 g

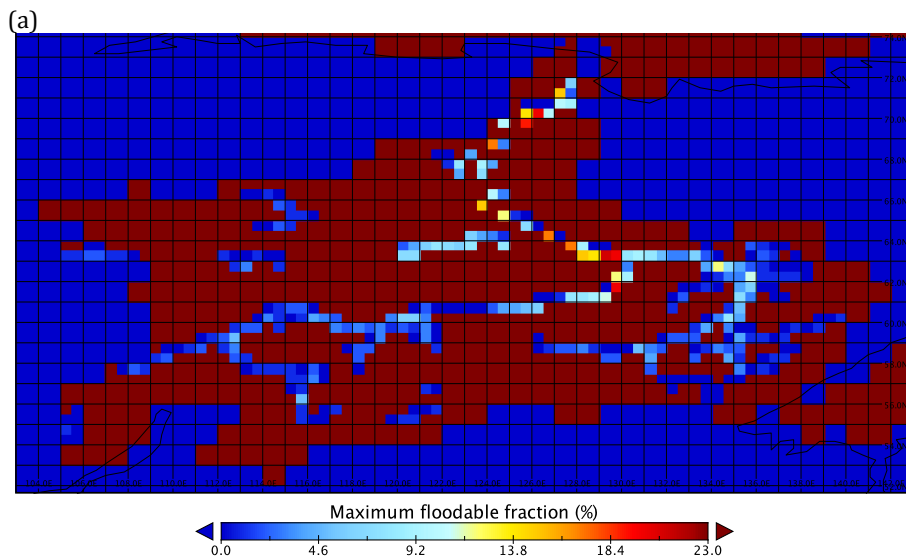


Viliui
Export 0.3 Tg C p^-1
ASE 0.8 g C m^-2 p^-1

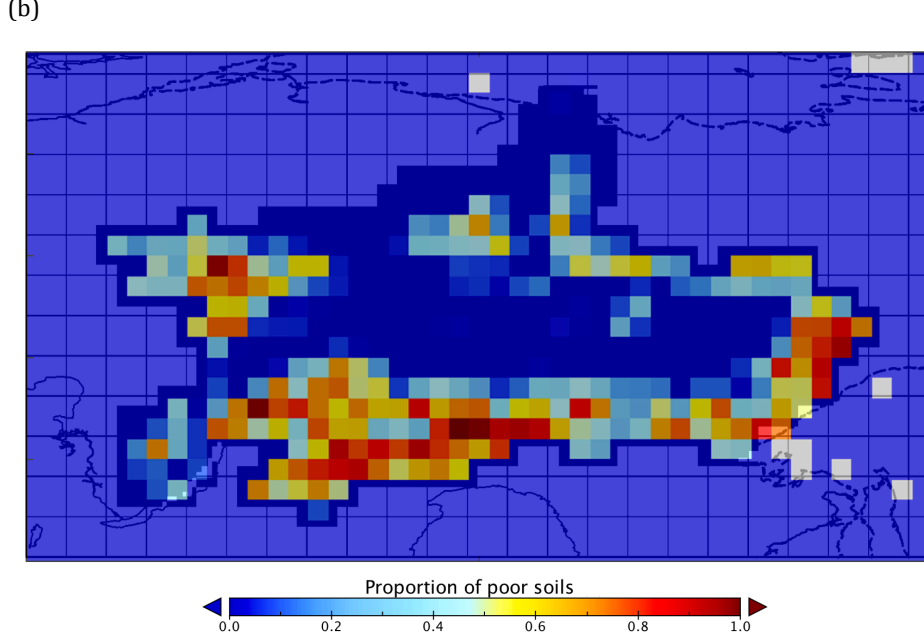


Supprimé: ... [2]

613



614



616

617 | **Figure S9:** (a) Maximum floodable fraction of grid cells for the Lena basin per the input
 618 | map from Tootchi et al. (2018). (b) Podzol and Arenosol map (Nachtergael, Freddy,
 619 | Harrij van Velthuizen, Luc Verelst, N. H. Batjes, Koos Dijkshoorn, V. W. P. van Engelen,
 620 | Guenther Fischer, Arwyn Jones, Luca Montanarella, Monica Petri, Sylvia PrielerB,
 621 | Xuezheng Shi, Edmar Teixera and David Wiberg, 2010) used as input to the 'poor soils'
 622 | module, basin mask in the background.

623

624 |

Simon Bowring 10/10/y 11:13

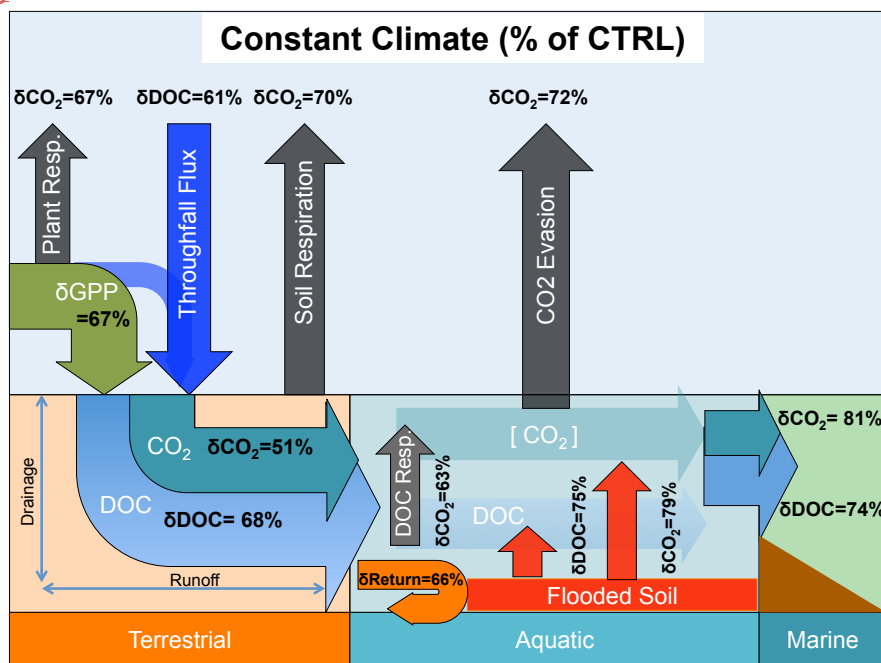
Supprimé: S3

Simon Bowring 9/10/y 09:38

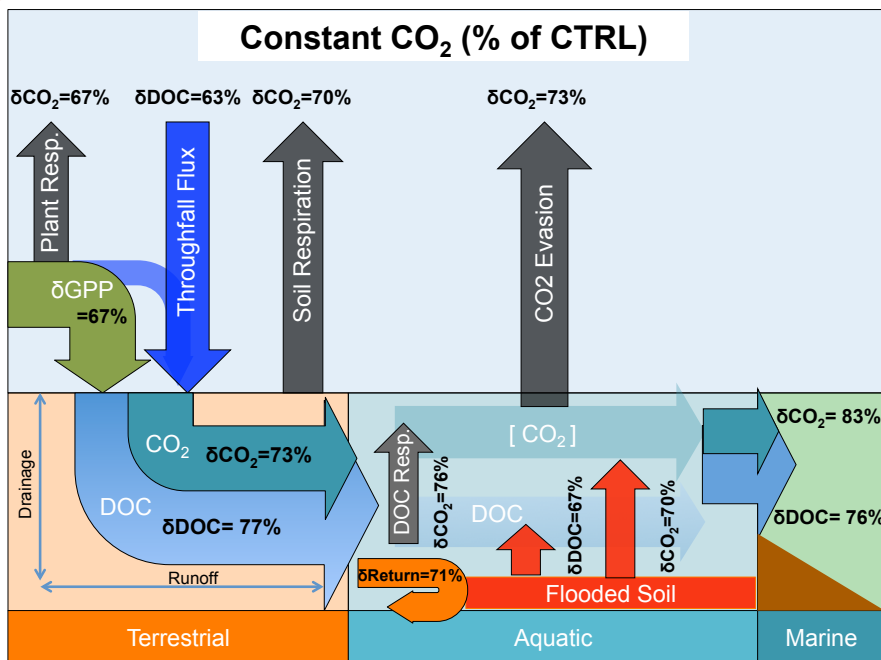
Supprimé:

... [3]

(a)

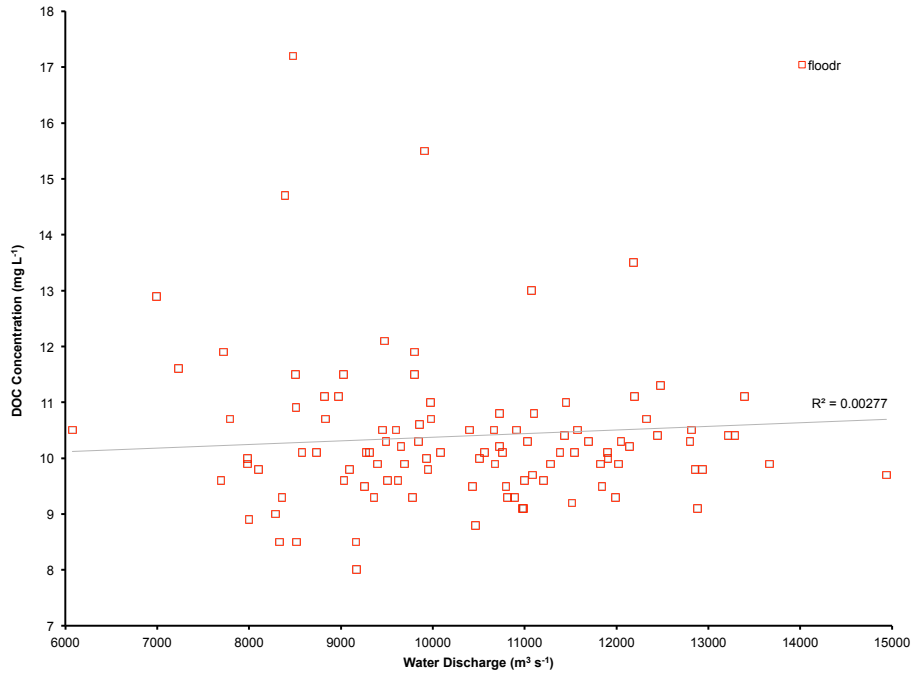


(b)



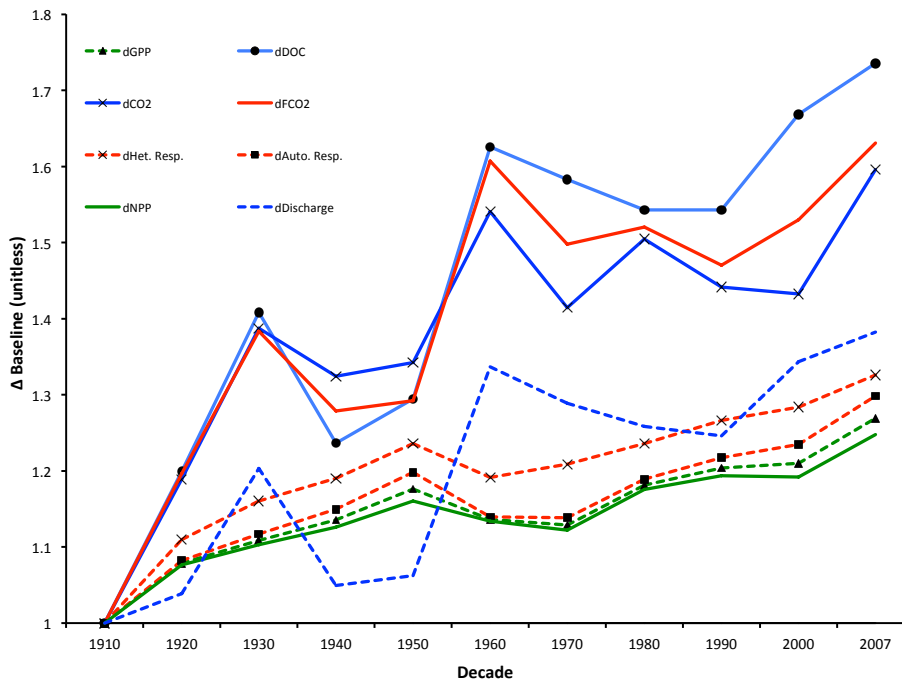
632 | **Figure S10: (a-b): Schematic diagrams detailing the major yearly carbon flux outputs**
633 | **from simulations averaged over the period 1998-2007 as they are transformed and**
634 | **transported across the land-aquatic continuum. Figures (b) and (c) give the same fluxes**
635 | **as a percentage difference from the Control (CTRL-Simulation), for the constant climate**
636 | **and CO₂ simulations, respectively.**

Simon Bowring 9/10/y 09:41
Mis en forme: Police :Gras



638 | **Figure S11:** Simulated basin-mean annual DOC concentrations (mg L^{-1}) for the
639 | floodplain water pool regressed against mean annual simulated discharge rates at Kusur
640 | ($\text{m}^3 \text{s}^{-1}$) over 1901-2007. A linear regression with R^2 is plotted.
641 |
642 |

Simon Bowring 10/10/y 11:13
Supprimé: S6



644
645 | **Figure S12:** Time series showing the decadal-mean fractional change in carbon fluxes
646 normalised to a 1901-1910 average baseline (=1 on the y-axis) for NPP, GPP,
647 autotrophic and heterotrophic respiration, DOC inputs to the water column, CO₂ inputs
648 to the water column, CO₂ evasion from the water surface (FCO₂), and discharge.

Simon Bowring 10/10/y 11:13

Supprimé: S7

650 651 References

652
653 Beer, C., Lucht, W., Schmullius, C. and Shvidenko, A.: Small net carbon dioxide uptake by
654 Russian forests during 1981-1999, *Geophys. Res. Lett.*, doi:10.1029/2006GL026919,
655 2006.
656 Bekryaev, R. V., Polyakov, I. V. and Alexeev, V. A.: Role of polar amplification in long-term
657 surface air temperature variations and modern arctic warming, *J. Clim.*,
658 doi:10.1175/2010JCLI3297.1, 2010.
659 Biancamaria, S., Bates, P. D., Boone, A. and Mognard, N. M.: Large-scale coupled
660 hydrologic and hydraulic modelling of the Ob river in Siberia, *J. Hydrol.*,
661 doi:10.1016/j.jhydrol.2009.09.054, 2009.
662 Bontemps, S., Defourny, P., Radoux, J., Van Bogaert, E., Lamarche, C., Achard, F., Mayaux, P.,
663 Boettcher, M., Brockmann, C., Kirches, G., Zulkhe, M., Kalogirou, V., Seifert, F. . and
664 Arino, O.: Consistent global land cover maps for climate modelling communities: current
665 achievements of the ESA' and cover CCI, in *ESA Living Planet Symposium 2013*, pp. 9–
666 13., 2013.
667 Burke, E. J., Dankers, R., Jones, C. D. and Wiltshire, A. J.: A retrospective analysis of pan
668 Arctic permafrost using the JULES land surface model, *Clim. Dyn.*, doi:10.1007/s00382-
669 012-1648-x, 2013.

671 Connolly, C. T., Khosh, M. S., Burkart, G. A., Douglas, T. A., Holmes, R. M., Jacobson, A. D.,
672 Tank, S. E. and McClelland, J. W.: Watershed slope as a predictor of fluvial dissolved
673 organic matter and nitrate concentrations across geographical space and catchment size
674 in the Arctic, *Environ. Res. Lett.*, 13(10), 104015, doi:10.1088/1748-9326/aae35d, 2018.
675 Denfeld, B., Frey, K. and Sobczak, W.: Summer CO₂ evasion from streams and rivers in
676 the Kolyma River basin, north-east Siberia, *Polar Res.*, 32(1), 19704,
677 doi:10.3402/polar.v32i0.19704, 2013.
678 Drake, T. W., Wickland, K. P., Spencer, R. G. M., McKnight, D. M. and Striegl, R. G.: Ancient
679 low-molecular-weight organic acids in permafrost fuel rapid carbon dioxide production
680 upon thaw, *Proc. Natl. Acad. Sci.*, 112(45), 13946–13951,
681 doi:10.1073/pnas.1511705112, 2015.
682 Elberling, B.: Annual soil CO₂ effluxes in the High Arctic: The role of snow thickness and
683 vegetation type, *Soil Biol. Biochem.*, doi:10.1016/j.soilbio.2006.09.017, 2007.
684 Fekete, B. M., Vörösmarty, C. J., Roads, J. O. and Willmott, C. J.: Uncertainties in
685 precipitation and their impacts on runoff estimates, *J. Clim.*, doi:10.1175/1520-
686 0442(2004)017<0294:U_IPATI>2.0.CO;2, 2004.
687 Frey, K. E. and McClelland, J. W.: Impacts of permafrost degradation on arctic river
688 biogeochemistry, *Hydrol. Process.*, 169–182, doi:10.1002/hyp.7196, 2009.
689 Frey, K. E. and Smith, L. C.: Amplified carbon release from vast West Siberian peatlands
690 by 2100, *Geophys. Res. Lett.*, doi:10.1029/2004GL022025, 2005.
691 Frieler, K., Lange, S., Piontek, F., Reyer, C. P. O., Schewe, J., Warszawski, L., Zhao, F., Chini,
692 L., Denvil, S., Emanuel, K., Geiger, T., Halladay, K., Hurtt, G., Mengel, M., Murakami, D.,
693 Ostberg, S., Popp, A., Riva, R., Stevanovic, M., SuzGBRI, T., Volkholz, J., Burke, E., Ciais, P.,
694 Ebi, K., Eddy, T. D., Elliott, J., Galbraith, E., Gosling, S. N., Hattermann, F., Hickler, T.,
695 Hinkel, J., Hof, C., Huber, V., Jägermeyr, J., Krysanova, V., Marcé, R., Müller Schmied, H.,
696 Mouratiadou, I., Pierson, D., Tittensor, D. P., Vautard, R., Van Vliet, M., Biber, M. F., Betts,
697 R. A., Leon Bodirsky, B., Deryng, D., Frolking, S., Jones, C. D., Lotze, H. K., Lotze-Campen,
698 H., Sahajpal, R., Thonicke, K., Tian, H. and Yamagata, Y.: Assessing the impacts of 1.5°C
699 global warming - Simulation protocol of the Inter-Sectoral Impact Model
700 Intercomparison Project (ISIMIP2b), *Geosci. Model Dev.*, doi:10.5194/gmd-10-4321-
701 2017, 2017.
702 Guimbertea, M., Zhu, D., Maignan, F., Huang, Y., Yue, C., Dantec-N d lec, S., Ottl, C., Jornet-
703 Puig, A., Bastos, A., Laurent, P., Goll, D., Bowring, S., Chang, J., Guenet, B., Tifafi, M., Peng,
704 S., Krinner, G., Ducharme, A. s., Wang, F., Wang, T., Wang, X., Wang, Y., Yin, Z., Lauerwald,
705 R., Joetzjer, E., Qiu, C., Kim, H. and Ciais, P.: ORCHIDEE-MICT (v8.4.1), a land surface
706 model for the high latitudes: model description and validation, *Geosci. Model Dev.*,
707 11(1), 121–163, doi:10.5194/gmd-11-121-2018, 2018.
708 Haddeland, I., Clark, D. B., Franssen, W., Ludwig, F., Voß, F., Arnell, N. W., Bertrand, N.,
709 Best, M., Folwell, S., Gerten, D., Gomes, S., Gosling, S. N., Hagemann, S., Hanasaki, N.,
710 Harding, R., Heinke, J., Kabat, P., Koirala, S., Oki, T., Polcher, J., Stacke, T., Viterbo, P.,
711 Weedon, G. P. and Yeh, P.: Multimodel Estimate of the Global Terrestrial Water Balance:
712 Setup and First Results, *J. Hydrometeorol.*, doi:10.1175/2011JHM1324.1, 2011.
713 Kaiser, K. and Kalbitz, K.: Cycling downwards - dissolved organic matter in soils, *Soil*
714 *Biol. Biochem.*, doi:10.1016/j.soilbio.2012.04.002, 2012.
715 Klaminder, J., Grip, H., Mörth, C. M. and Laudon, H.: Carbon mineralization and pyrite
716 oxidation in groundwater: Importance for silicate weathering in boreal forest soils and
717 stream base-flow chemistry, *Appl. Geochemistry*,
718 doi:10.1016/j.apgeochem.2010.12.005, 2011.
719 Kutscher, L., Mörth, C. M., Porcelli, D., Hirst, C., Maximov, T. C., Petrov, R. E. and

720 Andersson, P. S.: Spatial variation in concentration and sources of organic carbon in the
721 Lena River, Siberia, *J. Geophys. Res. Biogeosciences*, 122(8), 1999–2016,
722 doi:10.1002/2017JG003858, 2017.

723 Lammers, R. B., Shiklomanov, A. I., Vörösmarty, C. J., Fekete, B. M. and Peterson, B. J.:
724 Assessment of contemporary Arctic river runoff based on observational discharge
725 records, *J. Geophys. Res. Atmos.*, doi:10.1029/2000JD900444, 2001.

726 Lange, S.: Earth2Observe, WFDEI and ERA-Interim data Merged and Bias-corrected for
727 ISIMIP (EWEMBI), GFZ Data Serv., doi:10.5880/pik.2016.004, 2016.

728 Lange, S.: Bias correction of surface downwelling longwave and shortwave radiation for
729 the EWEMBI dataset, *Earth Syst. Dyn.*, doi:10.5194/esd-9-627-2018, 2018.

730 Laudon, H., Buttle, J., Carey, S. K., McDonnell, J., McGuire, K., Seibert, J., Shanley, J.,
731 Soulsby, C. and Tetzlaff, D.: Cross-regional prediction of long-term trajectory of stream
732 water DOC response to climate change, *Geophys. Res. Lett.*, doi:10.1029/2012GL053033,
733 2012.

734 Lauerwald, R., Hartmann, J., Ludwig, W. and Moosdorf, N.: Assessing the nonconservative
735 fluvial fluxes of dissolved organic carbon in North America, *J. Geophys. Res. Biogeosciences*,
736 doi:10.1029/2011JG001820, 2012.

737 Lauerwald, R., Laruelle, G. G., Hartmann, J., Ciais, P. and Regnier, P. A. G.: Spatial patterns
738 in CO₂evasion from the global river network, *Global Biogeochem. Cycles*,
739 doi:10.1002/2014GB004941, 2015.

740 Lloyd, J., Shibalova, O., Zolotoukhine, D., Kolle, O., Arneth, A., Wirth, C., Styles, J. M.,
741 Tchebakova, N. M. and Schulze, E. D.: Seasonal and annual variations in the
742 photosynthetic productivity and carbon balance of a central Siberian pine forest, *Tellus, Ser. B Chem. Phys. Meteorol.*, doi:10.1034/j.1600-0889.2002.01487.x, 2002.

743 Nachtergael, Freddy, Harrij van Velthuizen, Luc Verelst, N. H. Batjes, Koos Dijkshoorn,
744 V. W. P. van Engelen, Guenther Fischer, Arwyn Jones, Luca Montanarella, Monica Petri,
745 Sylvia PrielerB, Xuezheng Shi, Edmar Teixera and David Wiberg: The harmonized world
746 soil database, *Proc. 19th World Congr. Soil Sci. Soil Solut. a Chang. World*, Brisbane, Aust.
747 1-6 August 2010, pp. 34-37., 34–37 [online] Available from:
748 <https://library.wur.nl/WebQuery/wurpubs/fulltext/154132>, 2010.

749 Qiu, C., Zhu, D., Ciais, P., Guenet, B., Krinner, G., Peng, S., Aurela, M., Bernhofer, C.,
750 Brümmer, C., Bret-Harte, S., Chu, H., Chen, J., Desai, A. R., Dušek, J., Euskirchen, E. S.,
751 Fortuniak, K., Flanagan, L. B., Friborg, T., Grygoruk, M., Gogo, S., Grünwald, T., Hansen, B.,
752 U., Holl, D., Humphreys, E., Hurkuck, M., Kiely, G., Klatt, J., Kutzbach, L., Laggeron, C.,
753 Laggoun-Défarge, F., Lund, M., Lafleur, P. M., Li, X., Mammarella, I., Merbold, L., Nilsson,
754 M. B., Olejnik, J., Ottosson-Löfvenius, M., Oechel, W., Parmentier, F. J. W., Peichl, M., Pirk,
755 N., Peltola, O., Pawlak, W., Rasse, D., Rinne, J., Shaver, G., Peter Schmid, H., Sottocornola,
756 M., Steinbrecher, R., Sachs, T., Urbaniak, M., Zona, D. and Ziemblińska, K.: ORCHIDEE-
757 PEAT (revision 4596), a model for northern peatland CO₂, water, and energy fluxes on
758 daily to annual scales, *Geosci. Model Dev.*, 11(2), 497–497, doi:10.5194/gmd-11-497-
759 2018, 2018.

760 Rawlins, M. A., Fahnestock, M., Frolking, S. and Vörösmarty, C. J.: On the evaluation of
761 snow water equivalent estimates over the terrestrial Arctic drainage basin, in
762 *Hydrological Processes*, 2007.

763 Reynolds, C. A., Jackson, T. J. and Rawls, W. J.: Estimating soil water-holding capacities by
764 linking the Food and Agriculture Organization soil map of the world with global pedon
765 databases and continuous pedotransfer functions, *Water Resour. Res.*, 36(12), 3653–
766 3662, doi:10.1029/2000WR900130, 1999.

767 Roser, C., Montagnani, L., Schulze, E.-D., Mollicone, D., Kolle, O., Meroni, M., Papale, D.,

769 Marchesini, L. B., Federici, S. and Valentini, R.: Net CO₂ exchange rates in three different
770 successional stages of the “Dark Taiga” of central Siberia, *Tellus B*, doi:10.1034/j.1600-
771 0889.2002.01351.x, 2002.

772 Sawamoto, T., Hatano, R., Yajima, T., Takahashi, K. and Isaev, A. P.: Soil respiration in
773 siberian taiga ecosystems with different histories of forest fire, *Soil Sci. Plant Nutr.*,
774 doi:10.1080/00380768.2000.10408759, 2000.

775 Schulze, E. D., Lloyd, J., Kelliher, F. M., Wirth, C., Rebmann, C., Luhker, B., Mund, M., Knohl,
776 A., Milyukova, I. M., Schulze, W., Ziegler, W., Varlagin, A. B., Sogachev, A. F., Valentini, R.,
777 Dore, S., Grigoriev, S., Kolle, O., Panfyorov, M. I., Tchebakova, N. and Vygodskaya, N. N.:
778 Productivity of forests in the eurosiberian boreal region and their potential to act as a
779 carbon sink - a synthesis, *Glob. Chang. Biol.*, doi:10.1046/j.1365-2486.1999.00266.x,
780 1999.

781 Serikova, S., Pokrovsky, O. S., Ala-Aho, P., Kazantsev, V., Kirpotin, S. N., Kopysov, S. G.,
782 Krickov, I. V., Laudon, H., Manasypov, R. M., Shirokova, L. S., Soulsby, C., Tetzlaff, D. and
783 Karlsson, J.: High riverine CO₂ emissions at the permafrost boundary of Western Siberia,
784 *Nat. Geosci.*, doi:10.1038/s41561-018-0218-1, 2018.

785 Shvartsev, S. L.: Geochemistry of fresh groundwater in the main landscape zones of the
786 Earth, *Geochemistry Int.*, doi:10.1134/S0016702908130016, 2008.

787 Shvidenko, A. and Nilsson, S.: A synthesis of the impact of Russian forests on the global
788 carbon budget for 1961-1998, *Tellus, Ser. B Chem. Phys. Meteorol.*, doi:10.1034/j.1600-
789 0889.2003.00046.x, 2003.

790 Sommerkorn, M.: Micro-topographic patterns unravel controls of soil water and
791 temperature on soil respiration in three Siberian tundra systems, *Soil Biol. Biochem.*,
792 doi:10.1016/j.soilbio.2008.03.002, 2008.

793 Tarnocai, C., Canadell, J. G., Schuur, E. A. G., Kuhry, P., Mazhitova, G. and Zimov, S.: Soil
794 organic carbon pools in the northern circumpolar permafrost region, *Global
795 Biogeochem. Cycles*, 23(2), doi:Gb2023\ n10.1029/2008gb003327, 2009.

796 Tootchi, A., Jost, A. and Ducharne, A.: Multi-source global wetland maps combining
797 surface water imagery and groundwater constraints, *Earth Syst. Sci. Data*, 11, 189-220,
798 doi:10.5194/essd-11-189-2019, 2019.

799 Vonk, J. E., Mann, P. J., Davydov, S., Davydova, A., Spencer, R. G. M., Schade, J., Sobczak, W.
800 V., Zimov, N., Zimov, S., Bulygina, E., Eglinton, T. I. and Holmes, R. M.: High biolability of
801 ancient permafrost carbon upon thaw, *Geophys. Res. Lett.*, 40(11), 2689-2693,
802 doi:10.1002/grl.50348, 2013.

803 Vonk, J. E., Tank, S. E., Mann, P. J., Spencer, R. G. M., Treat, C. C., Striegl, R. G., Abbott, B. W.
804 and Wickland, K. P.: Biodegradability of dissolved organic carbon in permafrost soils and
805 aquatic systems: A meta-analysis, *Biogeosciences*, 12(23), 6915-6930, doi:10.5194/bg-
806 12-6915-2015, 2015a.

807 Vonk, J. E., Tank, S. E., Bowden, W. B., Laurion, I., Vincent, W. F., Alekseychik, P., Amyot,
808 M., Billet, M. F., Canário, J., Cory, R. M., Deshpande, B. N., Helbig, M., Jammes, M., Karlsson,
809 J., Larouche, J., MacMillan, G., Rautio, M., Walter Anthony, K. M. and Wickland, K. P.:
810 Reviews and Syntheses: Effects of permafrost thaw on arctic aquatic ecosystems,
811 *Biogeosciences Discuss.*, 12(23), 7129-7167, doi:10.5194/bgd-12-10719-2015, 2015b.

812 Vorosmarty, C. J., Fekete, B. M., Meybeck, M. and Lammers, R. B.: Global system of rivers:
813 Its role in organizing continental land mass and defining land-To-Ocean linkages, *Global
814 Biogeochem. Cycles*, 14(2), 599-621, doi:10.1029/1999GB900092, 2000.

815 Wang, S., Huang, J., Yang, D., Pavlic, G. and Li, J.: Long-term water budget imbalances and
816 error sources for cold region drainage basins, *Hydrol. Process.*, doi:10.1002/hyp.10343,
817 2015.

818 Yang, D., Kane, D., Zhang, Z., Legates, D. and Goodison, B.: Bias corrections of long-term
819 (1973-2004) daily precipitation data over the northern regions, *Geophys. Res. Lett.*,
820 doi:10.1029/2005GL024057, 2005.

821 Ye, B., Yang, D. and Kane, D. L.: Changes in Lena River streamflow hydrology: Human
822 impacts versus natural variations, *Water Resour. Res.*, doi:10.1029/2003WR001991,
823 2003.

824 Ye, B., Yang, D., Zhang, Z. and Kane, D. L.: Variation of hydrological regime with
825 permafrost coverage over Lena Basin in Siberia, *J. Geophys. Res. Atmos.*, 114, D7,
826 doi:10.1029/2008JD010537, 2009.

827 Zhang, X., Hutchings, J. A., Bianchi, T. S., Liu, Y., Arellano, A. R. and Schuur, E. A. G.:
828 Importance of lateral flux and its percolation depth on organic carbon export in Arctic
829 tundra soil: Implications from a soil leaching experiment, *J. Geophys. Res.*
830 *Biogeosciences*, 122(4), 796–810, doi:10.1002/2016JG003754, 2017.

831

Text S1: Groundwater DOC Concentrations

The high groundwater reservoir DOC concentrations simulated in high altitude regions by ORCHIDEE MICT-L is related to the fact that, in the model, DOC is rapidly produced and infiltrated deep into soil above the permafrost table, to the point that it reaches the simulated groundwater pool relatively quickly, allowing it to enter this reservoir before being metabolised through the soil column –hence allowing for the relatively high groundwater concentrations found in mountain areas. Because of the prevailing low temperatures, this DOC is not quickly decomposed by microbes and instead feed the groundwater DOC pool.

Text S2: Evaluation of Simulated NPP and Soil Respiration

Rates of yearly net primary production (NPP) for Russian and Siberian forests have been inferred in situ from eddy flux and inventory techniques to range from 123-250 gC m⁻² yr⁻¹ (Beer et al., 2006; Lloyd et al., 2002; Roser et al., 2002; Schulze et al., 1999; Shvidenko and Nilsson, 2003). We likewise simulate a broad range of NPP carbon uptake rates, of 61-469 gC m⁻² yr⁻¹ averaged per grid cell over the Lena basin, with a mean value of 210 gC m⁻² yr⁻¹. NPP is heterogeneously distributed over space and between PFTs (SI, Fig. S5c), with forests averaging 90 gC m⁻² yr⁻¹ and grasslands averaging 104 gC m⁻² yr⁻¹ over the basin as a whole. Low values tended to originate in basin grid cells with elevated topography or high mean slope, while the maximum value was standalone, exceeding the next greatest by ~100 gC m⁻² yr⁻¹, and is most likely caused by the edge effects of upscaling a coastal gridcell's small fraction of terrestrial area where high productivity occurs in a small plot, to the grid cell as a whole. By evaluating NPP we are also evaluating at a secondary level litter production, which is at a third level a major component of DOC production.

Taken as a whole, gross primary production (GPP) was performed under simulations by four PFT groups, with the largest basin-wide bulk contributions coming from boreal needleleaf summer-green trees and C3 grasses (SI, Fig. S5a), the highest GPP uptake rates (3 TgC pixel⁻¹ yr⁻¹) generated by boreal needleleaf evergreen trees, and the remainder of GPP contributed by Boreal broad-leaved summer-green trees (SI, Fig. S5a).

Soil respiration rates, of combined soil heterotroph and plant root respiration in our Control simulation, averaged 208 gC m⁻² yr⁻¹ (0.57 gC m⁻² d⁻¹) over the Lena basin over the period 1990-2000, which is somewhat higher than those found by Elberling (2007) in tundra soils over Svalbard, of 103-176 gC m⁻² yr⁻¹ (0.28-0.48 gC m⁻² d⁻¹). Sawamoto, et al. (2000) measured in situ summertime soil respiration over the central Lena basin and found rates of 1.6-34 gC m⁻² d⁻¹, while Sommerkorn (2008) observed rates of 0.1-3.9 gC m⁻² d⁻¹ at higher latitudes, these appearing to vary with vegetation and fire history, water table depth and temperature. Mean heterotrophic respiration rates of 1.6 gC m⁻² d⁻¹ are simulated here during July and August, in the range 0.0.5-2.2 gC m⁻² d⁻¹ for each of the above PFT groups. The spatial distribution of, and difference in respiration rates between PFT groups largely mirrors those for NPP (SI Fig. S5c), with maximum rates of 1.4 gC m⁻² d⁻¹ over forested sites,

versus a maximum of $2.2 \text{ gC m}^{-2} \text{ d}^{-1}$ over grassland/tundra sites (SI, Fig. S5b).

Aggregated over the basin, results show that increases over the course of the 20th Century were simulated for NPP, GPP, River Discharge, DOC, $\text{CO}_{2(\text{aq})}$, autotrophic and heterotrophic respiration and CO_2 evasion, with percentage changes in the last versus first decade of +25%, +27%, 38%, +73%, +60%, +30%, +33% and +63%, respectively. (Fig. S7). It thus appears that rising temperatures and CO_2 concentrations disproportionately favoured the metabolism of carbon within the soil and its transport and mineralisation within the water column, fed by higher rates of primary production and litter formation as well as an accelerated hydrological cycle.

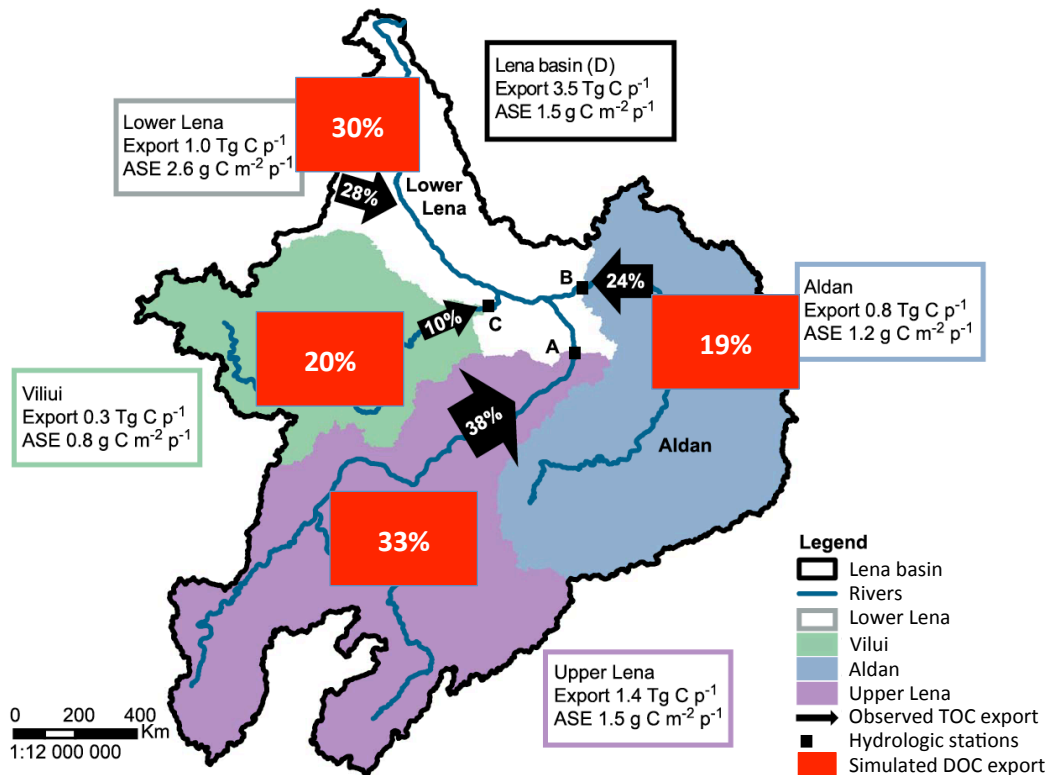


Figure S2: Map adapted from Fig. 2 in Kutscher et al. (2017) showing proportional sub-basin contributions of TOC outflow to total TOC discharge in June and July (designated as their sampling period ' p^{-1} ') of 2012-2013, as observed in Kutscher et al., 2017 (black arrows), and DOC export contributions as simulated over the period 1998-2007 by ORCHIDEE MICT-L (red boxes). Simulation pixels used in the calculation are correlates of the real-world sampling locations unless the site coordinates deviated from a mainstem hydrographic flowpath pixel -in which case a nearest 'next-best' pixel was used. Here the percentages are out of the summed mean bulk DOC flow of each tributary, not the mean DOC discharge from the river mouth, because doing so would negate the in-stream loss of DOC via degradation to CO_2 while in-stream.

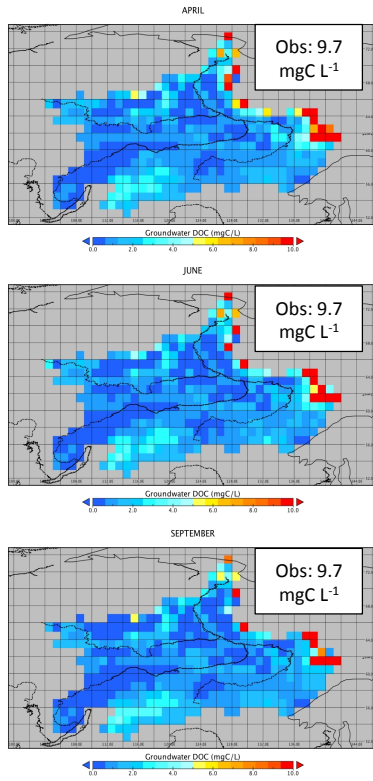
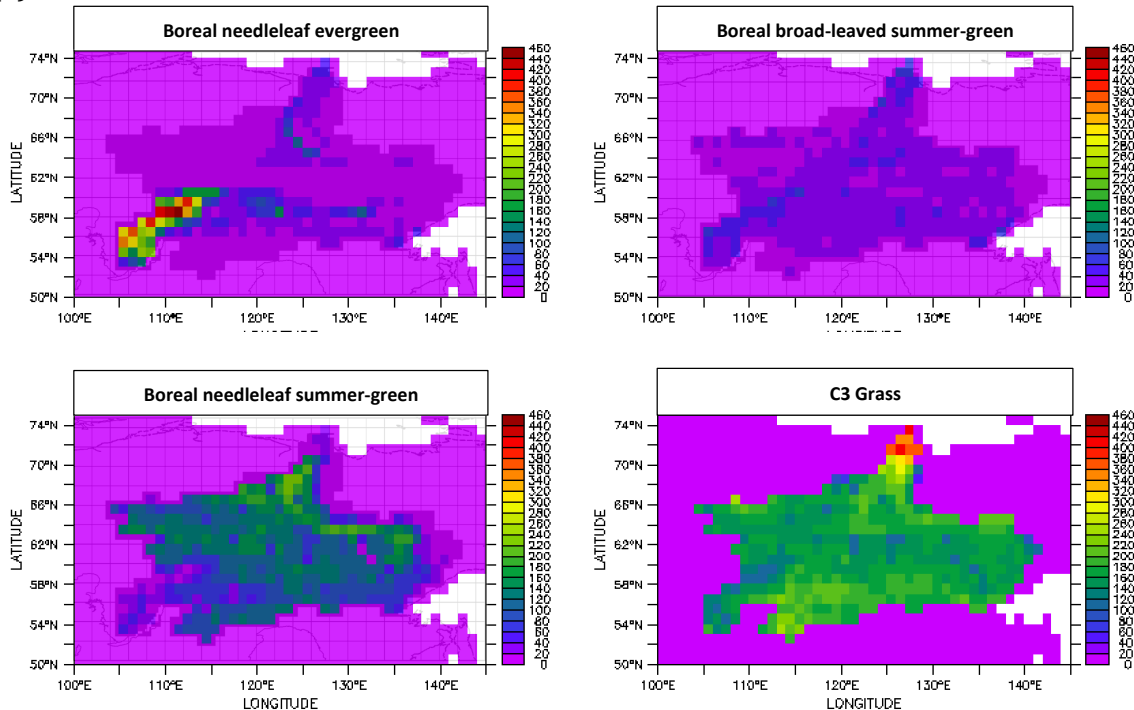
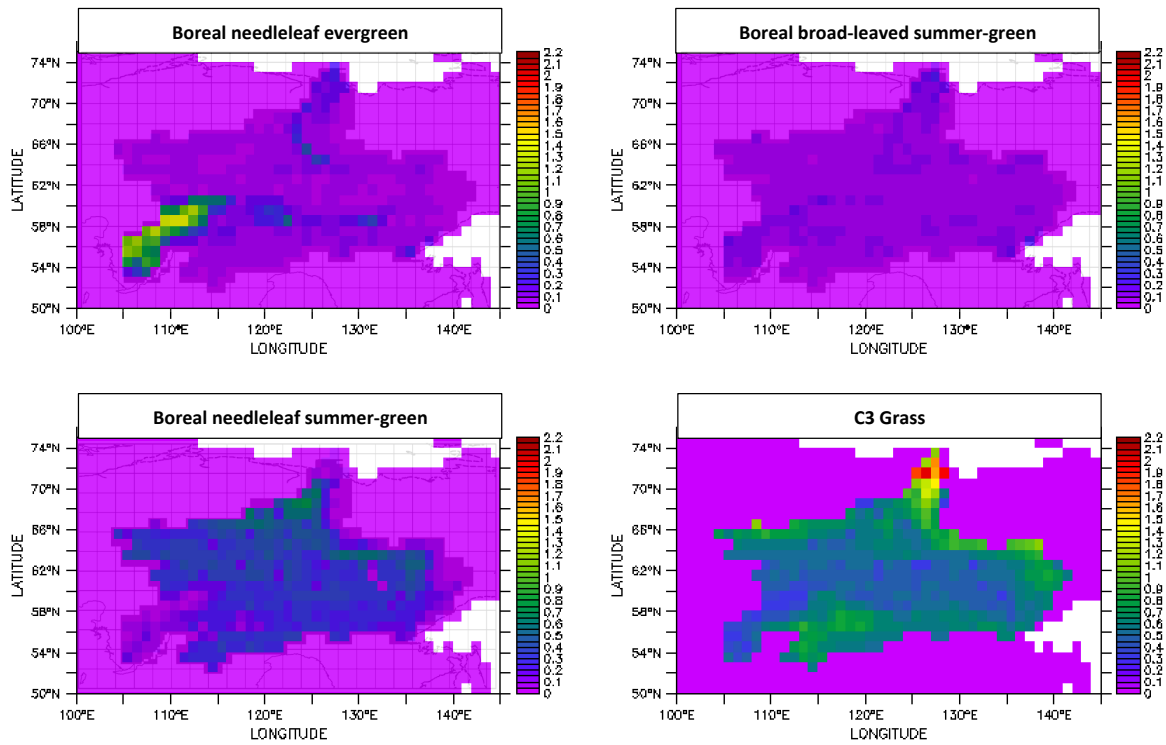


Figure S4: Groundwater DOC concentrations over the Lena basin for April, June and September averaged over 1998-2007, with mean observed concentrations for permafrost groundwater inset.

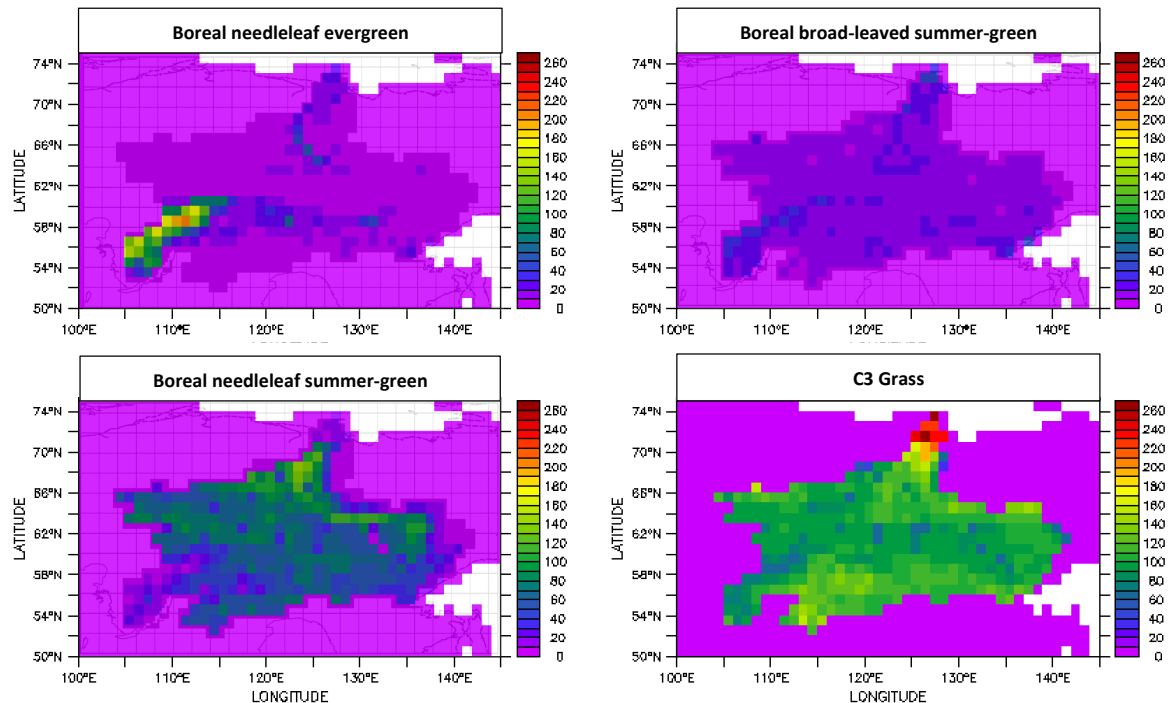
(a)



(b)



(c)



(d)

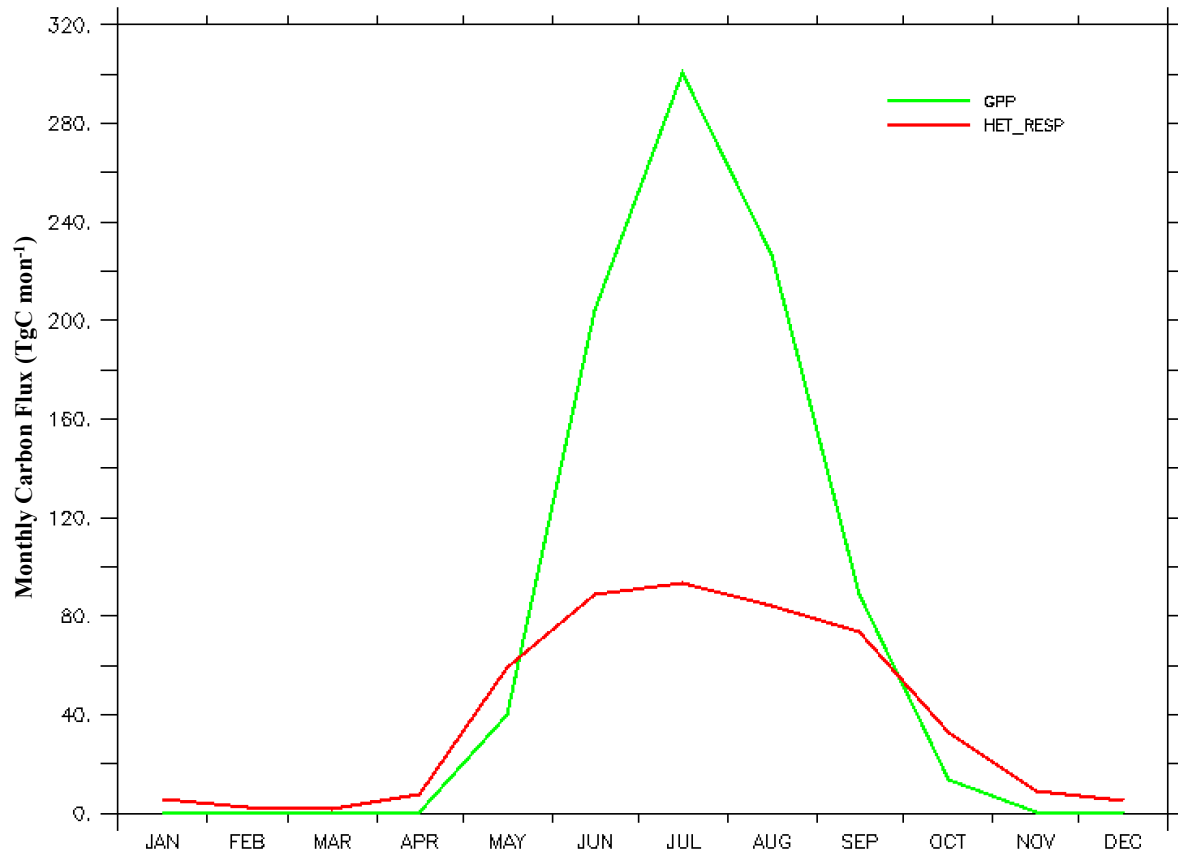


Figure S5: (a) Absolute yearly gross primary productivity (GPP, TgC yr^{-1}) for the four relevant PFT groups over the Lena basin, averaged over 1998-2007. (b) Mean July and August soil heterotrophic respiration rates ($\text{g m}^2 \text{ d}^{-1}$) for the same PFT groups as in (a), during the period 1998-2007. (c) Average yearly NPP ($\text{gC m}^2 \text{ yr}^{-1}$) averaged over the period 1998-2007. All maps have the Lena basin area shaded in the background. (d) Mean monthly carbon uptake (GPP) versus its heterotrophic respiration from the soil (Het_Resp) in TgC per month, over the period 1998-2007.